ADVANCED MATERIALS INTERFACES
www.advmatinterfaces.de

Hydrogel Nanocomposite Adsorbents and Photocatalysts for Sustainable Water Purification

*Neeraj Kumar, Rashi Gusain, Sadanand Pandey, and Suprakas Sinha Ray**

Hydrogels have been employed for water purification applications, but their performance and strength are unsatisfactory for widespread adoption. Recently, hydrogel nanocomposites have been proposed to resolve the inherent challenges faced by hydrogels for water treatment. This review comprehensively analyzes hydrogel nanocomposites for water treatment using adsorbent and photocatalysis techniques. The structure, classification, and tunable synthesis methods of hydrogels are explained. Further, how hydrogels can be incorporated with functional nanoparticles (NPs) and can be used as templates/precursors for developing advanced 3D architectures, including the formation of hydrogel nanocomposite beads and 3D printing objects are discussed. Finally, the structure-property relationships of hydrogel nanocomposites are critically reviewed by considering introductory gelation chemistry, such as swelling characteristics, mechanical properties, stimuli-responsiveness, and ionic/electronic conduction. The extensive cross-linking of polymer chains with NPs offers high mass/charge transport, high surface areas, and enhanced polymer-water interactions to achieve high-performing adsorbents and photocatalysts. Several motivating examples of emerging NP-containing hydrogel nanocomposites for use in adsorbents and photocatalysis have been discussed. Such efforts validated the excellent technological potential held by hydrogel nanocomposites for water purification applications. Finally, future directions of hydrogel nanocomposites for sustainable water treatment are proposed.

1. Introduction

The availability of clean water is the uppermost requirement for the survival of humankind and all ecosystems. However, based on the 2014 Global Water Intelligence Report, over 1.2 billion people are currently affected by the severe shortage of direct access to clean, drinkable water due to uncontrollable water pollution and physical or economic water scarcity.[1,2] Anthropogenic actions, environmental catastrophes, urbanization, population growth, and industrialization generate toxic pollutants in water bodies. The most pollutants are heavy metals and metalloids, dyes, volatile organic compounds, pharmaceuticals, pesticides, radionuclides, aromatic hydrocarbons, oils, polycyclic aromatic hydrocarbons, microbes/pathogens, and microplastics that can be in different forms and concentrations.[3–5] Globally, approximately 2 million tons of pollutants from agriculture, industrial, and sewage waste are released into water streams, which pose severe health risks and cause the deaths of more than 1400 people every day.[6] Thus, developing efficient, economical, environmental-friendly, and scalable technologies for the purification of wastewater and seawater is urgently required. To fulfill the shortage of clean water, affordable technologies can be used to transform unconventional water reserves (such as wastewater, rainfall, seawater, and brackish water) into potable water. Recently, numerous water treatment technologies, including coagulation/flocculation, filtration, chemical precipitation, aerobic/anaerobic processing, biological treatment, electrochemically precipitation, advanced oxidation processing, membrane separation, ion-exchange, adsorption, solar/thermal distillation/evaporation, crystallization, and photocatalysis, have emerged to offer practical solutions to water pollution management.[7–14] Among them, adsorption and photocatalysis technologies have garnered significant attention from the research community due to their cost-effectiveness, high performance,

N. Kumar, R. Gusain, S. S. Ray
Department of Chemical Sciences
University of Johannesburg
Doornfontein 2028, South Africa
E-mail: rsuprakas@csir.co.za

The ORCID identification number(s) for the author(s) of this article can be found under https://doi.org/10.1002/admi.202201375.

DOI: 10.1002/admi.202201375

N. Kumar, R. Gusain, S. S. Ray
Centre for Nanostructures and Advanced Materials
DSI-CSIR Nanotechnology Innovation Centre
Council for Scientific and Industrial Research
Pretoria 0001, South Africa

S. Pandey
Department of Chemistry
College of Natural Science
Yeungnam University
280 Daehak-Ro, Gyeongsan, Gyeongbuk 38541, Republic of Korea

S. Pandey
Particulate Matter Research Center
Research Institute of Industrial Science & Technology (RIST)
187-12, Geumho-ro, Gwangyang-si, Jeollanam-do 57801, Republic of Korea

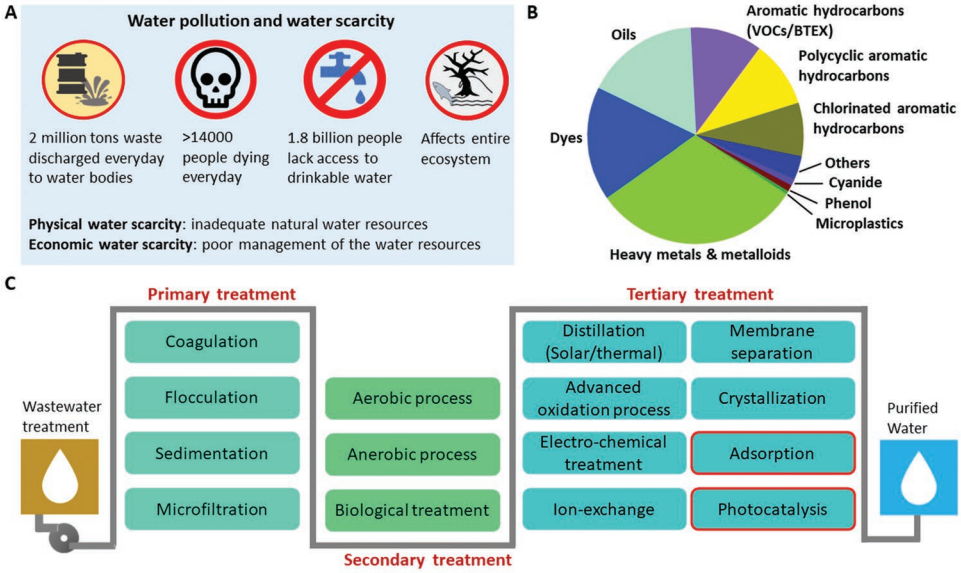

Figure 1. Summary of water pollution and available treatment technologies. A) Worldwide water pollution and water scarcity (Global Water Intelligence Report, 2014). B) Various types of water pollutants. C) Primary, secondary, and tertiary water treatment practices to eliminate inorganic, organic, and biological contaminants from wastewater.

and simple operation without requiring complex infrastructure.[15–17] **Figure 1** summarizes the global consequences of water pollution and scarcity, various water pollutants, and developed water purification technologies used at different treatment stages.

Although several nanomaterials-based adsorbents and photocatalysts have been developed recently, searching for ideal materials for water-treatment applications is still ongoing. The development of new sustainable materials with high performance and low cost is greatly desired to advance photocatalytic- and adsorption-based technologies toward practical operation. In particular, hydrogel-based materials have shown great potential for effective water treatment.

Hydrogels are macromolecular hydrophilic polymeric gels with cross-linked 3D structures that can easily entrap water molecules in their pores or interstitial spaces to swell up while remaining insoluble.[18] Hydrogels exhibit high structural flexibility, chemical stability, elasticity, and permeability, enhancing their water absorption capability.[19] Hydrogels consist of several hydrophilic groups, such as carboxylic (−COOH), amide ($-CONH_2$), amino groups ($-NH_2$), sulfonic acid ($-SO_3H$) and hydroxyl (−OH), which provide ample active space to accommodate foreign materials that are adsorbed on the surface of hydrogels.[20] Several natural polysaccharide polymers, such as chitin, gum, cellulose, alginate, starch, and proteins, have been used to prepare various hydrogels, which elevates their popularity due to the availability of renewably-sourced precursors.[21] In the last two decades, natural hydrogels, or a combination of natural and synthetic monomeric hydrogels have increasingly replaced synthetic hydrogels. The cross-linked structure of the polymeric chains provides viscoelastic or elastic behavior and mechanical properties.

Moreover, copolymerization using more than one type of monomer during hydrogel synthesis can effectively introduce more functional groups to improve desired characteristics for efficient pollutant removal.[22,23] In wastewater treatment, the biocompatibility, abundant surface functional groups, high surface-to-volume ratio, fast diffusion process, controllable pore structures, water holding capacity, permeability, and swelling and deswelling reversibility characteristics of hydrogels allow the adsorption of several inorganic and organic pollutants from wastewater with high adsorption capacities that rival that of conventional water adsorbents.[24–26] In addition, several hydrogels exhibit good recyclability for numerous successive cycles without reducing adsorption capacity, which promotes the economical and sustainable use of hydrogels in water treatment.[27]

The performance of hydrogels in water treatment can be enhanced by modulating their polymer networks with nanomaterials, resulting in hydrogel nanocomposites. The mechanical strength, swelling characteristics, and recovery/reusability of the hydrogels can be improved by impregnating hydrogels with organic/inorganic nanomaterials such as carbonaceous materials (viz., graphene and carbon nanotubes (CNTs)), metal chalcogenides, metal oxides/sulfides, magnetic materials, metals, nanoclays, layered double hydroxides (LDHs), MXenes, metal-organic frameworks (MOFs), and nanocellulose.[28–39] The addition of nanomaterials to hydrogels decreases the mesh size (open space in the networks) by extensive cross-linking of the polymer chains with nanomaterials, yielding a large number of interconnected pores and increased mass/charge transport, high surface areas, and enhanced polymer-water interactions to achieve high performing adsorbents and photocatalysts. In addition, nanomaterials and polymer networks enable synergistic surface functionality, making hydrogel nanocomposites excellent materials for water treatment. Furthermore, hydrogel nanocomposites are potent photocatalysts because their high porosity and specific surface area afford many available active sites for the adsorption of reactants.[40,41] In addition, it is often challenging to separate pristine nano-photocatalysts from the reaction medium following photocatalysis, leading to secondary contamination and poor reusability.[42] Hydrogels could be

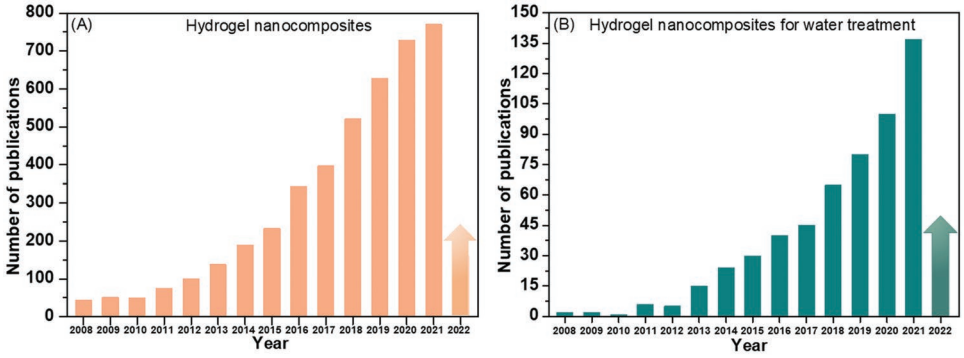

Figure 2. Histograms showing the number of publications based on the use of hydrogel nanocomposites in A) and B) water treatment applications (2008–2022). Data were obtained from a Web of Science search (30th April 2022).

used as attractive support materials for these photocatalysts to achieve efficient photocatalytic systems by providing adsorption sites, good environmental compatibility, and improved recycling characteristics.

A primary focus of this review is the latest developments in inorganic and organic hydrogel nanocomposites for water treatment. There is growing interest in developing hydrogel nanocomposites for water treatment and numerous other applications, as illustrated in **Figure 2**. Several reviews have been published on hydrogels and other 3D materials used in medical, environmental, energy, and other applications.[43–46] However, only a few reviews have been published specifically on the water treatment applications of hydrogels.[24,43,47–49] In addition, most recent reviews concerned only one type of hydrogel, for example, chitosan[44,50] or graphene-based hydrogels,[35] one class of pollutants, such as dyes[47] or heavy metals,[51–53] or one type of water treatment method, such as adsorption[23,49,54] or photocatalysis.[35] After considering the various applications of hydrogel nanocomposites for wastewater treatment via adsorption and photocatalysis, we have explored the limitations of parent hydrogels in water treatment. Except for graphene-based hydrogels or the removal of dyes, only a limited number of reviews focus on the use of hydrogel nanocomposites for photocatalytic applications or the removal of organic contaminants.

Moreover, none of the reviews are solely dedicated to hydrogel nanocomposites. Therefore, a summary of published applications of hydrogel nanocomposites to remove organic and inorganic water contaminants is warranted. This review provides a brief overview of the classification, synthesis, properties, and applications of hydrogels and hydrogel nanocomposites in the adsorptive and photocatalytic removal of aqueous organic and inorganic pollutants. The sustainable application of hydrogels in water treatment will face significant challenges related to recovery and reusability. The adsorption mechanism of hydrogels is also discussed. Finally, the remaining challenges are discussed and future directions of hydrogel nanocomposites for sustainable water treatment are proposed.

2. Hydrogels: Structure and Classification

Hydrogels are 3D network structures comprising chemically or physically cross-linked polymer chains with absorbed water molecules. Each hydrogel offers a characteristic mesh size (microscopic pores) depending on polymer concentration and cross-linking density. Various characteristics of hydrogels are summarized in **Figure 3**. Based on their formulation, hydrogels exhibit porous or nonporous structures. At the molecular level, mesh size and the molecular weight of the polymer chain between the crosslinks are the most critical features of polymer networks, which control the state and transport of water in the hydrogels.[55] The cross-linking of hydrogels can be achieved by physical (entanglement/H-bonding) and chemical (covalent bonding) crosslinks. The swelling properties of hydrogels are attributed to hydrophilic functional groups in polymer chains, such as $-COOH$, $-CONH_2$, $-NH_2$, $-SO_3H$, and $-OH$. Water molecules can be bound to functional groups of polymers via noncovalent interaction, including electrostatic interactions and hydrogen bonding (H-bonding).[56] Based on the water-polymer interaction, the imbibed water in hydrogels can be described as free, bound, and intermediate water.[57] Bound water has strong interactions with polymer functionalities, while intermediate water has weak interactions with polymer functionalities and neighboring water molecules. In contrast, free water is equivalent to bulk water, indicating minimum interactions with polymer functionalities. The swelling of hydrogels depends on the cross-linking density and polymer concentration; for example, a high degree of cross-linking density decreases the swelling ratio, but it increases the brittleness of the hydrogel.

Moreover, the well-defined shape of hydrogels can be fabricated from miniaturized building blocks via spontaneous assembly. The miniaturized building blocks of microgels with intrinsic morphological configurations self-assemble to produce bulk forms under the synergic influence of surface tension, external energy, and gel dimensions at liquid-liquid interfaces.[58] To stabilize the bulk structure of hydrogels, microgels may undergo further cross-linking. Various shapes and sizes of hydrogels can be fabricated, such as spheres, sheets, rods, cubes, films, and hollow tubes, by passing fluidic gel (low viscosity) into a template of the desired shape.[59] Various well-defined forms of the hydrogel are shown in **Figure 4**. Hydrogels with irregular surfaces (e.g., a surface with rods or pillars) can be fabricated using templates with specific hollows or cavities. Various shapes of hydrogels have also been obtained using 3D printing (including nozzle-based and

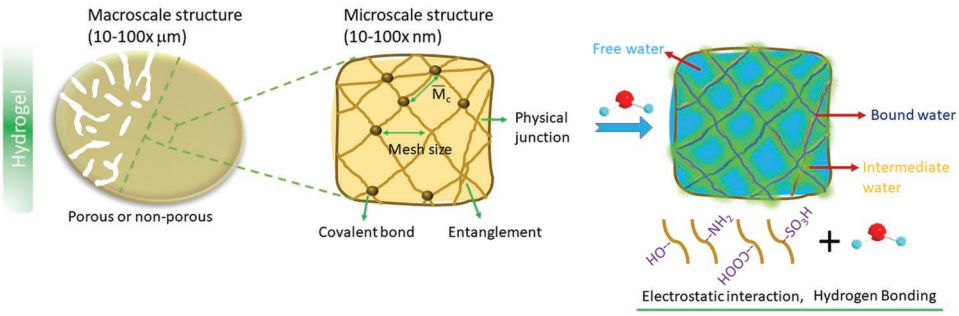

Figure 3. Structural characteristics of a hydrogel and its interaction with water molecules. Noncovalent interactions between functional groups of polymer chains and water molecules are responsible for the swelling attributes of the hydrogel.

stereolithography) and 4D bioprinting.[60,61] These printing methods produce hydrogels with defined architectures, multiplexed materials, and high spatial resolution. Hydrogel beads can be fabricated using metallic cross-linking (e.g., with $CaCl_2$) during synthesis.[62–64] Furthermore, hydrophobic hydrogels can also be prepared by introducing a stabilizing layer of hydrophobic substances on the surface of regular hydrogel, making them floatable on aqueous media.[65]

Hydrogels can be categorized in many ways based on the physical, biological, or chemical response, mode of preparation, physical state, origin, nature of swelling, ionic charge, size, nature of cross-linking, and rate of biodegradation.[68] **Figure 5** shows a general overview of the classification of hydrogels. Based on their composition or the preparation method, hydrogels can be divided into four types, namely homopolymer (consisting of a single monomer), copolymer (comprising

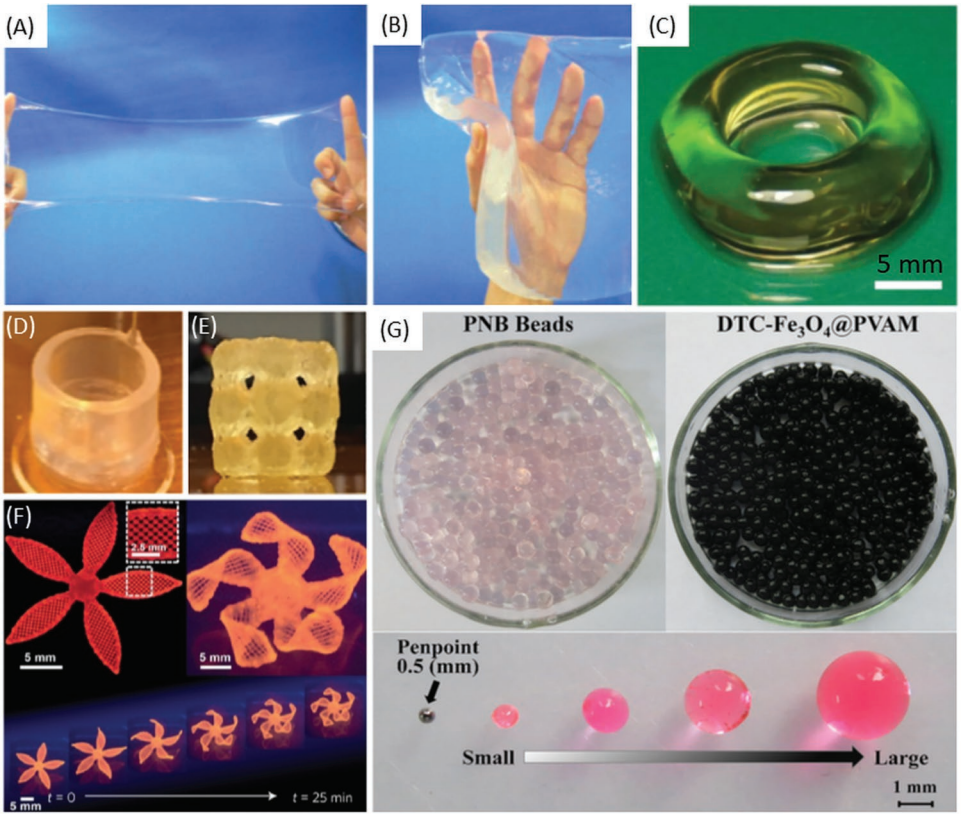

Figure 4. Various shapes of hydrogel: A) thin film (200 μm thick), B) sheet (30 mm thick). Reproduced with permission.[59] Copyright 2011, Springer Nature; C) Donut with a smooth surface 3D printed in highly deformable gelatin methacrylate hydrogel. Reproduced with permission.[66] Copyright 2019, American Association for the Advancement of Science. D) 3D printed cup and E) solid cube of chitosan and diacrylated Pluronic F-127 derived hydrogel. Reproduced with permission.[67] Copyright 2019, Wiley. F) Complex flower morphology constructed by biomimetic 4D printing, with time-lapse changes of the flowers during the swelling process (bottom panel). Reproduced with permission.[60] Copyright 2016, Springer Nature. G) Photographs of carmine-colored poly[(N-vinylformamide)-co-(butylenebis-N-vinylacetamide)] (PNB) precursor hydrogel beads and target dithiocarbamate-decorated poly(vinyl amine) hydrogel beads (DTC-Fe_3O_4@PVAM) beads. Reproduced with permission.[64] Copyright 2018, Springer Nature.

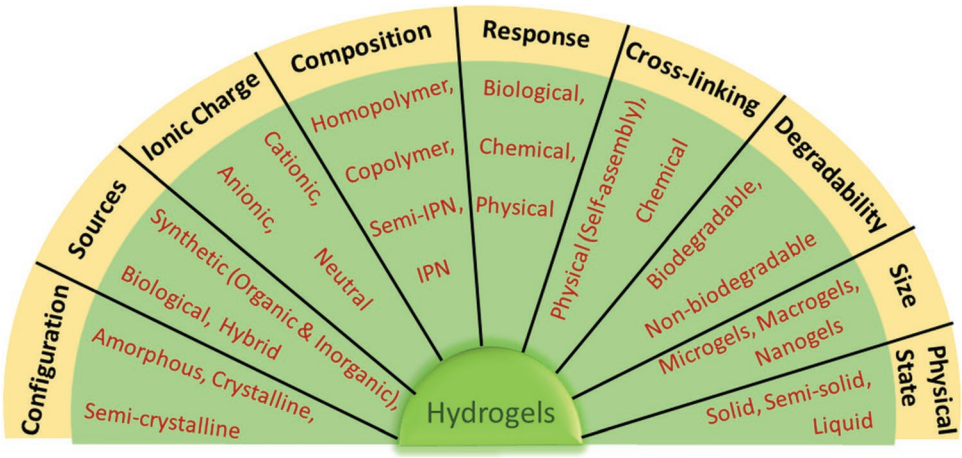

Figure 5. General classification of hydrogels.

two types of monomers), semi-interpenetrating (semi-IPN) network, and IPN network. Homopolymers and copolymers yield single hydrogel networks. Multiple functional groups can be achieved for a copolymer by selecting two distinct monomers, such as conductive and nonconductive or hydrophilic and hydrophobic monomers. A semi-IPN network is formed when one component with a linear structure penetrates the cross-linked network of another. It is a simple way to functionalize cross-linked polymers and improve their properties. In IPN networks, one polymer is a pre-crosslinked hydrogel that is immersed in a solution of an initiator and the monomers of the second polymer. The two polymer networks are interconnected, forming an IPN structure that is a relatively dense and compact matrix with enhanced mechanical properties.[69]

In terms of sources, hydrogels are divided into natural (biological), synthetic, and semi-synthetic (hybrid) hydrogels. Natural hydrogels are derived from natural resources, such as insects (e.g., chitosan and chitin), plants (e.g., alginate, cellulose, agarose, and gums), and mammalian extracellular matrix (e.g., fibrin, collagen, and hyaluronate).[70] These natural polymers are either protein or polysaccharides with comparatively weak mechanical strength. Various strategies have been developed to improve the mechanical and desired properties, such as combining natural hydrogels with synthetic hydrogels to produce hybrid or double-network hydrogels and introducing dual chemical and physical cross-linking in a single network. Synthetic hydrogels can be inorganic or organic. Inorganic hydrogels can be further divided into metal- and non-metal-based. Cyanogels are examples of metal-based hydrogels that are prepared by ligand-substitution reactions between the main polymer backbone or noble-metal chloride/chlorometallates (Sn, In, Sb, Pd, Pt, and Rh) and transition-metal cyanometallates (Fe, Co, and Ni).[71] The interconnected porous structure with heterometallic elements enables effective mass and charge transport for energy storage and conversion applications. Moreover, hygroscopic hydrogels are prepared using nonstoichiometric amorphous Zn or ZnO compounds, which offer unusual swelling and electrical and electrochemical properties.[72] Non-metal-based hydrogels are primarily composed of carbon materials, including CNTs, graphene, graphene oxide (GO), and reduced graphene oxide (rGO).

Synthetic organic hydrogels are derived from synthetic polymers such as poly(vinyl alcohol) (PVA), poly(2-hydroxyethyl methacrylate), poly(ethylene oxide) (PEO), and poly(ethylene glycol) (PEG) (M_w < 100k). Due to high solubility in water and organic solvents, PEO and PEG are ideal materials to produce hydrogels for potential energy storage and water purification applications. PVA is also commonly used to create stable and elastic synthetic hydrogels using freezing/thawing and cross-linking of aldehydes (e.g., glutaraldehyde and formaldehyde). Synthetic organic hydrogels can also be prepared using synthetic conductive polymers. The electrical properties of conductive polymers are ascribed to delocalized π electrons in their backbones. Common examples of conductive synthetic polymers that have been used to form hydrogels are polythiophene (PTh), poly(3,4-ethylenedioxythphene), polyaniline (PANI), polyacetylene (PAc), and polypyrrole (PPy).[73–75]

Furthermore, ionic hydrogels are divided into cationic, anionic, and neutral hydrogels. They are prepared using polymer chains that have chemically bonded ions in their chains in the form of a pendant or enchained. Hydrogels with both cationic and anionic ions are called ampholytic hydrogels. Ionic polymers are labeled polyelectrolytes when they carry counter-ions to neutralize bound ions. Polyionic hydrogels can be weak or strong based on their degree of ionization. For example, the quaternary NR_3^+ cation (R = organic group) is stronger than the amine (NH_3^+) cation, and the carboxylate ($RCOO^-$) anion is weaker than the sulfonate (RSO_3^-) anion.

The physical-state category of hydrogels is subdivided based on phase characteristics into solid, semi-solid, and liquid hydrogels. Biodegradable and non-biodegradable hydrogels are divided based on the rate of degradability. Macrogels, microgels, and nanogels are three classes of hydrogels based on the size of the hydrogels.[18] Based on their configuration, hydrogels can be classified as amorphous, crystalline, and semi-crystalline. However, the most popular classification of hydrogels is based on the cross-linking behavior of polymers: a) physically cross-linked (self-assembly) hydrogels and b) chemically cross-linked hydrogels.[76] Cross-linking approaches will be considered in more detail in the next section.

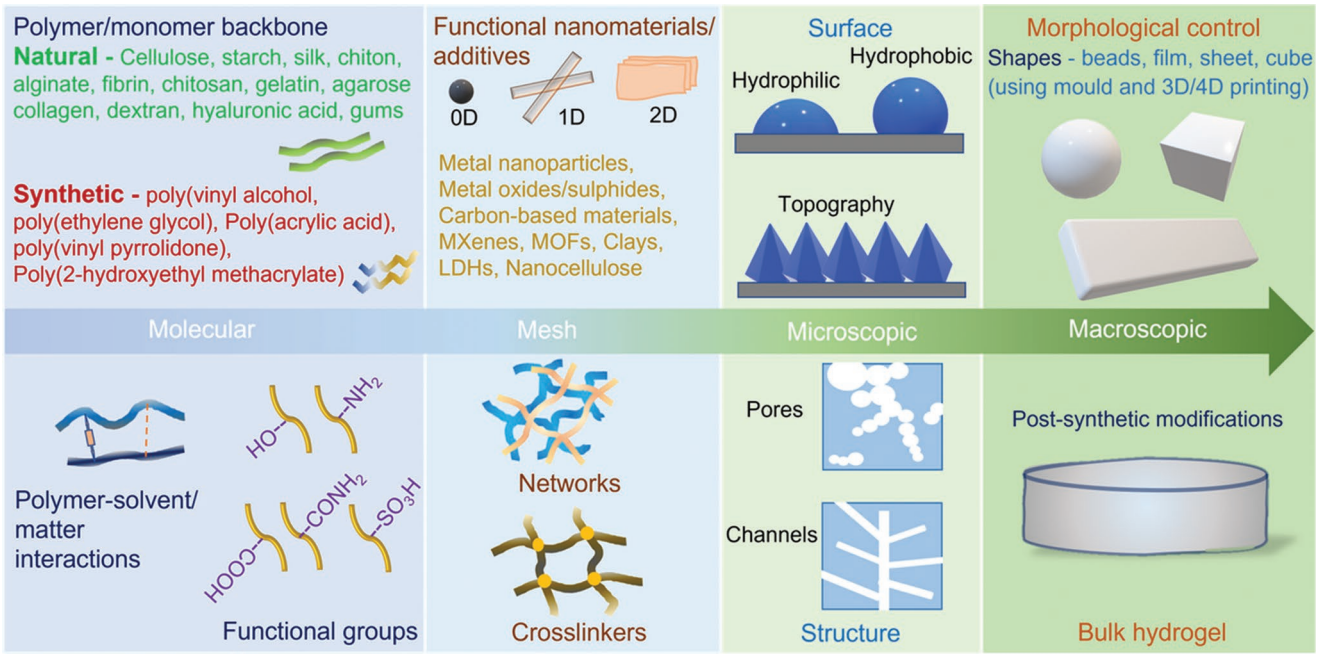

Figure 6. Tunability of hydrogel nanocomposites from the molecular to the macroscopic scale for the rational design of hydrogel materials for water treatment.

Hydrogel materials can be tailored at multiple scale levels to achieve various physicochemical properties by tuning polymer functional groups/monomers, cross-linking density, functional additives, synthesis environment (e.g., pH, ionic strength, and temperature), and others. **Figure 6** shows the rational design of various hydrogel materials used for water treatment. At the molecular level, the hydrogel building element (monomer/polymer backbone) defines essential characteristics, such as wettability, conductivity, and viscoelasticity, based on the interactions between the polymer networks and water/solvent. The functionalities (e.g., $-COOH$, $-CONH_2$, $-OH$, $-NH_2$, and $-SO_3H$) on polymer chains determine the chemical interactions (e.g., electrostatic, hydrogen linkage, metal coordination, and chelating linkage) between polymer chains and surrounding matter (e.g., water, solvent, and nanomaterial additives). Additional functional groups can be introduced to gels using two or more distinct monomers or polymers (e.g., synthetic and natural).[77] The choice of solvent or aqueous medium (acidic, alkaline, neutral) during synthesis controls the gelation chemistry and is responsible for the unique properties and structures of the obtained hydrogels.[78] Moreover, water-polymer interactions affect the extent of swelling and bound water, which can be regulated at the molecular level via different factors.[79] By judiciously selecting functional/semiconducting nanomaterial additives and hydrophilic polymer networks, synergistic intrinsic attributes result in highly effective hydrogel nanocomposites for water treatment.

The cross-linkers, polymer networks, and functional additives determine the mesh size, degree of networks, and porosity of hydrogels. A hydrogel can comprise more than one network, forming a double or IPN network system. The mesh size of hydrogels depends on cross-linking density, backbone concentration, and cross-linking type. High-density cross-linkers and high backbone concentrations produce hydrogels with a dense network (i.e., small mesh size), resulting in nonporous or low-porosity structures. By selecting cross-linkers appropriately, mechanically tough[80] and self-healing hydrogels[81,82] can be rationally designed for various applications. Furthermore, the microscopic tuning results in distinct structural and surface properties. The freeze-casting approach is commonly used to introduce differently shaped pores and channels by changing the solvent, temperature, and sequence of events. Aligned pore walls can be obtained when the hydrogel undergoes directional freezing and thawing in a salt mixture.

In contrast, non-directional freezing produces hydrogels with a nanofibril network.[83] Hydrogels with a larger surface area and a porous structure can be formed by employing supercritical drying. The surface properties of hydrogels can be tailored by grafting functional moieties during post-treatment or during the gelation step via a templating process.[84] Additionally, surface modifications/topographies can add various properties that a polymer network does not carry, such as antifouling,[85] anti-dehydration,[86] hydrophobicity,[65,87] and antireflection.[88] The morphological versatility of hydrogels further confers extra features to their practical applicability. Different shapes (such as beads, film, sheets, cubes, and hollow structures) can be fabricated using a molding method or 3D/4D printing. Owing to their tunability across multiple scales, ranging from adaptable synthesis to numerous post-synthetic modifications, multi-functional hydrogels can be produced to fulfill most of the requirements for effective adsorptive/photocatalytic removal of toxic pollutants from water.

3. Synthetic Approaches

3D hydrogel polymeric networks can be prepared using synthetic polymers (such as PEO, poly(acrylic acid) (PAA),

polypeptides, poly(vinyl pyrrolidone) (PVP), PVA, and their derivatives/copolymers), natural polymers (including starch, gelatin (Gel), collagen, agarose, alginate, and gums), or combination of both as starting materials. They differ in their properties due to different chemical structures, cross-linking, swelling tendency, and preparation techniques. Innovative materials can be achieved by a change in chemical composition or a slight change in one of the synthesis parameters, such as cross-linking agent, cross-linking method, reaction conditions, and preparation time. Various synthesis approaches for the preparation of hydrogels and their nanocomposites are discussed in this section.

3.1. Synthesis of Hydrogels

Any method that is suitable for the production of cross-linked polymers can be utilized to synthesize a hydrogel. Chemical and physical cross-linking, free-radical polymerization, free-radical or graft copolymerization, and irradiation cross-linking of polymers are commonly used methods for preparing hydrogel by mixing hydrophilic polymers with various functional group-carrying cross-linkers.[34,68,89–91] The primary constituents of hydrogel synthesis are the monomer, initiator, cross-linker, and solvent. For example, a biopolymer-based hydrogel has been prepared by free-radical graft copolymerization using acrylamide (AAm) and acrylic acid (AA) as monomers, N,N′-methylenebis (acrylamide) (MBA) as cross-linker, and the ascorbic acid/potassium persulfate redox pair as initiator.[33] The amount of water and the process of binding the polymer backbone in the gel network played crucial roles in synthesizing the hydrogel. The swelling characteristics or water absorption capacity of a hydrogel depend on the type of monomer used and the density of the backbone polymer.[92] The following sub-section provides a brief outline of physical and chemical cross-linking polymerization for the preparation of hydrogels.

3.1.1. Chemical Cross-Linking

Permanent covalent cross-linking between the monomeric units yields chemically cross-linked hydrogels that are stable against degradation. The excellent mechanical characteristics of chemically cross-linked hydrogels make them viable candidates for applications in industries such as pharmaceuticals, food, agriculture, and cosmetics. Chemical cross-linking polymerization approaches for synthesizing hydrogels can be described as follows.

Chain-growth polymerization involves free-radical polymerization, which proceeds in initiation, propagation, and termination steps. Hydrogels prepared by these methods generally use hydrophilic monomers with unsaturated bonds.[93] Initiation reactions in chain-growth polymerization can be achieved by using different kinds of initiators, such as various chemicals, electron beams, heat, light (photo-initiator), and γ radiation.[94] Hydrogels obtained by chain-growth polymerization have diverse network structural properties. This method is versatile and can be employed in suspension, solution, or grafting to support the synthesis of hydrogels of various structures.

In solution polymerization, the reaction starts with a high monomer concentration and minimum initiator, solvent, and catalyst concentrations. Then, the solvent is added to control the viscosity, and the concentrations of the catalyst and/or initiator are adjusted to control the reaction rate. In this method, the initiator, monomer, and formed polymer are soluble in the solvent or solvent mixture. The added solvent acts as a heat sink, which is the primary benefit of solution polymerization over bulk polymerization. Solution polymerization is broadly used for hydrogel preparation owing to its excellent polymerization rate and safe handling and can be performed under ambient conditions.[95]

Suspension polymerization or inverse-suspension polymerization requires both hydrophilic and lipophilic suspending agents and constant agitation. In this method, the initiator and monomers are dispersed as a uniform mixture in an organic phase. This means that the reaction mixture is suspended as tiny droplets in a continuous aqueous phase, and each droplet behaves as a miniature bulk reactor. The suspension gelation method yields hydrogel powders or microspheres (beads).[96] In addition, this process produces macroporous polymeric hydrogels.[97]

The photo-polymerization process facilitates the in situ preparation of cross-linked hydrogel networks. In this approach, free-radical polymerization is carried out by an initiator and broad-spectrum light irradiation spanning ultraviolet (UV) and visible to infrared wavelengths.[98] For example, Reeves et al.[99] prepared stable cross-linked carboxymethyl cellulose (CMC) hydrogel by employing a photo-initiator, viz., UV radiation.

Grafting is an essential technique to enhance the mechanical properties of hydrogel networks. This method involves attaching the hydrogel to more robust support. A typical reaction involves the formation of free-radicals on the more stable support. The monomers are then polymerized directly onto the support, resulting in a covalently attached hydrogel. Various polymeric supports have been used to prepare hydrogel via the grafting method.[100–102]

Irradiation polymerization involves using energy-intensive radiations such as gamma rays and electron beams as initiators to polymerize unsaturated substances for hydrogel synthesis.[103,104] Hydrophilic polymers can be easily converted into hydrogels using different kinds of irradiation. During irradiation of the polymeric solution, numerous active sites are produced on the polymer chains, which results in extensive cross-linking.[105] Irradiation polymerization produces residue-free, sterile, and highly pure hydrogels. Swelling factors (viz., pore size and cross-linking) of hydrogels can be readily regulated using this method by changing the radiation exposure.[106,107] Compared to chemical cross-linking, this method requires no additional catalysts or chemicals to modify the materials.[108]

Step-growth polymerization occurs via the reaction of distinct functional groups of the monomer molecules to form new covalent bonds.[109,110] This method is governed by a single reaction mechanism. The hydrogels prepared by this approach are homogeneous because they are synthesized by mixing at least two monomers with equally reactive functional moieties. The presence of reactive groups in each monomer acts as cross-linking points. For example, Lin et al.[111] used step-growth polymerization to produce chemically cross-linked hydrogels

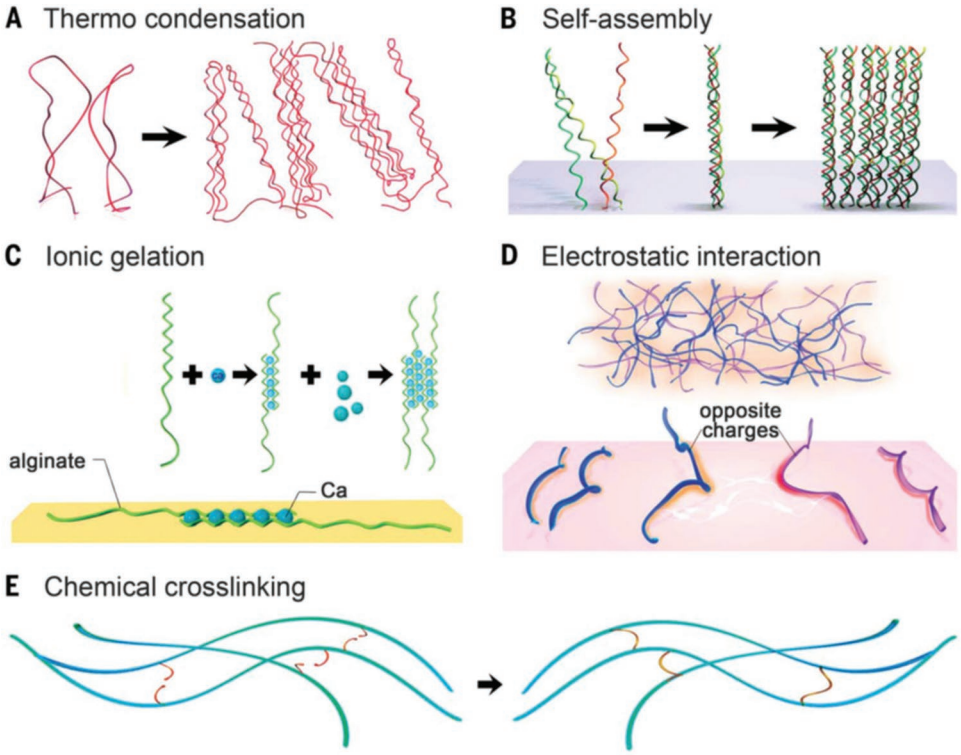

Figure 7. Schematic presentations of the preparation methods of hydrogels. Different cross-linking of hydrogels: A–D) Physical cross-linking and E) chemical cross-linking. Reproduced with permission.[56] Copyright 2016, American Association for the Advancement of Science.

using a four-arm PEG norbornene monomer and dithiol-containing cross-linkers. **Figure 7**A–E shows commonly used synthesis routes of the hydrogel.

3.1.2. Physical Cross-Linking

The spontaneous self-organization of monomers allows physical cross-linking via intermolecular interactions, resulting in self-assembled hydrogels.[112,113] In physical cross-linking polymerization, the interactions between the monomers can be interrupted by controlling environmental conditions, including ionic strength, temperature, presence of solutes, temperature, and stress, resulting in the reversible nature of the physically cross-linked hydrogels.[112] Physically cross-linked hydrogels exhibit entangled polymeric chains due to H-bonding, crystallite formation, or hydrophobic interactions that are not permanent. The application of physically cross-linked hydrogels has received much attention owing to the advantages of not requiring harmful cross-linking agents and the ease of preparation. Traditional hydrogel synthesis is complex due to the inability to control chain lengths, sequence types, and 3D arrangements and the need to check for side reactions. Generally, physically cross-linked hydrogels are prepared using multiblock or graft copolymers.[68] Polysaccharides are typical examples of graft copolymers that exhibit water-soluble polymer backbones attached to hydrophobic units. Reported physical cross-linking hydrogel synthesis methods include self-assembly, H-bonding/freeze-thawing, ionic gelation, electrostatic interaction, hydrophobic interactions, stereo-complex formation, thermal condensation, photo-induced gelation, and protein interactions cross-linking.[56,76,114] Due to their reversible nature, these interactions can be interrupted by varying physical conditions or stress.[115] **Figure 8** summarizes the various preparation methods of hydrogels and hydrogel nanocomposites.

3.2. Synthesis of Hydrogel Nanocomposites

Hydrogel nanocomposites have been prepared through the addition of a broad range of nanomaterials, such as metallic NPs, metal oxide/sulfide NPs, polymeric NPs, carbonaceous nanomaterials, and other 2D nanomaterials.[34,116–120] The combination of hydrogel and nanomaterials produces nanocomposite with multi-functional characteristics, which provide hydrogel with better swelling characteristics, mechanical stability, and hydrophilicity for water treatment and several other applications. Five approaches can be employed to integrate the nanomaterials into hydrogels to yield hydrogel nanocomposites (Figure 8): i) formation of hydrogel in NPs suspension, ii) physically mixing of the NPs into hydrogel matrix after gelation, iii) In situ synthesis of NPs within the hydrogel, iv) using NPs as a cross-linkers to form a hydrogel, and v) nanocomposite formation using NPs, distinct gelators, and polymers. For example, Sershen et al.[121] used the first approach to prepare AuNPs- containing hydrogel nanocomposite by mixing AuNPs suspension into a solution of N-isopropylacrylamide (NIPAm)/AAm (monomer), followed by the addition of ammonium persulfate (initiator) and tetramethylethylenediamine (accelerator). However, the formation of hydrogel in NPs

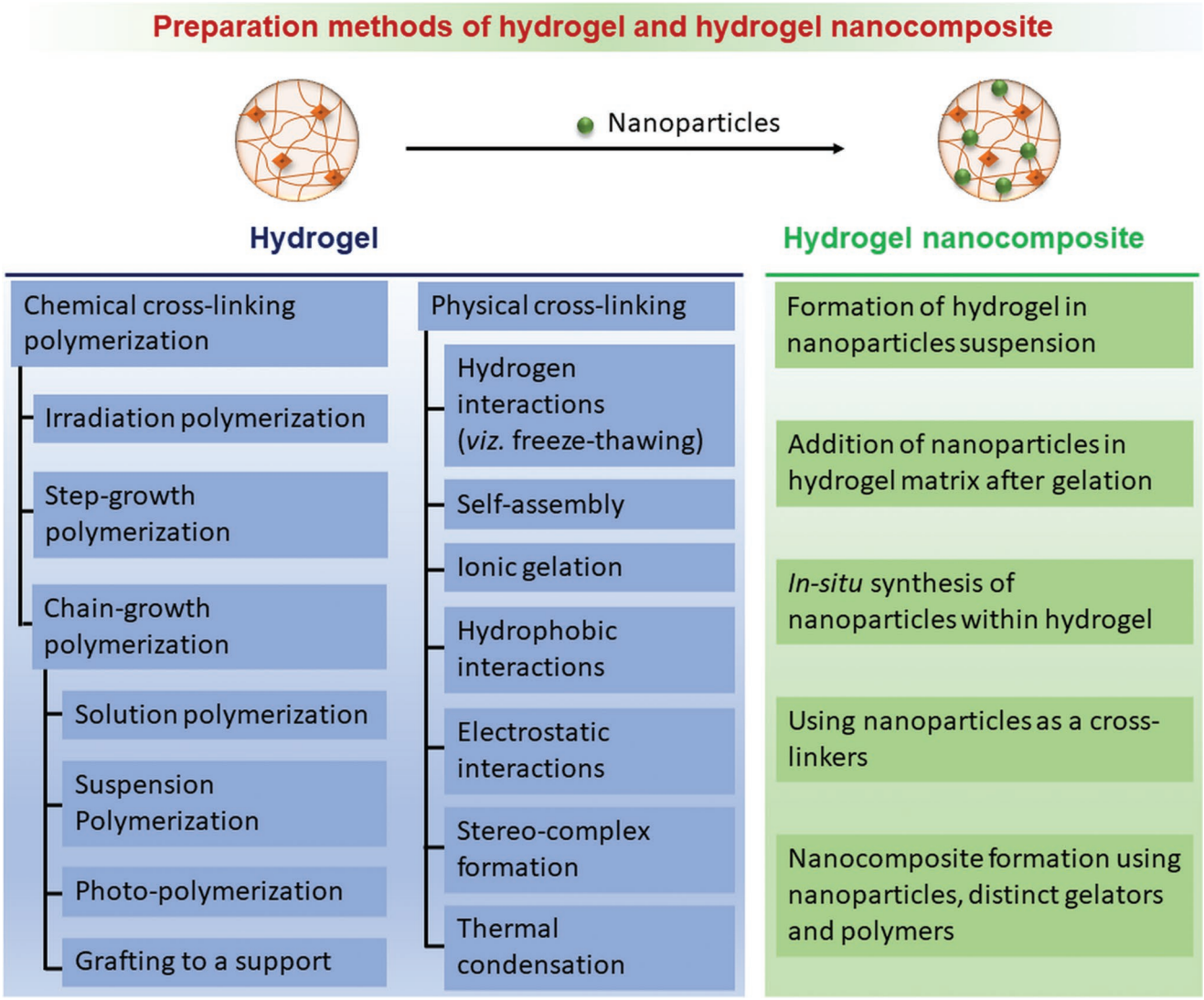

Figure 8. Summary of the various preparation methods of hydrogels and hydrogel nanocomposites.

suspension has a few drawbacks, such as the leaching of NPs from the hydrogel matrix when the cross-linking density is low. A second approach was later introduced to prepare a hydrogel by incorporating Au NPs into a polyacrylamide (PAAm) gel after electro-polymerization.[122] This approach involves the separate synthesis of the NPs and hydrogel, and then physically combining the two components. To further simplify the synthesis route of hydrogel nanocomposites, Langer et al.[123] demonstrated a third approach, which entails the addition of NP precursors into a hydrogel to prepare hydrogel nanocomposite in situ, rather than synthesizing NPs separately. The hydrogel nanocomposite prepared using this method exhibit uniformly distributed NPs. Functional groups in the polymer branch, for example, catechol side-chain in NIPAm, help to reduce the Au precursor to AuNPs to prepare NIPAm/Au hybrid hydrogels.[124] The fourth approach uses functional groups of NPs as cross-linker or initiators to develop hydrogel nanocomposites. For example, Prestwich et al.[125] utilized the thiophilicity and multivalent nature of Au NPs to cross-link thiolated hyaluronic acid into extrudable, printable, and biocompatible hydrogels. In another study, in situ copolymerization of 2-acrylamido-2-methylpropane sulfonic acid (AMPS) and AA was carried out using Al_2O_3 NPs as the cross-linker to form the stretchable and self-healing poly(AA-co-AMPS)/Al_2O_3 hydrogel nanocomposite.[126] In the fifth approach, a hydrogel nanocomposite is prepared using NPs, distinct gelator molecules, and polymers. For example, Wu et al.[127] used in situ polymerization to produce a hydrogel framework consisting of SiO_2 NPs coated with the conducting polymer PANI for applications as anodes. They performed solution-phase synthesis by mixing aniline, Si NPs, and phytic acid (used as gelator) in water, followed by the addition of ammonium persulfate (used as oxidizer).

3.2.1. Synthesis of Hydrogel Nanocomposite Beads

Numerous synthesis strategies have been developed to prepare hydrogel nanocomposite beads using various cross-linkers,

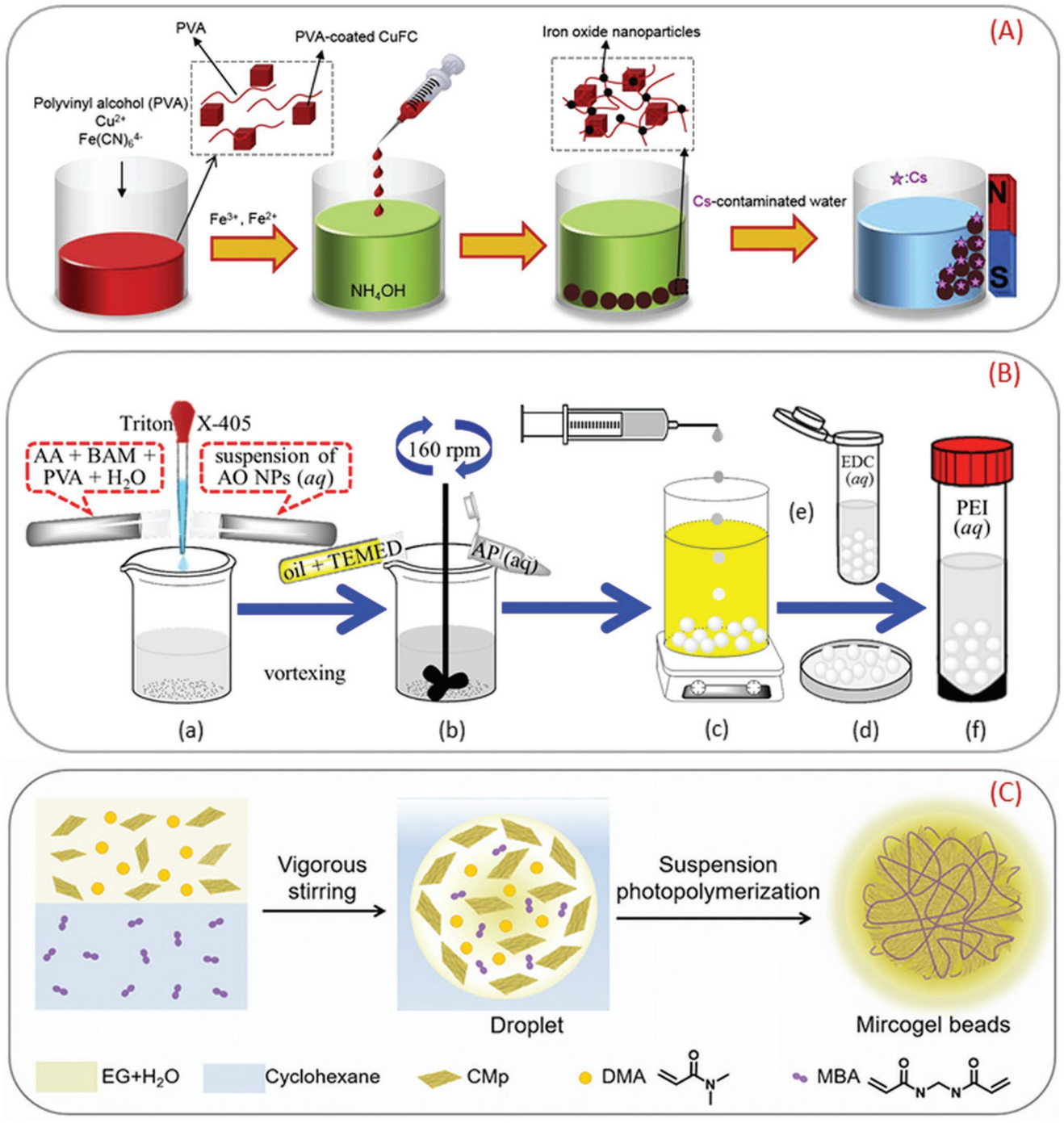

Figure 9. Synthesis of hydrogel nanocomposite beads. A) Preparation steps of the PVA-coated copper ferrocyanide-embedded magnetic hydrogel beads (PVA-CuFC-MHBs) for removal Cs from water. Reproduced with permission.[134] Copyright 2019, Elsevier Science Ltd. B) Schematic shows the preparation of PAA–AO–PEI nanocomposite beads a) synthesis of the aqueous phase, b) O/W emulsification and initiation of polymerization, c) beads formation via O/W/O sedimentation polymerization, d) purified PAA-AO nanocomposite beads, e) soaking of beads in EDC solution, and f) PAA-AO-PEI nanocomposite beads. Reproduced with permission.[138] Copyright 2021, American Chemical Society. C) Synthetic process for PDMA/g-C_3N_4 microgel beads via inverse suspension photopolymerization. Reproduced with permission.[139] Copyright 2020, American Chemical Society. CMp, phenol-modified g-C_3N_4; PDMA,poly (N,N′-Dimethylacrylamide); N-(3-(dimethylamino)propyl)-N′-ethylcarbodiimide hydrochloride, EDC.

polymer systems, and nanostructured materials for effective water treatment.[118,128–133] A summary of various methods that have been used for the synthesis of hydrogel nanocomposite beads is shown in **Figure 9**. Commonly used cross-linkers for hydrogel beads are NaOH,[129,130] NH_4OH,[134] $CaCl_2$,[62,135] $MgCO_3$,[136] $FeCl_3$,[137] $CuSO_4$,[135] and $ZnCl_2$.[62] For example, Lee et al.[134] demonstrated the preparation of PVA-coated copper ferrocyanide-embedded magnetic hydrogel beads

(PVA-CuFC-MHBs) for the removal of Cs from water. The synthesis processes are depicted in Figure 9A. Firstly, $CuSO_4$ $5H_2O$ and $K_4Fe(CN)_6$ $3H_2O$ were added to a PVA solution to produce PVA-CuFC. The cross-linkers $FeCl_2$ $4H_2O$ and $FeCl_3$ were then added to the PVA-CuFC mixture to cross-linking the polymer chains. Finally, the reaction mixture was added dropwise to an NH_4OH solution (pH = 11.2) to yield PVA-CuFC-MHBs. In another study, hierarchically porous poly(acrylic acid)-alumina (Al_2O_3) nanocomposite (PAA-AO nanocomposite) beads were fabricated by solidifying droplets of emulsions co-stabilized using a surfactant (Triton X-405), co-surfactant (PVA), and Al_2O_3 NPs, as described in Figure 9B.[138] To improve the mechanical properties and surface positive charge, the PAA-AO nanocomposite beads were further modified by hyperbranched polyethylenimine (PEI) via initial treatment with N-(3-(dimethylamino) propyl)-N′-ethylcarbodiimide hydrochloride to produce PAA-AO-PEI nanocomposite beads. Phenol-modified g-C_3N_4 has also been investigated[139] as a water-dispersible photo-initiator for the synthesis of poly (N,N′-Dimethylacrylamide)/g-C_3N_4 microgel beads using MBA as cross-linker and cyclohexane as a continuous oil phase (Figure 9C). Furthermore, Bandara et al.[129] reported a simple approach to synthesizing chitosan-polyethylenimine-graphene oxide (CS-PEI-GO) hydrogel beads to effectively remove Se from polluted water. A homogenized CS-PEI-GO solution was added dropwise to a 1.5 M NaOH solution using a 10 mL syringe with a 23G needle to produce CS-PEI-GO hydrogel beads.[130] In a similar approach, CS/AgCl/ZnO NC beads were prepared using a 0.5 NaOH solution for the photodegradation of methylene blue (MB) dye.[129]

3.2.2. Scalable Production of Hydrogel Nanocomposites

Large-scale hydrogel nanocomposites are necessary to attain their full potential in various industrial applications, including sprayable carriers, hydraulic or injection fluids, complex viscosity modifiers, tissue engineering scaffolds, wound healing, and water treatment. Recently, scalable routes to produce hydrogel nanocomposites at a large scale have been demonstrated.[140–143] **Figure 10** presents various scalable manufacturing processes of hydrogel nanocomposites. For example, Yu et al.[141] reported a scalable route for the preparation of biomimetic polymer NP-based hydrogels via the self-assembly (involving noncovalent interactions) between colloidal SiO_2 NPs and environment-friendly and renewable polysaccharides hydroxyethyl cellulose (HEC) and methylcellulose (MC). The developed method could be easily scaled up linearly from 0.5 mL to over 15 L without compromising the mechanical characteristics of the hydrogel (Figure 10A). Another study developed a scalable method to produce micrometer-sized core-shell microgels (CSMG) as a solid powder.[141] Hydrophobic SiO_2 NPs and an aqueous solution of gel precursors (AAm (monomer), potassium persulfate/$NaHSO_3$ (initiator), and MBA (crosslinker)) were mixed in a domestic mixer at 22 000 rpm for 90 s to yield a dry water system, which was heated at 38 °C for 4 h under nitrogen to produce the CSMG. Compared to solution-phase polymerization methods, the solid microgel could be easily obtained with a high yield (96%) and without any purification steps. This scalable dry water method produced a microgel with core-shell morphology comprising hydrophilic cores (hydrogel) and porous hydrophobic shells (SiO_2 NPs), enabling the ability to absorb both oil and water. Furthermore, Rutgeerts et al.[144] used a solvent-free ball-milling approach to produce supramolecular hydrogels using bis-urea derivatives.

Recently, 3D printing (also known as additive manufacturing) has emerged as a continuous industrial technique to produce prototypes, find design variations to improve yield, and verify the scalability of a process. Using this technology, 3D objects can be rapidly fabricated via a layer-by-layer deposition. 3D printed hydrogels have been manufactured and employed in numerous applications, such as electronics, food production, and tissue engineering,[145–147] and have recently garnered much attention for fast and effective water treatment.[67,145,148–151] For example, a highly stretchable in situ synthesized MOF-hydrogel nanocomposite was 3D printed using a combination of prepolymers of a double network hydrogel (AAm and sodium alginate (SA)), a shear-thinning agent (HEC), ligands for the HKUST-1 MOF (trimesic acid (H_3BTC)), and a deprotonating agent (triethylamine), Figure 10B.[152] MBA and Irgacure 2959 were used as crosslinker and photo-initiator, respectively. UV-curing (365 nm UV LED) was applied to produce a primary polymer network of PAAm, which was immersed in a $Cu(NO_3)_2$ water/acetone solution (1:1 ratio) solution to produce a secondary polymer network of Cu^{2+}cross-linked SA. Concurrently, the copper ions were coordinated by the BTC ligands to in situ synthesize the MOF and, finally, form the HKUST-1 hydrogel nanocomposite. Different hydrogel structures (i.e., dumbbell, grid, and pyramid) have been designed using SolidWorks (Dassault Systèmes) for the efficient absorption of dye. For example, Baniasadi et al.[153] illustrated the use of direct ink writing (a 3D printing technique) for the preparation of bio-hydrogels that consist of aloe vera/TEMPO-oxidized cellulose nanofibril (TEMPO = (2,2,6,6-tetramethylpiperidin-1-yl)oxidanyl). In addition, electron-beam irradiation was used to cross-link alginate, nanoclay, and AA to prepare a nanocomposite ink-based suspension.[154] The suspension was introduced to an extrusion-based 3D printer to successfully fabricate a superabsorbent hydrogel for the removal of heavy metal ions from contaminated water.

4. Properties of Hydrogels-Based Materials

Hydrogels are cross-linked polymers with high elastic and swelling characteristics and are used in various applications, including water treatment. Combining hydrogels with other nanomaterials elevates the advantages of the components through synergetic effects while counteracting the disadvantages of each. The excellent swelling properties, mechanical strength, and ionic and electronic conduction of hydrogel-based nanomaterials have helped to advance several fields. The following sections thoroughly explain the inherent properties of hydrogel-based materials.

4.1. Swelling Characteristics

The swelling behavior of hydrogel-based materials is a very critical feature, which promotes their potential use in numerous

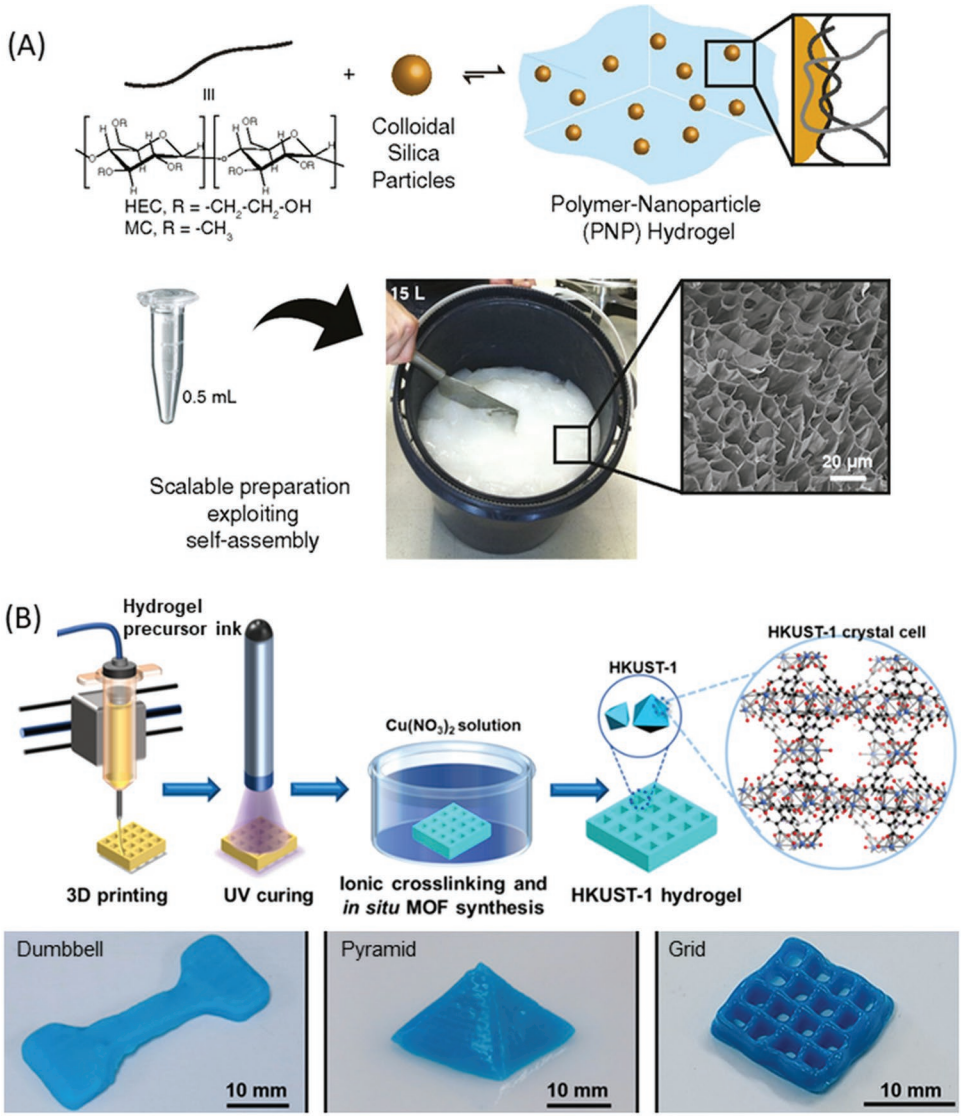

Figure 10. Scalable manufacturing of hydrogel nanocomposite. A) Polysaccharides (HEC and MC) on mixing with SiO_2 NPs yield robust PNP hydrogels. Reproduced with permission.[140] Copyright 2016, United States National Academy of Sciences. B) The graphic illustrates the three critical steps in the 3D printing process: printing, UV curing, and ionic cross-linking. Various shapes (dumbbell, pyramid, and grid) of 3D printed MOF-hydrogel could be obtained using a 0.8 mm diameter nozzle. Reproduced with permission.[152] Copyright 2020, American Chemical Society.

applications. The swelling properties of hydrogels are accredited to the presence of several hydrophilic functional groups, such as −OH, $-CONH_2$, −CONH−, and $-SO_3H$.[155] The weight ratio of a hydrogel in a swelled and deswelled state defines the swelling ratio and quantifies the swelling capacity of a hydrogel. Hydrogel-based materials with large swelling capacities are also called super-absorbents. They are widely used in environmental remediation applications,[156] while those with low swelling capacities are used in gas capture and catalysis.[157] Several factors affect the swelling ability of hydrogels, such as the skeleton structure, the chemical structure of repeating units, the quality and concentration of solvent, the cross-linking ratio, and the specific stimuli. The hydrophilic functional groups on the hydrogel skeleton significantly impact the swelling capacity of the hydrogel. For example, Xu et al.[158] have found that fabricating GO with a poly(acrylic acid-co-acrylamide) (P(AA-co-AM)) hydrogel enhances the swelling characteristics of the hydrogel.[158] The swelling capacity of the P(AA-co-AM) hydrogel improved from 757 to 1094 g/g after adding a low quantity (0.10 wt.%) of GO sheets. The noteworthy improvement of the swelling capacities of the GO/P(AA-co-AM) hydrogel nanocomposite was ascribed to the presence of functional groups, such as −OH, −C=O, −COOH, and −C−O−C−, on the GO surface.

The swelling characteristics of a hydrogel can be easily tuned by altering the pH or salt concentration of a solution. The ionization state of functional groups of the hydrogel is sensitive to the influence of pH and ionic strength of the solution and affects the swelling capacity. It has been found that the swelling capacity of the sodium alginate-g-poly(acrylic acid-co-acrylamide)/clinoptilolite hydrogel nanocomposite increases with an increase in pH from 2 to 10 but declines when pH > 10.[159] At

pH 10, the −COOH groups on the hydrogel nanocomposite are converted to $-COO^{-}$, and the hydrogel shows a high swelling capacity due to anion-anion repulsion. However, the −COOH groups are protonated at low pH, preventing efficient anion-anion electrostatic repulsion. Additionally, at pH > 10, the swelling ratio of hydrogel is reduced due to the presence of Na^{+} from NaOH, which shields the $-COO^{-}$ groups and prohibits anion-anion repulsion. Similarly, the ionic strength of the solution also exhibits an influence on the swelling characteristics of a hydrogel. With increasing NaCl concentration in the solution, cationic hydrogels show a significant decline in swelling capacity.[160] However, hydrogels with zwitter-ionic monomers usually show an increased swelling ratio with increasing NaCl concentration.[161,162]

The cross-linking of the polymer backbones in hydrogel also affects their swelling characteristics. Under appropriate reaction conditions (such as temperature and pressure), increased cross-linking density results in a denser network, negatively impacting swelling capacity. In addition, a high concentration of cross-linking agents also impedes swelling properties. The presence of cross-linkers with long spacers strongly reduces the swelling properties of hydrogels. As the cross-linker concentration increases, the mechanical stability and rigidity of the hydrogel network also increase, which has adverse effects on swelling.[163] Furthermore, the swelling characteristics of hydrogel nanocomposites increase with increasing temperature. However, some hydrogels may exhibit the separation of polymer chains at high temperatures, resulting in collapsing or shrinkage.[164]

Swelling and deswelling of hydrogels cause reversible volume changes and, thus, affect their mechanical properties, structure, and surface morphologies.[165] Hoshino et al.[166] performed experimental and theoretical investigations of the relationship between the swelling ratio and Young's modulus of tetra-PEG-based hydrogels. They found that Young's modulus of the hydrogel decreases with an increasing swelling ratio. Knowledge of the relationships between the moduli and swelling ratio of a hydrogel is valuable for designing hydrogel-based materials with strong mechanical strength and large swelling ratios for environmental remediation applications. Swelling and deswelling also induce structural changes in the hydrogels. By controlling the swelling process of a hydrogel material, various surface patterns can be obtained.[167] These surface patterns are stable in both dry and swollen states and enhance the potential of hydrogels for multiple applications.

4.2. Mechanical Properties

Hydrogels exhibit excellent elasticity, flexibility, and self-healing properties, making them suitable candidates for several applications, including biomedical engineering, energy storage, and environmental remediation. Self-healing properties enable the self-repairing of cracks that form in hydrogels during operation, which is desirable in wearable energy storage and conversion devices. Self-healing is a reversible process and promotes the lifetime and durability of devices composed of self-healing hydrogel materials. Self-healing is introduced to hydrogels through physical interactions, such as H-bonds, electrostatic interaction, metal coordination, or chemical bonds.[81] Covalent bonds, such as disulfide, imine, boronate ester, and acylhydrazone bonds, aid in the chemical self-healing of hydrogels. Wearable electronics require materials that can work under uninterrupted bending, stretching, and twisting conditions and must have high strength and elasticity. Unfortunately, several hydrogels demonstrate poor stretchability and elasticity despite good mechanical properties, which are unsuitable for practical applications. Therefore, hydrogels that exhibit exceptional elasticity and high compressive and tensile strength should be developed. The most common approach to designing such hydrogels is to employ double-network hydrogels and hydrogel nanocomposites.[168]

Hydrogel nanocomposites are a popular route to enhance the properties of hydrogels. Several nanomaterials, such as graphene-based materials, CNT, clay, silica, metals, and metal oxides, have been employed to strengthen the polymer matrix of hydrogels. Yin et al.[169] reported the graphene oxide/sodium alginate/polyacrylamide (GO/SA/PAAm) hydrogel nanocomposite with enhanced mechanical strength and demonstrated dye adsorption.[169] **Figure 11**A shows the effect of pressure on these hydrogels. Parts (a) to (c) of Figure 11A show that a PAAm-based hydrogel was damaged under pressure, whereas the GO/SA/PAAm (GSP) hydrogel nanocomposite delivers outstanding performance in ductility and was not damaged under pressure, as shown in parts (d) to (f) of Figure 11A. The GSP hydrogel nanocomposite quickly recovered its original shape after removing the pressure, which demonstrates the flexibility and elasticity of the hydrogel nanocomposite. The mechanical characteristics of a hydrogel can be measured using the following parameters: tensile modulus, storage, and loss modulus, compression modulus, fracture energy, and fracture stress and tension. Figure 11B,C shows the mechanical properties of the pure SA/PAAm and GSP hydrogels, revealing that the compressive and tensile strengths of the GSP hydrogel nanocomposite are significantly higher than those of the SA/PAAm hydrogel. The introduction of GO and SA to the hydrogel matrix provides strong interfacial interactions with PAAm polymer chains and, thus, enhanced the mechanical properties of the hydrogel.

4.3. Stimuli-Responsiveness

Stimuli-responsive hydrogels can undergo exceptional changes in response to external stimuli, such as pH, ionic strength, humidity, temperature, light, solvent, electric field, magnetic field, and pressure, as illustrated in **Figure 12**. Stimuli-responsive hydrogels are also called intelligent hydrogels and have garnered much attention in biomedical (such as drug delivery, tissue regeneration, and gene delivery), energy, and environmental applications.[170–172] The utility of several materials for various applications can be enhanced through the integration of stimuli-responsive hydrogels that can easily adjust their shape and size under external stimuli. External stimuli can be distinguished to be physical or chemical. Physical stimuli include magnetic and electric fields, mechanical forces, light, and pressure,[173] with the temperature being the most extensively investigated.[174] Stimuli-responsive hydrogels provide an alternative prospect to enhance the removal efficiency of

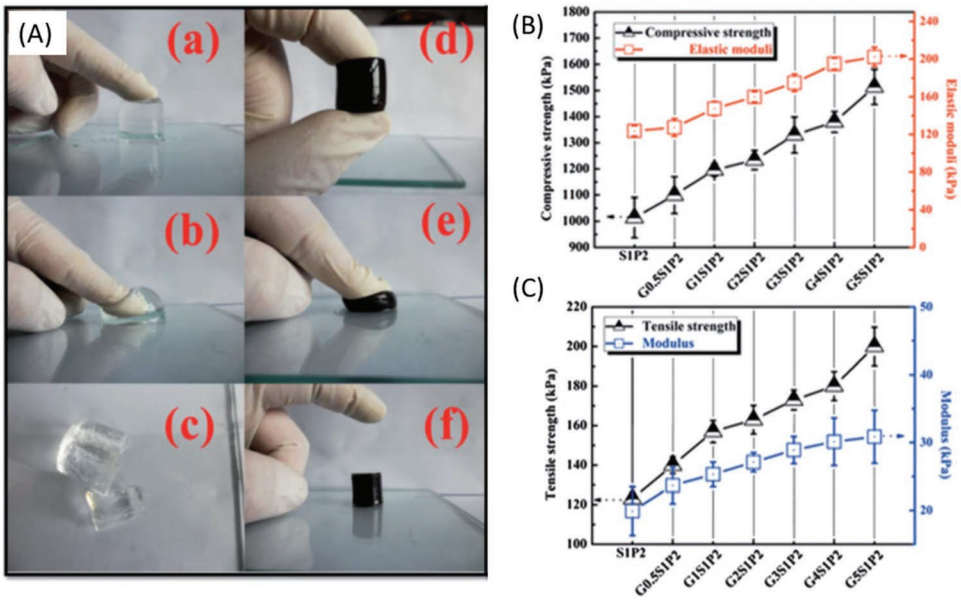

Figure 11. A) Photographs of a–c) PAm hydrogel and d–f) GSP hydrogel nanocomposite under pressure. B) Compressive strengths and elastic moduli of SP and GSP hydrogels. C) Tensile strengths and modulus of SP and GSP hydrogels. Reproduced with permission.[169] Copyright 2013, Royal Society of Chemistry.

wastewater contaminants: following the removal of contaminants through adsorption, reversible desorption can be induced by simply altering environmental conditions. Responsive materials are introduced into the 3D gel network to bestow stimuli-responsive behavior to hydrogels.

Poly(N-isopropylacrylamide) (PNIPAm) is highly sensitive to temperature and is one of the most widely used thermo-responsive polymers. It can quickly transform from a hydrophilic hydrated state to a dehydrated state at temperatures below its lower critical solution temperature, that is, 32 °C.[175] Saad et al.[176] fabricated PNIPAm hydrogel-functionalized polyvinylidene fluoride membranes for the adsorption and desorption of perfluorooctanoic acid (PFOA) from water via temperature-responsive behavior.[176] The adsorption of PFOA was efficient

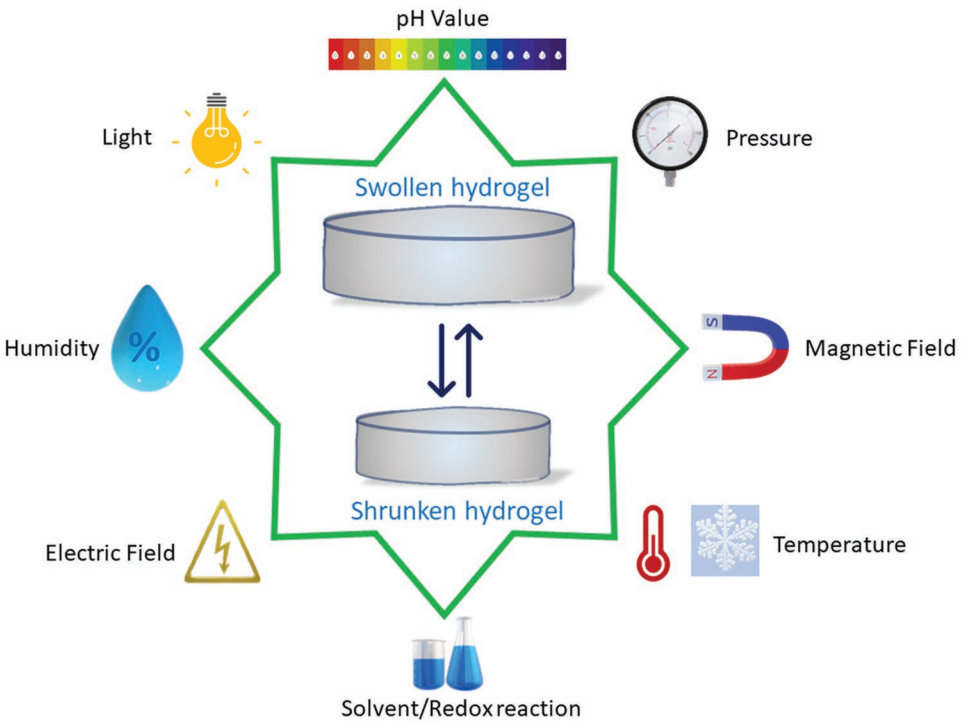

Figure 12. Graphic illustration of stimuli-responsive characteristics of hydrogels.

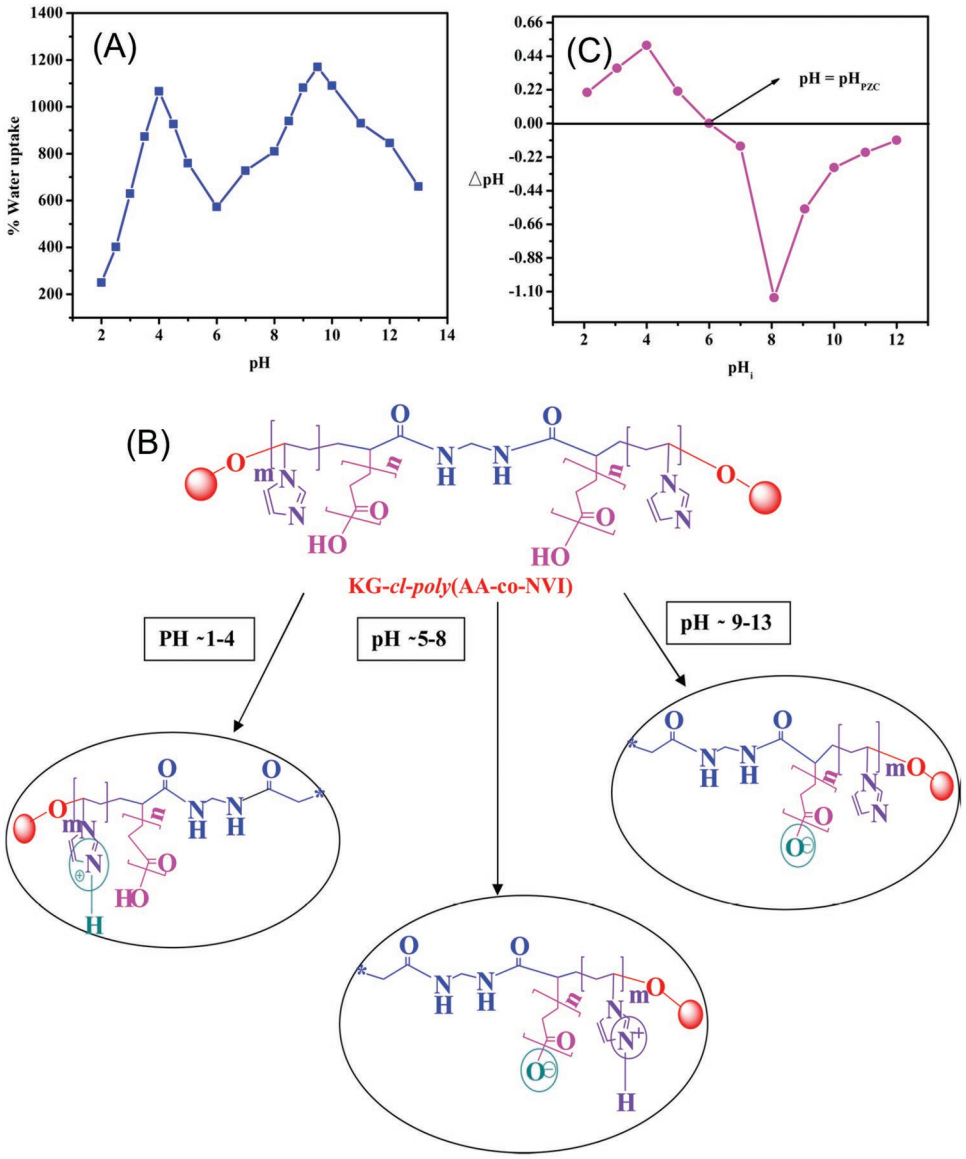

Figure 13. A) Water uptake percentage of the hydrogel at different medium pH. B) Effect of pH on the KG-cl-poly(AA-co-NVI) hydrogel and C) The value of point of zero charges (pH_{pzc}) of the pH-sensitive hydrogel with changing in pH value. Reproduced with from.[178] Copyright 2018, Elsevier Science Ltd.

at 350 °C and 3.5 bar. However, desorption of PFOA took place when pure water was passed through the membrane at 20 °C and 3.5 bar pressure. The adsorption capacity remained approximately constant during cycling experiments. An electric field is another effective external stimulus to induce a response in responsive hydrogels. Electric responsive hydrogels can readily transform their shape and size by swelling and deswelling under the influence of an electric field.[177] PPy is a popular electric-responsive polymer that can transform under electrochemical activation.

In addition to physical stimuli, chemical stimuli, including solvent composition, pH, and concentration, can also significantly impact the performance of hydrogels. For example, a pH-responsive dual hydrogel based on katira gum and poly(acrylic acid-co-N-vinyl imidazole) (KG-cl-P(AA-co-NVI)) exhibit enhanced adsorption characteristics for water-soluble dye molecules in wastewater treatment.[178] **Figure 13**A shows the pH-responsive water uptake capacity of KG-cl-P(AA-co-NVI) hydrogel. The maximum water uptake was obtained at pH 4.5 and 9, which might be due to the pH-responsive functional groups on hydrogel, as shown in Figure 13B. The hydrogel surface charge at different pH is depicted in Figure 13C. The water uptake of the hydrogel is governed by the presence of imidazole groups and the secondary amide. In acidic conditions, the imidazolic nitrogen is protonated and generates more space through steric repulsion between polymeric chains, resulting in enhanced swelling characteristics and an increase in the adsorption of water (Figure 13C). In contrast, at neutral pH (pH = 5–8), the carboxylic acid dissociates into carboxylate ions ($RCOO^-$), resulting in electrostatic attraction between the carboxylate groups and positively charged imidazole rings and reducing the water uptake. However, upon increasing the pH further (≈9), all

the carboxylic acid groups are converted into $RCOO^-$ ions and generate more intramolecular space due to electrostatic repulsion, thus enhancing the water uptake capacity. At higher pH (pH = 9–13), the electrostatic repulsion between the $RCOO^-$ ions decrease as a result of the formation of $RCOO^-Na^+$ ionic pairs, and, thus, the water uptake is decreased. Moreover, at low pH (<5), the protonated hydrogel favors the adsorption of anionic dyes, and at higher pH, it supports the elimination of cationic dyes. Therefore, the KG-cl-P(AA-co-NVI) hydrogel can be used for the pH-dependent selective adsorption of different dyes.

4.4. Ionic Conduction in Hydrogels

Hydrogels can also be used as quasi-solid-state electrolytes and have performed well in flexible aqueous batteries and other electronics due to their outstanding durability.[179] A hydrogel should exhibit high ionic conductivity, low resistance, and excellent chemical stability to be used as an electrolyte. Ionic conductive hydrogels are generally transparent and demonstrate high potential for practical applications, such as skin-contact electrodes, by enabling visualization of internal settings or conditions of electronic devices and skin. Therefore, the research on ionic hydrogels is growing exponentially. The conductivity of hydrogels is generally improved through functionalization with a conductive polymer backbone, active electrode materials, metal cross-linkers, and solid electrolyte particles.

In contrast to traditional conductive materials, the conductivity of ionic conductive hydrogels is due to free-moving ions. Incorporating aqueous electrolytes into hydrophilic hydrogels significantly improves ionic conductivity because hydrophilic functional groups in hydrogels can retain a high-water content.[165] Aqueous electrolytes generally exhibit charges (cationic or anionic) and can easily solvate in the water because water molecules also possess Lewis acidity and basicity.[180] Furthermore, the low viscosity of water also facilitates the mobility of ions and enhances the conductivity of hydrogel.

Recently, transporting Li^+ ions has become a popular option for ionic conductive hydrogels. Zhang et al.[181] fabricated an ionic conductive hydrogel based on a PAAm-PVP dual network with Li^+ (LiCl) as an electrolyte.[181] The conductivity of the hydrogel increased with an increasing amount of LiCl. For example, the highest conductivity (2.0 S m^{-1}) was observed with 31.8% LiCl. Similarly, a hydrogel nanocomposite was constructed by photo-initiated cross-linking a PAAm skeleton with a bio-inspired agar into a dual network with Li^+ as conductive ions.[182] The ionic hydrogel nanocomposite was found to exhibit high stretchability (approx. 1600% extension), high mechanical strength, toughness, and transparency. These and other ionic-conductive hydrogels show promise for applications in flexible electronic devices, such as robots, sensors, actuators, and luminescence displays.

4.5. Electronic Conduction in Hydrogels

The high demand for smart wearable devices requires efficient conductive materials for outstanding performance and durability. Hydrogels based on conductive polymers have garnered much interest due to advantages such as high conductivity, large surface area, facile synthesis, and flexible modification.[183–185] The high electronic conductivity of conductive polymers is mainly attributed to delocalized π electrons.[186] Conductive polymers that are commonly used in hydrogels include PAc, PANI, PPy, PTh, and their derivatives. Furthermore, the electronic conductivity of conductive hydrogels can be enhanced through the incorporation of dopants into the hydrogel matrix.[187] For example, the use of acids (H_2SO_4, HCl, $HClO_4$) as dopants in PAAm/PANI hydrogels resulted in a significantly enhanced electrical conductivity.[188] The highest and lowest electrical conductivity was obtained for the H_2SO_4 and $HClO_4$-doped PAAm/PANI hydrogels, respectively.

In addition to the conductive polymer backbone, conductive fillers, such as carbonaceous materials, MXenes conductive polymers, and metal-based NPs, can be introduced to hydrogels. Certain conductive fillers can act as multifunctional additives to enhance the conductivity and improve other functionalities of the hydrogel. For example, Li et al.[189] constructed a self-healing, strain-sensitive, and conductive hydrogel nanocomposite of poly(vinyl alcohol)-polydopamine-partially reduced graphene oxide (PVA-PDA-pRGO) by the self-polymerization of dopamine and borax into the PVA network, followed by impregnation with pRGO.[189] pRGO acted as a nano-reinforcer and conductive component and improved the mechanical and conductive properties of the hydrogel material. Jing et al.[190] fabricated a self-healing, biocompatible, conductive, and highly stretchable hydrogel nanocomposite composed of PAA and rGO for sensor applications. He et al.[191] introduced tannic acid-carbon nanotubes (TA-CNTs) into the matrix of a PVA hydrogel. The TA coating on the CNTs enhanced the dispersion of the nanocomposite in an aqueous medium. In contrast, the addition of CNTs enhanced the mechanical and conductive characteristics of the parent PVA hydrogel.

Several hydrogels also exhibit dual ionic and electronic conductivity, which is useful for several electrochemical devices. A dual ionic-electronic conductive hydrogel nanocomposite can be prepared by immersing an electronic-conductive hydrogel in an aqueous electrolyte. For example, the electronic conductivity of PANI is enhanced with increased humidity in ambient air, which might be due to the higher ionic conduction in the wet state.[192] A PANI hydrogel film immersed in 1 M $H_2SO_{4(aq)}$ electrolyte exhibit a conductivity of $\approx 10^3$ S cm^{-1}.[193] However, the electrical conductivity of the PANI film is in the range of 10^{-2} to 10^0 S cm^{-1}, while the conductivity of 1 M $H_2SO_{4(aq)}$ is $\approx 10^{-1}$ S cm^{-1}. Therefore, the significant increase in the conductivity of PANI in 1 M $H_2SO_{4(aq)}$ cannot be solely ascribed to the combination of PANI and 1 M $H_2SO_{4(aq)}$, and the weakly bound protons in PANI helped increase electronic conductivity through a synergistic mixed ionic-electrical conductivity effect. However, the main challenge regarding mixed ionic-electronic conductivity is to explore the impact of each component (viz., polymer chain, dopants, functional groups, and additives) on the conductivity of a hydrogel nanocomposite. Nevertheless, mixed ionic-electrical conducting hydrogels are gaining attention and have been investigated as electrodes in batteries, conductive additives, and polymer binders. Hydrogels with appropriate mechanical strength, swelling properties, and enhanced conductivity harbor great potential for various energy and environmental remediation applications.

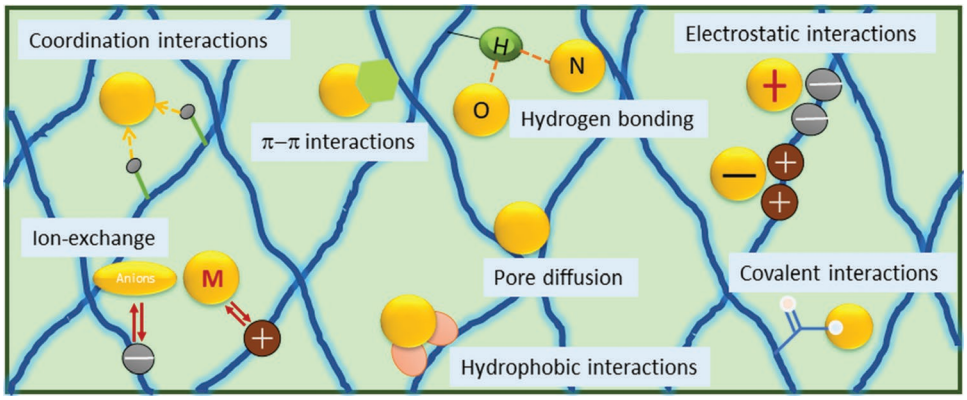

Figure 14. Pollutants can be adsorbed on hydrogel-based materials via various interactions based on the physiochemical attributes of individual pollutants.

5. Mechanisms of Adsorptive and Photocatalytic Removal of Pollutants by Hydrogels

To improve the adsorption performance, a complete understanding of the adsorption approach and removal mechanism of different contaminants in hydrogels is crucial. The adsorption of pollutants onto hydrogel-based materials could occur via one or many mechanisms. The mechanisms involved in the adsorption can be found in **Figure 14**, such as electrostatic interactions, H-bonding, hydrophobic interactions, intermolecular interactions, π-π bonding, ion-exchange, complexation/coordination/chelation, and ion/molecules diffusion in inter- and intra-fibrillar pores/capillaries.[11,194] Several of these types of adsorption interactions are greatly dependent on the functionalities present in hydrogels (e.g., −COOH, −OH, $-H_3PO_4$, $-NH_2$, −SH), the chemical composition of contaminants, adsorbent properties, and experimental factors, including solution pH, initial pollutant concentration, ionic strength, and co-existence of multiple pollutants.[24] Electrostatic interactions are considered to be the most common mechanism for eliminating inorganic and organic contaminants by hydrogel nanocomposites. However, the synergic combination of electrostatic interactions with other interactions has also been demonstrated in numerous adsorption studies.[33,54,195–198] The possible types of mechanisms can be predicted based on the result obtained from various characterization techniques, such as transmission electron microscopy (TEM), Fourier-transform infrared spectroscopy (FTIR), X-ray photoelectron spectroscopy (XPS), and X-ray diffraction (XRD).[23] Overall, hydrogel-based adsorbents with extensive functionalities and high porosity are ideal materials for removing pollutants from wastewater.

The photocatalytic degradation of water pollutants on hydrogel nanocomposites can be explained by the following steps:[199–201] i) Light absorption: a semiconductor material in hydrogel absorbs the photons. ii) Excitation and separation: when the wavelength of photons is equal to or greater than the band-gap of the semiconducting material in the hydrogel, and the photo-induced electrons are excited from the fully occupied valence band to the unoccupied conduction band. iii) Charge migration: the photo-generated electrons and holes migrate to the surface of the hydrogel. iv) Surface reactions: the photo-generated holes participate in surface oxidation reactions, whereas photo-generated electrons participate in surface reduction reactions. **Figure 15** shows the working principle of the photocatalytic degradation of pollutants on hydrogel-based materials. Simultaneously, the recombination of separated holes and electrons takes place at the surface and in the bulk of hydrogels, which is accompanied by the release of heat or light. The fast recombination of photogenerated charge carriers in hydrogels is unfavorable and decreases the surface redox reaction and, consequently, the efficiency of a photocatalyst. Several strategies have been employed to improve the photocatalytic performance of semiconducting materials, including doping, heterostructures/heterojunctions, the addition of cocatalyst, the addition of another light harvester (viz., dye sensitization and surface plasma resonance), and crystalline phase or morphological control.[42,200,202] In addition to semiconducting materials and their dispersion, the light source and its distance from the photocatalyst are critical to the overall performance of hydrogel nanocomposites. It

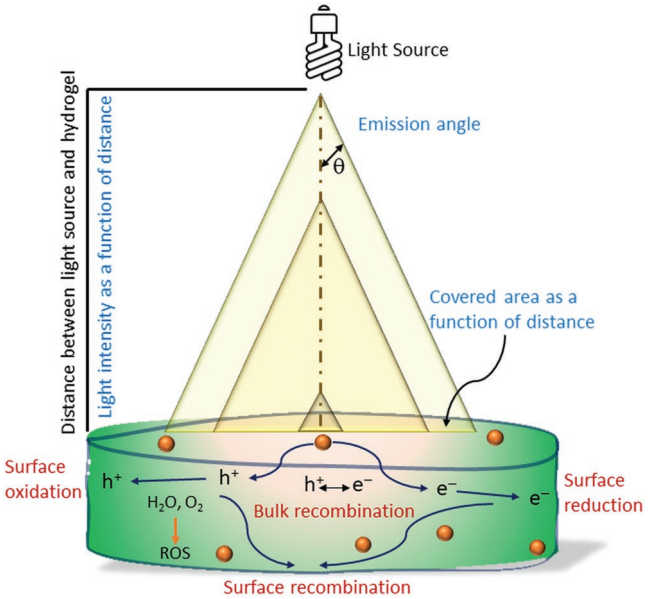

Figure 15. Schematic shows the working principle of photocatalytic degradation of pollutants on hydrogel-based materials.

has been reported that the larger the distance between the hydrogel/photocatalyst and the light source, the greater the illuminated area, but the lower the light intensity. The highest light intensity is achieved when the emission angle becomes zero with respect to the light source.[203]

Furthermore, the 3D network structure of hydrogels is excellent support for semiconducting photocatalysts because of its high surface area and porosity, which expose a large number of reactive sites, resulting in enhanced surface photocatalytic reactions.[41] In hydrogel-based photocatalysis, contaminants are first adsorbed onto the interconnected hydrogel structures, then adsorbed contaminants undergo in situ reduction or oxidation via photocatalysis. The 3D interconnected framework also prevents the stacking/aggregation of nano-sized photocatalysts, which further improves their structural stability. Moreover, these photocatalysts offer more efficient light-harvesting capability due to easy light distribution through the multiple reactions within the interconnected structures. Therefore, the high adsorption capacity, high pollutant retention ability, large surface area with accessible pores, and environmentally-friendly nature of hydrogel-based materials make them attractive for water and wastewater treatment.

6. Adsorptive and Photocatalytic Performance of Various Hydrogel Nanocomposites for Water Treatment

Hydrogels and hydrogel nanocomposites have been proven to be successful candidates in numerous multidisciplinary fields of research, such as biomedical engineering, agriculture, the food industry, and environmental remediation.[204–207] In wastewater purification, hydrogels effectively remove a broad class of water pollutants through adsorption and photocatalysis. Hydrogels have attracted much attention for purification applications owing to their low-cost, high-water retention, large surface area, high porosity, ease of modification, insolubility in water, rapid swelling kinetics, fast diffusion process, permeability, and hydrophilicity.[54,208] However, investigations regarding the recycling of hydrogel adsorbents are rare, which limits their use in a more economical approach.

To overcome this issue, various hydrogel nanocomposites have been synthesized to improve their separation from aqueous solution after wastewater treatment and recycling. In the following sub-sections, the use of the most important hydrogel nanocomposites in wastewater treatment for the removal of a wide range of organic, inorganic, and biological water contaminants is discussed.

6.1. Metallic Nanoparticles-Based Hydrogel Nanocomposites

Various inorganic/organic NPs are being studied to eliminate organic and inorganic pollutants from wastewater. This is possible due to significant features, such as high surface area, good porosity, small size, and maximizing interactions with pollutant molecules by providing several reactive binding sites, which increases adsorption efficiency by several-fold. Recently, in polymer chemistry, metallic NPs incorporated in hydrogel play a significant role in various applications.

Among all metal NPs, Ag NPs are the most explored in developing hydrogel nanocomposites for wastewater treatment applications due to their advanced biological properties (e.g., antibacterial and cytotoxicity) and nontoxicity to normal human cells.[209–211] Babaladimath et al.[212] described the preparation of Ag NPs embedded in a pectin-based hydrogel using microwave synthesis. In this process, pectin is polymerized by free-radical polymerization using MBA, ammonium persulfate, and AMPS. The silver nitrate (Ag precursor) and trisodium citrate (reducing agent) were used to incorporate Ag NPs into the parent hydrogel. The Ag NPs impregnated pectin-grafted-poly(2-acrylamido-2-methylpropanesulfonic acid) hydrogel-silver NPs nanocomposite (Pec-g-PAMPS-SN) was used to remove MB dye. The parent gel (Pec-g-PAMPS) shows a maximum adsorption capacity of 62 mg g^{-1}, while Pec-g-PAMPS-SN exhibited a higher adsorption capacity of 89 mg g^{-1} for MB uptake. The results revealed that MB uptake on hydrogel was a heterogeneous process and controlled mainly by electrostatic interactions. Thermodynamic studies investigated spontaneous and exothermic adsorption. The adsorption isotherm and kinetics indicated that adsorption followed the Freundlich and pseudo-second-order kinetic models.

In another study, Ag NPs were fabricated in poly(acrylic acid)/guar gum (GG/PAA/AgNPs) for MB dye removal from wastewater.[213] The preparation of the AgNPs/GG/PAA hydrogel nanocomposite involved a two-step process of free-radical graft copolymerization of GG (biopolymer) with AA (monomer), followed by instantaneous cross-linking and in situ embedding with Ag NPs. The hydrogel nanocomposite exhibits excellent adsorption efficiency (833 mg g^{-1}) for MB, which might be due to the enhancement in active surface area and reactive binding sites upon introducing NPs to the hydrogel matrix. The adsorption mechanism of MB dye on AgNPs/GG/PAA hydrogel is shown in **Figure 16**A. In an alkaline medium, the AgNPs/GG/PAA nanocomposite surface becomes negatively charged due to deprotonation and successfully adsorbs the cationic dye via electrostatic interactions. Additionally, the hydroxyl and carboxylic groups on the surface of the hydrogel nanocomposite strongly interact with the electronegative atoms of the MB dye via H-bonding. The thermodynamic study indicates that dye adsorption onto AgNPs/GG/PAA hydrogel is a spontaneous, endothermic, and favorable process. Similarly, Ag NPs were also incorporated using the co-precipitation method into a polymer matrix consisting of different molar ratios of AA, MBA, and 2-hydroxyethyl methacrylate in the presence of SA in water.[214] The prepared hydrogel nanocomposite showed very high adsorption capacity and removal% (>95%) of brilliant cresyl blue dye in a batch study, which reduced significantly in a fixed bed column study (≈25–30% removal). The nanocomposite also showed excellent regeneration ability without any measurable change in the morphology and adsorption efficiency.

The photocatalytic degradation ability of an Ag-incorporated hydrogel nanocomposite has also been investigated. The introduction of noble metals such as Ag notably improves visible-light absorption via surface plasmonic effects and enhances photocatalytic performance. Tang et al. prepared a Ag@AgCl containing cellulose hydrogel for the photo-degradation of methyl orange (MO) dye.[215] The Ag@AgCl-containing

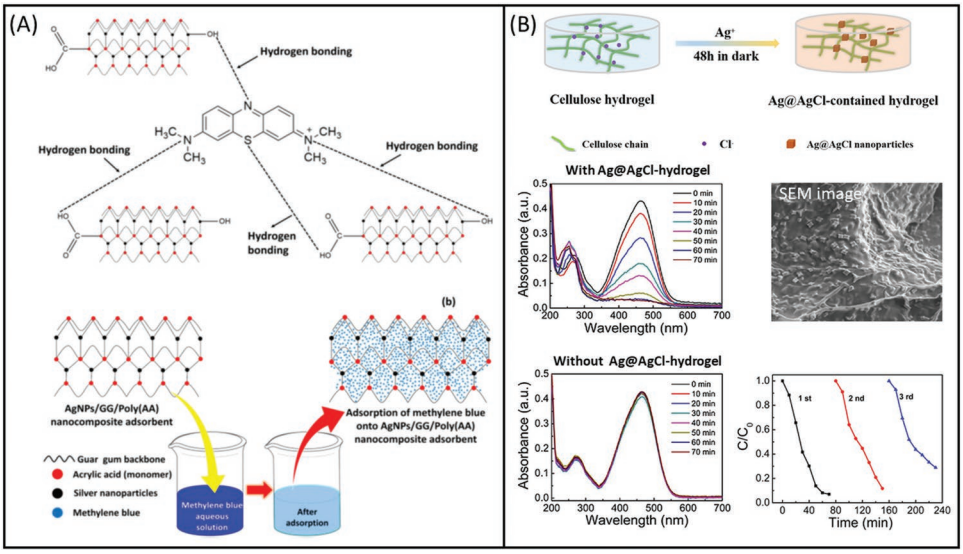

Figure 16. A) Adsorption mechanism of MB dye on AgNPs/GG/Poly(AA) hydrogel nanocomposite. Reproduced with permission.[213] Copyright 2021, Springer Nature. B) Ag@AgCl-contained cellulose hydrogels preparation and application in MO dye photocatalytic degradation. Reproduced with permission.[215] Copyright 2018, Elsevier Science Ltd.

cellulose hydrogel was prepared by mixing the dried cellulose hydrogel in an $AgNO_3$ solution and kept in the dark for 48 h. Figure 16B shows the formation of Ag@AgCl containing cellulose hydrogel nanocomposite and its application to the photocatalytic degradation of MO dye. The Ag@AgCl cube-like particles were found well-dispersed on the hydrogel matrix. Furthermore, the MO photocatalytic degradation was performed without Ag@AgCl-loaded cellulose hydrogel photocatalyst under visible light, also reported in Figure 16B. Without a photocatalyst, negligible photo-degradation of MO dye was observed. However, under similar conditions, in the presence of Ag@AgCl loaded cellulose hydrogel nanocomposite, 93% MO dye was degraded within 70 min of visible light exposure. To investigate the reusability of the Ag@AgCl loaded cellulose hydrogel nanocomposite, the hydrogel nanocomposite was used for ten consecutive cycles, revealing only a slight decrease in the photocatalytic performance. This indicates the potential of the Ag@AgCl-loaded cellulose hydrogel nanocomposite for sustainable water purification applications.

In addition to adsorption and photocatalytic reduction, Gao et al. reported the catalytic hydrogenation of p-nitrophenol (PNP) using 3D silver/poly(ethylenimine)/alginate hydrogel beads (Ag@PEI@AHB) prepared by a facile one-pot assembly method.[216] The experimental results show that the 20% silver-loaded Ag@PEI@AHB catalysts can exhibit 90% PNP conversion at 298 K (120 s) under fixed-bed conditions. The catalytic conversion follows the pseudo-first-order kinetic. The 20% Ag@PEI@AHB showed better conversion due to higher silver content, indicating that the PEI hydrogel not only enhanced the ability to reduce silver ions but also improved the silver loading, which greatly enhanced the catalytic activity of the catalyst and expedited the reaction process. A regeneration study revealed a negligible loss in catalytic efficiency after ten cycles, which confirmed the long-term stability of the Ag@PEI@AHB catalysts. In another study, biosynthesized Ag NPs were incorporated into 2-hydroxypropyl-β-cyclodextrin/alginate to yield the HPCD/Alg/AgNPs hydrogel nanocomposite, which was investigated for the photo-degradation of contaminants such as PNP, MO, and rhodamine B (RhB) using $NaBH_4$ as reductant.[217] Ag NPs were prepared using an aqueous extract of *Jasminum subtriplinerve* leaves. The nanocomposite showed a high crystallinity with an average diameter of 13.5 nm. AgNPs/HPCD/Alg could completely degrade the studied organic pollutants in 22–25 min by the electron transfer mechanism. The catalytic activity of the nanocomposite was very fast, with pseudo-first-order rate constants ranging from 1.51×10^{-3} to 2.23×10^{-3} s^{-1}.

Not many metals other than Ag metal have been combined with the polymeric hydrogel matrix and evaluated for wastewater treatment efficiency. Wang et al.[218] studied the Pd-supported nanocellulose-alginate hydrogel beads (PdNPs@CNCC-AHB) for catalytic MB dye degradation. Within 5 min of introducing PdNPs@CNCC-AHB to the MB aqueous solution in the presence of $NaBH_4$, the solution became discolored and was observed by UV–vis spectroscopy at 664 nm. The mechanism behind the catalytic reduction of the MB dye can be explained in two steps: initially, the cationic MB dye is successfully adsorbed on the negatively charged CNCC-alginate hydrogel matrix, followed by the catalytic borohydride reduction of the MB dye by Pd NPs located on the hydrogel surface.

In summary, although Ag is most frequently used as metallic NPs, several metals have been explored as the co-adsorbent/co-catalysts in various hydrogel nanocomposites for the removal of organic/inorganic water pollutants. They have shown an effective response in wastewater treatment. Therefore, there is ample scope to explore the effect of several other metals in hydrogel matrix for wastewater treatment.

6.2. Metal Oxides-Based Hydrogel Nanocomposites

Metal oxide nanostructured materials are of considerable interest in various applications due to their unique

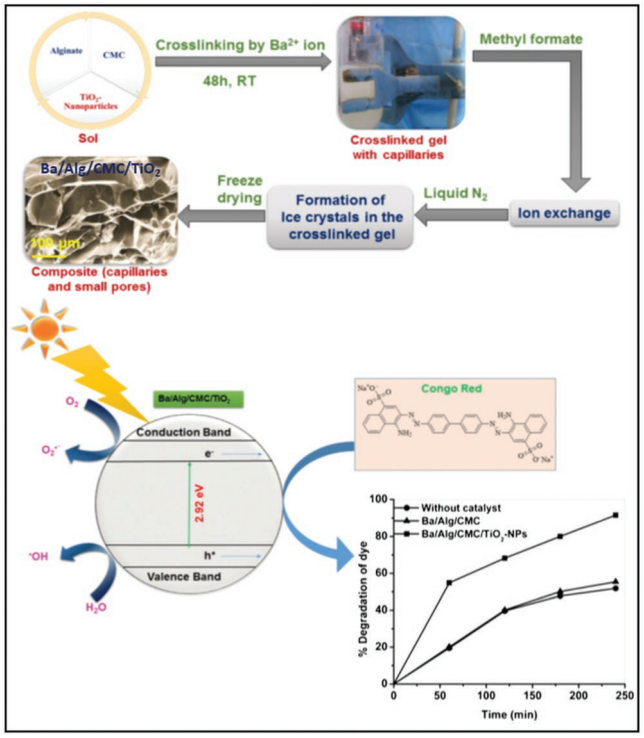

Figure 17. Photo-degradation of CR dye using Ba/Alg/CMC/TiO_2 hydrogel composite under visible light irradiation. Reproduced with permission.[234] Copyright 2016, Elsevier Science Ltd.

characteristics and abundant availability.[219] The high surface energy and large active surface area of metal oxide-based nanomaterials enhance the uptake of organic/inorganic sorbates. Therefore, metal oxide-based NPs are versatile materials that show excellent proficiency in cleaning wastewater as quick adsorbents or photocatalysts.[220–222] However, there are several challenges to using metal oxide nanomaterials in water applications. For example, reducing the size of metal oxides to the nanoscale may increase the surface area of the material. Still, it also makes the material unstable and more susceptible to aggregation, which affects the mechanical strength, selectivity, adsorption capacity, and quantum yield of the material. To overcome this issue, the metal oxide can be immobilized onto other supports, for example, polymers.[223] Therefore, metal oxide hydrogel nanocomposites are suitable for wastewater treatment with high efficiency.

TiO_2 is a commonly used chemically inert metal oxide with broad-ranging applications, including wastewater treatment as a standalone or nanocomposite photocatalyst.[224–226] However, the ease of agglomeration, wide band gap, and photosensitivity only to UV light are major drawbacks of TiO_2 for wastewater treatment applications. Modifying TiO_2 with biopolymers (e.g., chitosan, gum, and starch) to form TiO_2-hydrogel nanocomposites reduces aggregation and enhances the functional characteristics of the nanocomposite material.[227] TiO_2 is one of the most extensively investigated metal oxides that have been embedded into hydrogel matrices for wastewater treatment, with many reports on the utilization of TiO_2-based hydrogel nanocomposites as photocatalysts.[228–233] Thomas et al.[234] demonstrated Congo red (CR) dye degradation by a Ba^{2+}-crosslinked-alginate/carboxymethyl cellulose with embedded TiO_2-NPs- hydrogel nanocomposite (Ba/Alg/CMC/TiO_2) under sunlight. The Ba/Alg/CMC/TiO_2 hydrogel nanocomposite was prepared by a dissipative convective approach and dried by the freeze-drying method. **Figure 17** shows scanning electron microscopy (SEM) images of Ba/Alg/CMC/TiO_2 hydrogel nanocomposite.

The hydrogel nanocomposite consists of ordered capillaries 50–100 µm in diameter with apertures of 5–20 µm. The hydrogel nanocomposite was investigated for the photo-degradation of CR dye under solar light irradiation by varying reaction parameters. The photocatalytic reaction begins with the absorption of solar light irradiation by TiO_2, which generates photo charge carriers, active species, and radicals (Figure 17). The radicals degraded the dye molecules into intermediates that are converted into ammonium ions, nitrate ions, water, and carbon dioxide. To evaluate the role of TiO_2 in the hydrogel nanocomposite, photo-degradation of CR was also evaluated for Ba/Alg/CMC. CR dye was only degraded by 51% and 55% in the absence of the nanocomposite and by Ba/Alg/CMC, respectively, under solar irradiation, whereas 91.5% was degraded using Ba/Alg/CMC/TiO_2 under identical conditions.

Neeraj et al.[33] proposed a circulatory concept for water purification using TiO_2 nanorods incorporated gum ghatti (Gg) hydrogel bio-nanocomposite (TGB) (**Figure 18**A). According to this concept, the secondary waste generated from any water process is considered a resource for a new approach unless the used material properties deteriorate entirely. A schematic presentation of the formation of the hydrogel bio-nanocomposite is shown in Figure 18B. The free-radical graft copolymerization method was used to prepare the hydrogel (Gg-cl-(AAM-co-AA)) from AAm, AA, and Gg in the presence of an initiator and MBA (cross-linking agent). To introduce TiO_2 into the matrix, an aqueous TiO_2 nanorod dispersion was added to the above mixture. The TGB-hydrogel was used for the adsorption of toxic brilliant green (BG) dye, exhibiting a maximum adsorption capacity 740.9 mg g^{-1} at 30 °C. Figure 18C also shows the possible interactions and interaction sites for the uptake of BG dye by the TGB-hydrogel. Electrostatic interaction, hydrogen bonds, and π-π interactions are the driving interaction forces for the removal of BG dye.

Furthermore, the BG-adsorbed TGB-hydrogel was used to photodegrade the antibiotic ciprofloxacin (CIP). Before being used in photocatalysis, BG-adsorbed TGB-hydrogel was heated in a furnace at 550 °C for 3 h to produce C-TiO_2 active sites. The C-TiO_2 successfully degraded the CIP in 180 min under visible light illumination (Figure 18C). The high photocatalytic performance was ascribed to the presence of TiO_2 NPs on the activated hydrogel, which delayed the recombination of electron-hole pairs and produced large reactive sites for photodegradation. In another study, TiO_2 was incorporated into the SA-crosslinked poly(acrylic acid) hydrogel (SA-cl-PAA-TiO_2) and evaluated for the removal of MB dye from water.[235] The hydrogel was fabricated via graft copolymerization of SA with AA with the assistance of a free-radical initiator and a cross-linking agent and impregnated with TiO_2 NPs. The fabricated SA-cl-PAA-TiO_2 hydrogel nanocomposite exhibited a high swelling ratio of 412.98 g g^{-1}. The adsorption of MB dye on the hydrogel nanocomposite followed the Langmuir isotherm

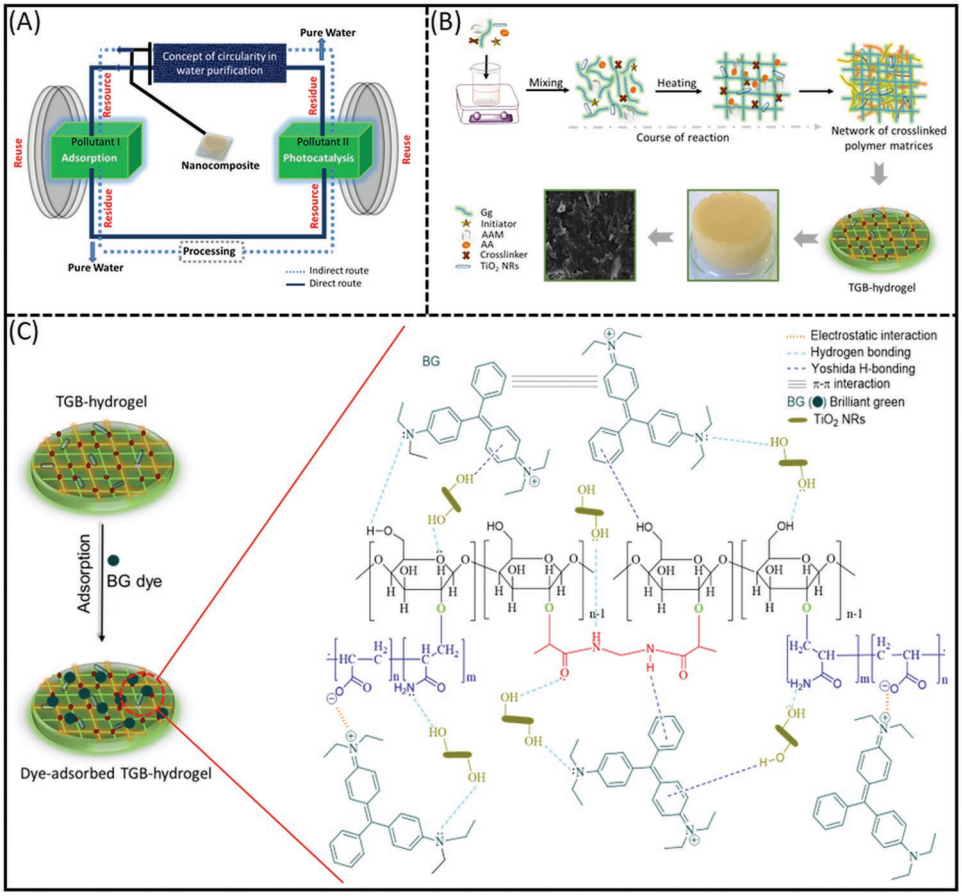

Figure 18. A) Illustration of circularity concept in water purification using hydrogel nanocomposite. B) Preparation of TGB-hydrogel and reuse of dye-adsorbed TGB hydrogel as photocatalyst. C) The probable interaction sites for adsorption of the BG dye on TGB-Hydrogel. Reproduced with permission.[33] Copyright 2018, American Chemical Society.

equation (R^2 = 0.998) and pseudo-second-order kinetics. The hydrogel nanocomposite exhibited an excellent MB adsorption capacity of 2257.36 mg g^{-1}, making it can be an appropriate material for water purification.

Zarrini et al.[129] investigated the photocatalytic potential of zinc oxide (ZnO)-based hydrogel for the photocatalytic degradation of MB under visible light illumination. Chitosan/AgCl/ZnO (CS/AgCl/ZnO) hydrogel beads were added to an MB aqueous solution at pH 11 and irradiated with visible light. For comparison, MB dye was also treated under dark conditions with CS/Ag/Cl and under visible light irradiation using CS, CS/AgCl, CS/ZnO, and CS/AgCl/ZnO hydrogel beads. Complete decolorization was obtained only with CS/AgCl/ZnO under visible light illumination. The incorporation of the semiconductor ZnO onto the hydrogel improved the photocatalytic performance by producing various highly active species on the surfaces. The photocatalyst was also recovered and reapplied with high efficiency observed for consecutive cycles.

In addition to photocatalysis, hydrogel nanocomposites embedded with metal oxide nanomaterials have also been utilized in water purification via adsorption.[236,237] Mittal et al.[238] reported the synthesis of a gum karaya (GK)-based hydrogel by grafting GK with copolymerized poly(acrylic acid-acrylamide) in the presence of MBA (cross-linker) and a mixture of potassium persulfate and ascorbic acid (redox initiator). The hydrogel nanocomposite of GK-cl-P(AA-co-AAM) with nanosilica was prepared by water condensation reactions of tetraethylorthosilicate in an aqueous dispersion of the parent hydrogel GK-cl-P(AA-co-AAM) at 50 °C for 12 h. The surface area of hydrogel significantly increased upon producing the nanocomposite with nanosilica. The high adsorption efficiency (96%) was obtained for the removal of MB dye from water at a low adsorbent dose (0.2 g L^{-1}). The hydrogel nanocomposite exhibits exceptionally high adsorption capacity (1408.67 mg g^{-1}) due to the increased surface area and porosity of the hydrogel and the dispersed SiO_2 NPs in the polymer matrix. The abundant functionalities of the polymer network and the −OH functional groups of SiO_2 likely contribute the most to the adsorption of MB. The hydrogel nanocomposite exhibited good regeneration ability by desorption of MB in an acidic medium followed by alkaline treatment to restore the binding sites and was effectively employed over three adsorption-desorption cycles.

The same group also demonstrated the removal of MB dye using a TiO_2 NPs-embedded polyacrylamide-grafted gum ghatti (PAAm-g-Gg) hydrogel nanocomposite.[239] The MB adsorption by the hydrogel nanocomposite was performed in batch experiments. It was observed that dye adsorption depended on adsorbent dosage, ionic strength, temperature, and solution

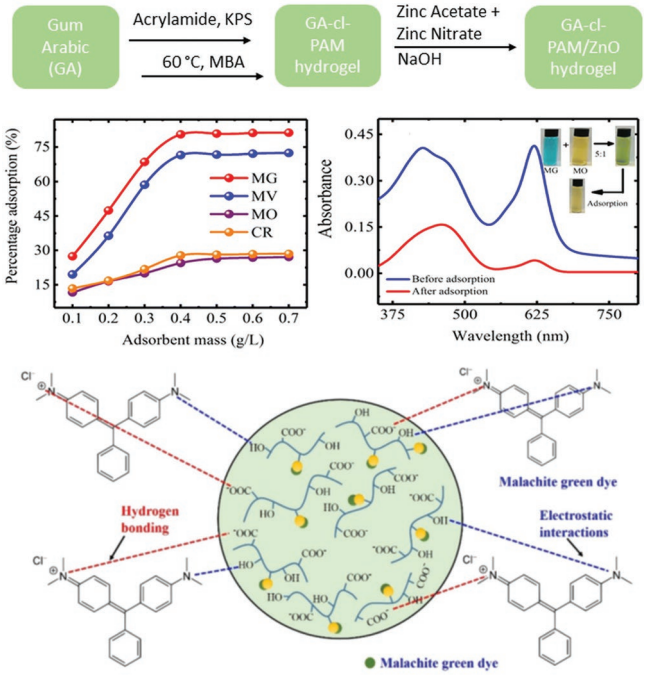

Figure 19. Synthesis steps of GA-cl-PAM/ZnO hydrogel; removal of various cationic and anionic dyes using GA-cl-PAM/ZnO and selective MG removal from the mixture of MG and MO dyes using GA-cl-PAM/ZnO; Best possible interactions for the MG adsorption onto GA-cl-PAM/ZnO. Reproduced with permission.[241] Copyright 2020, Springer.

pH. The hydrogel nanocomposite demonstrated a high maximum adsorption capacity of 1305.5 mg g^{-1} for MB, following the Langmuir adsorption isotherm and pseudo-second-order kinetic rate model. In addition, the hydrogel nanocomposite exhibited higher performance cationic dyes (e.g., MB, RhB, malachite green (MG), and methyl violet (MV)) than anionic dyes (e.g., MO and CR) due to the overall negative charge on the adsorbent surface. The hydrogel nanocomposite could be recovered and regenerated for five adsorption-desorption cycles without losing its initial adsorption capacity. In summary, these hydrogel nanocomposites display significant potential for eliminating toxic cationic dyes from industrial wastewater.

ZnO-based hydrogel nanocomposites also show high adsorption capacity toward water contaminants.[237,240,241] Alhassan et al.[241] proposed the preparation of ZnO NPs using the polyacrylamide-grafted Gum Arabic (GA-cl-PAAm) hydrogel. The prepared GA-cl-PAAm/ZnO hydrogel nanocomposite was used to remove the MG dye from the wastewater. Different mechanisms for the adsorption of MG on GA-cl-PAAm/ZnO are illustrated in **Figure 19**. The electrostatic interaction between the MG dye and GA-cl-PAAm/ZnO hydrogel nanocomposite is particularly strong. The composite exhibits a negative charge at high pH, and the cationic dye can readily be adsorbed. Another major interaction between the dye and composite is H-bonding, which is facilitated by hydroxyl groups present on ZnO. At low pH, the polar N atom of the dye molecule interacts with the hydrogel composite via H-bonding with carboxylate groups. The third adsorption mechanism is the pore diffusion mechanism. The hydrogel nanocomposite exhibits interconnected capillary channels, through which MG dye molecules can diffuse and adsorb on the hydrogel via pore diffusion or capillary condensation.

Furthermore, the adsorption selectivity of GA-cl-PAAm/ZnO hydrogel nanocomposite towards anionic and cationic dyes was also investigated. Figure 19 shows that the hydrogel nanocomposite more easily adsorbs the cationic dyes than anionic dyes. In addition, the hydrogel nanocomposite efficiently adsorbs MG from a mixture of MO and MG dyes (Figure 19), which is ascribed to the strong electrostatic interaction between MG dye and the hydrogel nanocomposite.

Similarly, many hydrogel nanocomposites based on other metal oxides, such as MnO_2,[236,242] CuO,[243] NiO,[244] and Al_2O_3,[245] have been employed for the adsorption of water pollutants. **Tables 1** and **2** summarize various metal oxide-based hydrogel nanocomposites for wastewater treatment as adsorbents and photocatalysts, respectively. While metal oxide hydrogel nanocomposites are well-studied for the adsorption of water contaminants, their photocatalytic efficiency has only been extensively investigated for various other applications. In particular, only TiO_2 and ZnO-based hydrogel nanocomposites have been widely explored as photocatalysts for wastewater treatment. Thus, there is a need to investigate the photocatalytic potential of other metal oxides-based hydrogel nanocomposite materials for the photo-degradation of water pollutants.

6.3. Magnetic Nanoparticles-Based Hydrogel Nanocomposites

The efficient recovery of any adsorbent or photocatalyst after being used in wastewater treatment is essential and challenging. The magnetic-separation method of a material is an economical and straightforward approach. Functionalization of magnetic NPs (generally iron or iron oxide) into organic/inorganic materials enhances the water contaminant removal efficiency of the composite material. It enables the easy separation process of material from the aqueous solution using an external magnet.[258] Magnetic hydrogels, also known as ferrogels, can effectively remove many aqueous cationic and anionic pollutants.[259] Zero-valent iron and iron oxide (Fe^{2+} or Fe^{3+}) NPs have been integrated into several hydrogels to impart magnetic characteristics and have been applied in wastewater treatment as an adsorbent or photocatalyst.[260–262]

Mainly magnetite (Fe_3O_4) or γ-Fe_2O_3 has been integrated into the hydrogel matrices for water treatment applications. γ-Fe_2O_3-based magnetic cationic hydrogel has been proven to be an efficient adsorbent for various pollutants. Fe_3O_4-incorporated chitosan-Fe(III) hydrogel shows high efficiency in the adsorption of a variety of anionic dyes.[263] **Figure 20**A illustrates the cycle of fast adsorption of dye using the chitosan-Fe(III) hydrogel, followed by desorption of the dye, regeneration of the hydrogel, and reuse for the adsorption of dye. The rapid adsorption of dye (within 10 min) using chitosan-Fe(III) is due to the high density of active sites on the hydrogel surface. Under alkaline conditions, the free amino groups of pristine chitosan are not protonated and, therefore, cannot participate in the adsorption of anionic dye via electrostatic interactions. However, in the chitosan-Fe(III) complex, negative groups in the dye molecule readily replace water molecules to chelate to Fe(III) centers in the hydrogel, resulting in fast adsorption.

Table 1. Various metal oxide-based hydrogel nanocomposites are employed as adsorbents for the removal of water contaminants from water.

Metal oxide based hydrogel	Water pollutant	Experimental conditions	Adsorption capacity [mg g^{-1}]	Ref.
3D MnO_2 modified biochar-based porous polyacrylamide hydrogel	Cu (II) Pb(II)	Temp: 25 °C Time: 72 h pH: 6 & 4	84.76 70.90	[236]
3D MnO_2 nanotubes@rGO hydrogel	Pb(II)	Temp: RT Time: 12 h pH: 5	356.37	[242]
Chitosan/poly(vinyl alcohol)/CuO	Pb(II)	Temp: 323K Time: 60 min pH: 5	116.8	[243]
Al_2O_3/GO cellulose	Fluoride	Temp: 30 °C Time: 120 min pH: 5	5.34	[245]
ZnO/Alginate	MB	Temp: 50 °C Time: 90 min pH: 7	2.543	[237]
ZnO/gum arabic grafted polyacrylamide	MG	Temp: 25 °C Time: 60 min pH: 7	766.52	[241]
ZnO –clay- Alginate	CR	Temp: 30 °C Time: 120 min	546.89	[246]
ZnO/Chitosan	Reactive Black 5 (RB-5)	Temp: 40 °C Time: 360 min pH: 4	189.44	[240]
Sodium alginate poly(acrylic acid) @ZnO	MB	Temp: 30 °C Time: 40 min pH: 6	1529.6	[247]
GK-cl-P(AA-cl-AAM)/SiO_2	MB	Temp: RT Time: 90 min pH: 7	1408.67	[238]
Gum tragacanth cross-linked 2-hydroxyethyl methacrylate-co-acrylamide/ZnO [GT-cl-(HEMA-co-AAm)/ZnO)]	Hg^{2+}	Temp: 25 °C Time: 400 min pH: 3.2	154.8	[248]
Xanthan gum grafted poly(acrylic acid-co-itaconic acid)/ZnO [XG-cl-p(AA-co-IC)/ZnO]	MB	Temp: RT Time: 70 min	212.8	[249]
Sodium alginate cross-linked poly (N,N-dimethyl Acrylamide-co-2 acrylamino-2-methyl-1-propane sulfonic acid) /TiO_2 [SAG-cl-poly(N,N-DMA-co-AMPS)/TiO_2]	MB, Carmosine-A (CR-A)	Temp: 27 °C Time: 90 min pH: 7	403.2 106.2	[250]

Lu et al.[264] immobilized Fe_3O_4 NPs in the chitosan/PEI hydrogel to prepare the magnetic hydrogel beads (MBH1), followed by the covalent functionalization with gallic acid to form MBH2 hydrogel beads for Cr(VI) removal. This hydrogel could successfully adsorb Cr(VI) and reduce it into less toxic Cr(III). The mechanism of adsorption and reduction of Cr(VI) is depicted in Figure 20B. Cr(VI) absorption is achieved via electrostatic interactions between the protonated amine groups at low pH (pH 2.0). A significant amount of Cr(VI) is reduced by electron donors on MHB2, whereas the grafted gallic acid further accelerates the reduction of Cr(VI). Moreover, the chitosan/PEI hydrogel captures Cr(III) via a chelating mechanism. MHB2 exhibits exceptionally high adsorption capacity (476.2 mg g^{-1}) for Cr(VI) at low pH and could be used in successive cycles after regeneration.

In another study, the poly(κ-carrageenan-co-PVA)/Fe_3O_4 magnetic hydrogel nanocomposite was fabricated by integration of PVA, magnetic Fe_3O_4 NPs, and κ-carrageenan (κ-C), and showed high adsorption capacity for crystal violet (CV) dye removal from water.[265] Fe_3O_4 NPs were synthesized via an in situ co-precipitation method in the presence of κ-C and PVA (Figure 20C). A thermodynamic study revealed that the adsorption of CV on the hydrogel nanocomposite occurred spontaneously. The maximum adsorption capacity achieved was 79 mg g^{-1} for the adsorption of CV dye, and the adsorption isotherm followed the Langmuir model. The adsorption of CV decreased by integrating Fe_3O_4 NPs and was increased by increasing the concentration of κ-C. The reduction in the adsorption capacity of hydrogel with Fe_3O_4 NPs can be attributed to the reduction in the weight ratio of anionic κ-C centers and the lower degree of swelling of the hydrogel nanocomposite.

Furthermore, an increase in κ-C content of the hydrogel nanocomposite enhanced the swelling characteristics and, therefore, increased the adsorption of CV. The adsorption of CV on

Table 2. Various metal oxide-based hydrogel nanocomposites are employed as photocatalysts for the photodegradation of water pollutants.

Metal oxide-based hydrogel	Water pollutant	Experimental Conditions	% Degradation	Ref.
TiO_2/Chitosan	MO Alizarin red S (ARS)	UV light Temp = RT Time = 3–6 h	100 100	[251]
TiO_2/chitosan/ poly(N-isopropylacrylamide)	Acid fuchsin (AF)	UV light Temp = 25 °C Time = 160 min	90.5	[252]
TiO_2/Chitosan	Amoxicillin	UV light Temp = 24 °C Time = 2h	100	[253]
Cu_2O/Cu/rGO@ carbon/ sodium alginate	p-nitrochlorobenzene (p-NCB)	Visible light Temp = RT Time = 150 min	96.35	[254]
TiO_2/MgO/ Chitosan	MO ARS	UV light Temp = RT Time = 90 min	82.4 41.8	[255]
AgCl/ZnO/ Chitosan	MB	Visible light Temp = 25 °C Time = 135 min	100	[129]
Alginate/ carboxymethyl cellulose/TiO_2	CR	Sunlight Temp = RT Time = 240 min	91.5	[234]
CeO_2/TiO_2	MO	125 W Hg lamp Temp = RT Time = 90 min	95.27	[256]
PAA/15-CuZnO	MB	Sunlight Temp = RT Time = 60 min	100	[257]

the hydrogel nanocomposite was followed by intraparticle diffusion and electrostatic interactions. To regenerate hydrogel nanocomposite, dye-adsorbed poly(κ-C-co-PVA)/Fe_3O_4 was treated in different solutions (Figure 20C). The desorption of the dye was most efficient in a 0.5 M KCl ethanol/water solution. The regenerated poly(κ-C-co-PVA)/Fe_3O_4 was used in consecutive cycles and showed a slight decrease in the adsorption efficiency.

Sharma et al.[260] reported the synthesis of a pectin-crosslinked guar gum/superparamagnetic iron oxide nanocomposite (Pec-cl-GG/SPION) hydrogel via a co-precipitation/polymerization method using MBA as cross-linker and utilized the hydrogel for the adsorption of the organic pollutants m-cresol (mC) and o-chlorophenol (OCP). The adsorption of organic contaminants on Pec-cl-GG/SPION was improved at low pH (pH < 3). mC and OCP are both good nucleophiles. At low pH, the surface of Pec-cl-GG/SPION is positively charged, accelerating the interaction between the adsorbate and adsorbent. The adsorption capacity of Pec-cl-GG/SPION towards mC and OCP was 176.1 and 75.6 mg g^{-1}, respectively. The adsorption of mC was more favorable than OCP, which might be due to the difference in the nucleophilicity of the pollutants. The superparamagnetic iron oxide in the hydrogel nanocomposite acted as an active magnetic material and simplified the separation process.

In another study, Fe NPs were introduced into the poly(vinyl alcohol/acrylamide) matrix along with Ag particles. The prepared P(VA/AAm)-Fe-Ag hydrogel nanocomposite was evaluated for the adsorption of heavy metal ions (viz., Cu(II)) and dyes from the wastewater (viz., MB and MG).[266] A high pH of the aqueous medium favors the swelling behavior of P(VA/AAm)-Fe-Ag hydrogel nanocomposite. For Cu(II) removal, P(VA/AAm)-Fe-Ag shows quick adsorption behavior and reaches maximum adsorption within 30 min. The rapid adsorption of Cu(II) might be due to the 3D structure of P(VA/AAm)-Fe-Ag, which exhibits several super-hydrophilic hydroxyl and amide groups, facilitating the adsorption of heavy metal ions. In contrast, the maximum adsorption of dyes was reached after 5 h.

Apart from Fe_3O_4, other iron derivatives, such as Fe_2O_3, β-FeOOH, and zero-valent Fe, have also been used in magnetic hydrogel matrices to enhance wastewater treatment efficiency. Wang et al.[261] reported the fabrication of β-FeOOH@tunicate cellulose hydrogel nanocomposite and their application to the photodegradation of MB. The β-FeOOH@tunicate cellulose hydrogel nanocomposite was prepared by the in situ growth of β-FeOOH NPs in the cellulose hydrogel matrix. The β-FeOOH NPs were uniformly dispersed and strongly anchored in the hydrogel matrix (**Figure 21**A). Within 30 min of exposure to visible light irradiation, β-FeOOH@tunicate cellulose could degrade 99.89% MB. Figure 21A displays the possible photocatalytic MB dye degradation mechanism. Under visible light illumination, charge pairs are generated from the excited β-FeOOH NPs. The excited electron jumped from the lowest unoccupied molecular orbital of the dye molecule to the conduction band of the β-FeOOH, which resulted in the reduction

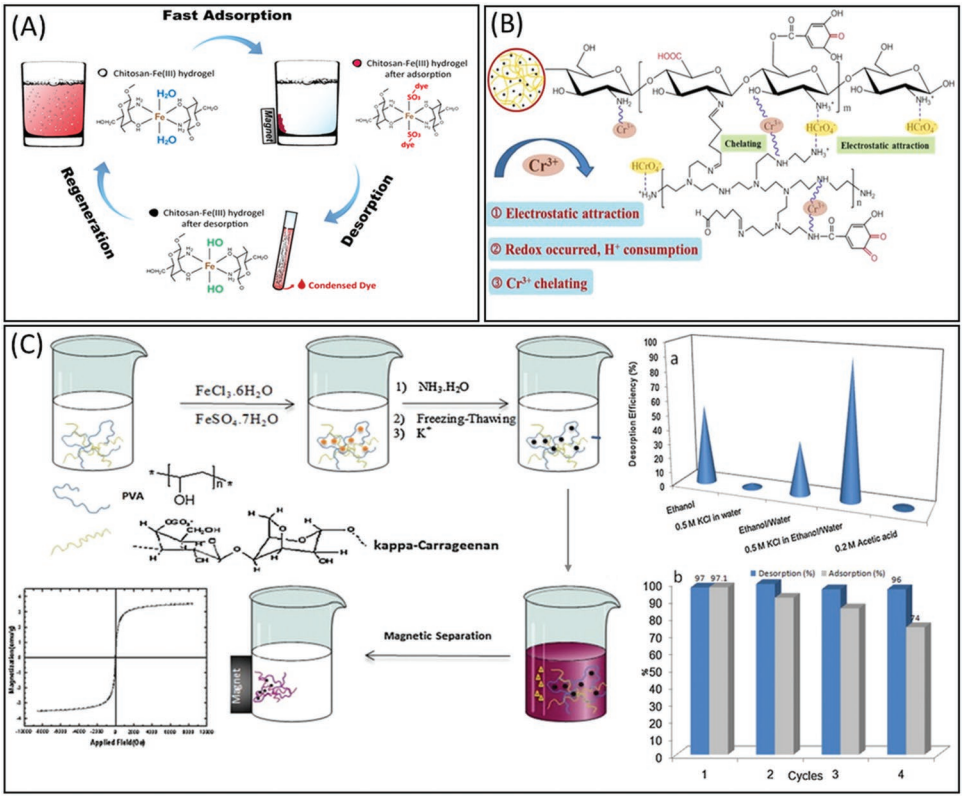

Figure 20. A) The cycle of anionic dye adsorption, dye desorption, regeneration, and reuse of hydrogel. Reproduced with permission.[263] Copyright 2011, Elsevier Science Ltd. B) Best possible mechanism for Cr(VI) adsorption and reduction to Cr(III) using magnetic chitosan/poly(ethylenimine) hydrogel. Reproduced with permission.[264] Copyright 2021, Elsevier Science Ltd. C) Representation of Poly(κ-carrageenan-co-PVA)/Fe_3O_4 synthesis; regeneration of poly(κ-carrageenan-co-PVA)/Fe_3O_4 after dye adsorption in various solutions and recyclability of Poly(κ-carrageenan-co-PVA)/Fe_3O_4 hydrogel nanocomposite. Reproduced with permission.[265] Copyright 2014, Elsevier Science Ltd.

of Fe^{3+} to Fe^{2+}.[267,268] Subsequently, in the presence of H_2O_2 and Fe^{2+}, the ·OH radicals and Fe^{3+} are generated. Finally, ·OH and charge holes react with MB for mineralization, and Fe^{3+} is regenerated. The effect of scavengers was also investigated to understand the most reactive species for dye degradation. The decreased degradation efficiency in the presence of triethanolamine and tert-butylalcohol confirmed that the ·OH radical and holes are the primary active species for dye degradation.[269] The hydrogel nanocomposite also shows excellent durability and stability for five successive cycles, maintaining 96% dye degradation efficiency.

Duan et al.[270] reported the green synthesis of a multifunctional 3D AgNPs@MIL-100(Fe)/GG hybrid hydrogel by the blending and self-cross-linking processes and the efficient degradation of MB dye. To prepare the hydrogel nanocomposite, Ag NPs were dispersed onto the MOF MIL-100(Fe), followed by ultra-sonication of AgNPs@MIL-100(Fe) and the GG hydrogel. As shown in Figure 21B, the AgNPs@MIL-100(Fe)/GG hydrogel nanocomposite exhibited excellent photocatalytic MB degradation ability and could degrade 100% MB within 100 min upon exposure to visible light irradiation. UV–vis absorbance spectra of revealed the continuous decrease of the absorption peak at 664 nm (characteristic peak of MB) with increased irradiation time and confirmed complete degradation. Figure 21B also shows a comparison of the adsorption and photocatalytic potential of MIL-100(Fe), GG, and MIL-100(Fe)/GG, revealing the enhanced performance of AgNPs@MIL-100(Fe)/GG. The high photocatalytic degradation ability of the hydrogel nanocomposite was due to the synergistic adsorption and photocatalysis of dye molecules. The possible mechanism is depicted in Figure 21B. Firstly, the dye molecules are adsorbed onto the nanocomposite surface. Then, charge carriers are generated under light illumination, and the Ag NPs accept the e^-, which effectively delays the recombination of e^- and holes. During the reaction, H_2O molecules and holes generated ·OH radicals and e^- react with oxygen to produce superoxide ions ($\cdot O^{2-}$). $\cdot O^{2-}$ further reacts with H_2O_2 to produce OH^- ions, which are also converted into ·OH. These ·OH radicals react with dye molecules for mineralization. It was reported that the Ag NPs present in the hydrogel enhanced both photocatalytic and antibacterial activity.

Zero-valent iron has also been incorporated in a GG cross-linked soya lecithin nanocomposite hydrogel (Fe^0@GG-cl-SY NCH) via the ultrasonication method and used for the MV dye photocatalytic degradation.[271] Fe^0@GG-cl-SY NCH could successfully degrade 81% MV in 120 min in the presence of H_2O_2 under natural sunlight irradiation. High adsorption efficiency and photo-response characteristics of the hydrogel nanocomposite facilitate the photocatalytic degradation of the dye molecules. The degradation of dye was also studied with and without H_2O_2. The maximum photo-degradation of MV (81%) was observed in the presence of H_2O_2, whereas Fe^0@GG-cl-SY NCH could degrade only 68% of the dye molecule in the

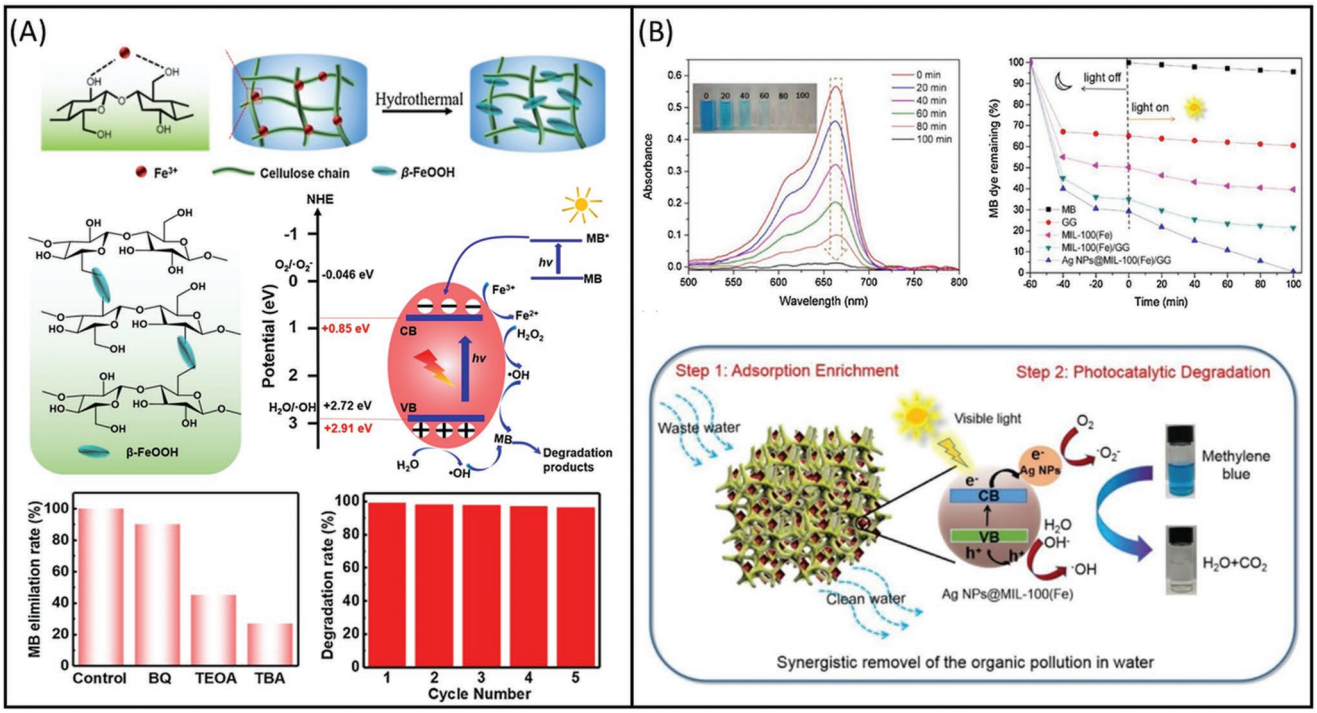

Figure 21. A) Schematic representation of β-FeOOH@tunicate cellulose hydrogel nanocomposite fabrication; mechanism of MB dye photocatalytic degradation using β-FeOOH@tunicate cellulose; effect of scavenger on MB photo-degradation and recyclability of β-FeOOH@tunicate cellulose hydrogel nanocomposite. Reproduced with permission.[261] Copyright 2020, Elsevier Science Ltd. B) UV–vis absorbance spectra of MB dye photo-degradation and percentage of remaining MB dye in solution after visible light illumination using Ag NPs@MIL-100(Fe)/GG as photocatalyst with different time intervals; mechanism of MB dye adsorption and photocatalytic degradation in the presence of Ag NPs@MIL-100(Fe)/GG hydrogel nanocomposite. Reproduced with permission.[270] Copyright 2020, Elsevier Science Ltd.

absence of H_2O_2. In the MV photocatalytic degradation process, dye molecules are initially adsorbed on the hydrogel nanocomposite surface. Under sunlight irradiation, electrons and holes are generated, which initiate the formation of free radicals. The addition of H_2O_2 further improved photo-degradation by generating more free radicals.

There are several other magnetic hydrogel nanocomposites that have been used as adsorbents in wastewater treatment. **Table 3** lists the application of various magnetic hydrogel nanocomposites to remove several types of water pollutants. Thus, apart from the removal of water contaminants from wastewater, the incorporation of iron and iron oxide in hydrogel nanocomposites ease the recovery of nanocomposite via the application of an external magnetic force. Integration of iron oxide NPs with several other hydrogel nanocomposites to improve the recovery, reusability, and performance can be studied for wastewater treatment via enhanced adsorption as well as photocatalysis.

6.4. Metal Sulfide-Based Hydrogel Nanocomposites

Metal sulfides, such as MoS_2,[295,296] CdS,[297] ZnS,[298] FeS,[299,300] and NiS,[34] are semiconductor materials that are incorporated with hydrogels to enhance the visible light adsorption properties and improve other hydrogel nanocomposite characteristics, such as mechanical strength, selective adsorption, and ease the separation. However, little work has been done in this direction. MoS_2 is actively being used in wastewater treatment as an adsorbent and photocatalyst.[301–304] Wang et al.[305] fabricated a MoS_2-embedded smart PNIPAm hydrogel nanocomposite using NIPAm monomers via a simple photo-initiated polymerization for selective Ag^+ adsorption. In a photo-initiated polymerization process, photo-initiators adsorb a particular frequency of light to initiate the polymerization process by producing free radicals.[306] The MoS_2-PNIPAm hydrogel nanocomposite material was added to an aqueous solution containing several ions (Ag^+, Ca^{2+}, Cd^{2+}, K^+, Zn^{2+}, and Mg^{2+}) and showed high selective adsorption towards Ag^+. The high affinity of sulfur atoms (soft base) in MoS_2 nanosheets towards Ag^+ (soft acid) promotes this selective adsorption according to the hard-and-soft-acids-and-bases) principle.[305] MoS_2 nanosheets and PNIPAm polymer exhibit noncovalent interactions, enabling direct heat transfer from MoS_2 to the polymer chains under photo-thermal induction. Therefore, the MoS_2-PNIPAm hydrogel nanocomposite quickly shrinks following a burst release of Ag^+ after adsorption under near-infrared (NIR) laser irradiation (808 nm) and is effectively regenerated for use in several cycles successfully. The MoS_2 nanosheets ease the desorption process by "squeezing out" activity under NIR irradiation.

The photo-regeneration of an adsorbent can also be achieved by degrading the adsorbed pollutant molecule under light irradiation, which offers an economical approach to hydrogel nanocomposites in wastewater treatment. Porous MoS_2-hydroxypropyl cellulose (HPC) (MoS_2-HPC/HPC) hydrogel nanocomposite was fabricated for the adsorption and photo-degradation of water-soluble dyes.[295] **Figure 22**A

Table 3. Various magnetic hydrogel nanocomposites as adsorbents for the removal of several organic/inorganic water pollutants.

Magnetic hydrogel	Water pollutant	Experimental conditions	Adsorption capacity [mg g^{-1}]	Ref.
NCHG (Fe_3O_4/polystyrene-co-polymethacrylic acid/co (sodium styrene sulfonate – acrylic acid)/PAM)	Cs(I) Co(II) Sr(II)	T = 25 °C time = 2 h pH = 4	66.12 96.95 76.25	[272]
Chitosan-Fe(III)	Acid Red 73	T = 25 °C time = 30 min pH = 12	294.5	[264]
γ-Fe_2O_3 based magnetic cationic hydrogel	Acid Red 27 Acid Orange 52	T = 22 °C time = 5 min pH = 5.5–7.5	833 1430	[273]
Fe_2O_3/xylan/poly(acrylic acid)	MB	T = 25 °C time = 48 h pH = 8	438.6	[263]
Chitosan/alginate/Fe_3O_4 @SiO2	Pb(II)	T = 20 °C time = 480 min pH = 4.2	234.77	[274]
Polyacrylamide/ chitosan/Fe_3O_4	MB	T = 25 °C time = 120 min pH = 7	1603	[275]
Lignin derivate magnetic hydrogel microspheres	MB MO MG Pb(II) Hg(II) Ni(II)	T = RT time = 24 h pH = 3–7	43 39 155 33 55 23	[276]
Magnetic hydrogel beads (MHB2)	Cr(VI)	T = 25 °C time = 24 h pH = 2	476.2	[264]
Magnetic PVA/sodium alginate/laponite RD	bovine serum albumin (BSA)	T = 25 °C time = 24 h pH = 4.5	127.3	[277]
Magnetic rGO-loaded PEGDMA	MB Cr(VI)	T = 25 °C time = 12 h pH = 7.4 & 4	119 313	[278]
Magnetic polyvinyl alcohol/laponite RD (PVA-mLap)	Cd(II)	T = 293K time = 10 h pH = 2	908 μmol g^{-1}	[279]
Magnetic PVA/chitosan	Co(II)	T = 30 °C time = 18 h pH = 6	14.39	[280]
Lanthanum-loaded magnetic cationic hydrogel	F^-	T = 25 °C time = 5 h pH = 7	136.78	[281]
carboxymethyl starch-g-poly(vinyl imidazole/ PVA/ Fe_3O_4(CMS-g-PVI/PVA/Fe_3O_4)	CV CR Pb(II) Cu(II) Cd(II)	T = 25 °C time = 0.5 – 24 h pH = 2–8	91.58 93.66 65.00 83.60 53.2	[282]
Fe_3O_4@SiO2/GO	CV	T = RT time = 120 min pH = 7	769.23	[283]
Fe_3O_4NPs/CS/glyoxal	Cr(VI)	T = 25 °C time = 110 min pH = 4	55.8	[284]
Gg-cl-PAA/Fe_3O_4	MB	T = 25 °C time = 24 h pH = 7	671.14	[285]

Table 3. Continued.

Magnetic hydrogel	Water pollutant	Experimental conditions	Adsorption capacity [mg g^{-1}]	Ref.
Fe_2O_3 based Magnetic hydrogel	Cr(VI)	T = 22 °C time = 240 min pH = 4.2	205	[286]
Poly(vinyl acetate-co-maleicanhydride)/melamine /Fe_3O_4.	CR	T = 25 °C time = 60 min pH = 5	48.6	[287]
Gum Acacia /polyvinyl pyrrolidone/SiO_2	Fuchsine basic (FC) MO	Temp: 25 °C Time: 300 min pH: 11 & 5	91.49 36.41	[288]
Alg/Fe_3O_4@C@TD	Tetracycline (TC) Amoxicillin (AMX)	Temp: 25 °C Time: 32 h pH: 5 & 7	476.19 416.67	[289]
γ-Methacryloxypropyl trimethoxysilane (KH570)-modified magnetic hydrogel	Pb(II)	Temp: RT Time: 120 min pH: 4.5	450	[290]
Arabic gum-g-polyamidoxime/$CuFe_2O_4$	Chlorpyrifos	Temp: 25 °C Time: 20 min pH: 6	769.23	[291]
Chitin/egg shell membrane @Fe_3O_4	Pb(II)	Temp: 20 °C Time: 24 h pH: 5	0.079 mmol g^{-1}	[292]
Chitosan/polypropenoic acid/ethylenediamine/ magnetite (Cs/PPA/EDA/Fe_3O_4-NPs)	Astrazon blue Lerui Acid Brilliant Blue	Temp: RT Time: 24 h pH: 10 & 3	193.21 51.9	[293]
CMC-Fe_3O_4	MB	Temp: 25 °C Time: 240 min pH: neutral	6.13	[294]

summarizes the preparation of the MoS_2-HPC/HPC hydrogel nanocomposite and its application to MB dye adsorption and photo-induced regeneration. To regenerate the hydrogel nanocomposite after the adsorption process, MB adsorbed MoS_2-HPC/HPC was exposed to sunlight for the photo-degradation of MB and regeneration of MoS_2-HPC/HPC for successive cycles. The regeneration potential of 5% MoS_2-HPC/HPC hydrogel nanocomposite is far better than that of the HPC hydrogel following absorption of MB. Moreover, the MoS_2-HPC/HPC hydrogel could also be used to adsorb and catalyze the degradation of other organic dyes.

Chen et al.[308] prepared the MoS_2-GO-based hydrogel (MGH) via hydrothermal synthesis for the photodegradation of MB dye. GO assists as an outstanding charge carrier for semiconductor materials and delays the recombination of e^-/h^+ to enhance photocatalytic characteristics.[202] MGH exhibits a higher photocatalytic degradation ability (99% degradation of MB in 60 min) than the pristine GO hydrogel, which might be due to the increased light adsorption and the delayed photo-induced e^-/h^+ recombination of the semiconductor during photocatalysis.[308] MoS_2-rGO hydrogel nanocomposites have also been studied for the catalytic reduction of PNP in an aqueous solution.[309]

CdS is another popular metal sulfide semiconductor material for the fabrication of hydrogel nanocomposites to enhance the adsorption and photocatalytic potential. Torkaman et al.[307] prepared a CdS quantum dots-based nanocomposite hydrogel (CdS QD-NCH) via in situ cross-linking copolymerization of AA and κ-C using MBA as a cross-linking agent, followed by the embedding of CdS QDs. Figure 22B shows the proposed synthesis route of CdS QD-NCH. CdS QD-NCH was employed for the adsorption and photocatalytic removal of water-soluble cationic dyes, that is, CV and MG. CdS QD-NCH successfully adsorbs the CV and MG dyes and achieves adsorption-desorption equilibrium in 120 and 75 min, respectively. The results reported in Figure 22B suggest that electrostatic interactions are the main driving force for the adsorption of dyes by the hydrogel nanocomposite.

Furthermore, the photocatalytic degradation of adsorbed dye on CdS QD-NCH was performed under visible light in 60 and 30 min for CV and MG, respectively. The regenerated hydrogel nanocomposite could be successfully used for several cycles. The generation of the hydroxyl radical was considered as the main active species for the degradation of the dyes. Similarly, CdS QDs were embedded in the cross-linked polymer chains of CMC and PAMPS to form a hydrogel nanocomposite for the adsorption of RhB dye.[310] The equilibrium swelling capacity of the CdS QD-NCH was observed to be higher than that of the pure hydrogel, which might be due to the higher surface area of CdS QDs. The adsorption of RhB on the CdS QD-NCH could be fitted by the pseudo-second-order kinetics and Langmuir isotherm models. In addition to cationic dyes, CdS-incorporated hydrogel nanocomposites have also been used for the removal of anionic dyes from wastewater.[311] CdS NPs were deposited on the semi-IPN hydrogel network of the AAm-grafted

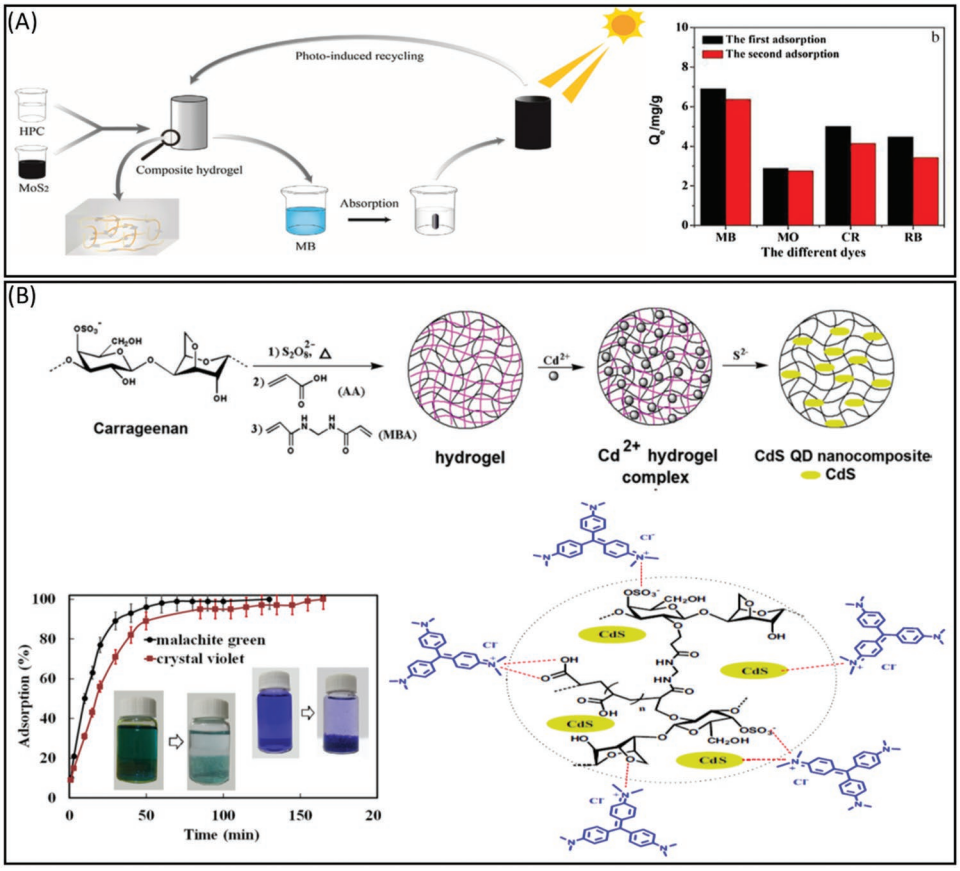

Figure 22. A) Schematic illustration of fabrication, MB dye absorption, and photo-induced recycling of the MoS_2-HPC/HPC hydrogel nanocomposite; 5% MoS_2-HPC/HPC hydrogel for MB and other different dyes. Reproduced with permission.[295] Copyright 2017, Elsevier Science Ltd. B) In situ preparation of CdS quantum dots in a hydrogel network; Adsorption of MG and CV dye with contact time; Possible electrostatic interactions between CdS QD-NCH hydrogel nanocomposite and dye. Reproduced with permission.[307] Copyright 2019, Springer Nature.

xanthan-agar hybrid. The hydrogel nanocomposite effectively adsorbs the anionic dyes eosin yellow and eriochrome black-T, following a Langmuir isotherm, and could be regenerated for successive batches.

On the other hand, Kumar et al.[34] showed that the nickel sulfide (NiS/Ni_3S_4) NPs incorporated PAAm-grafted GK hydrogel bio-nanocomposite (BioNC) is an excellent choice for the adsorption of RhB dye from the wastewater. The prominent interaction forces between cationic dye and BioNC were identified as van der Waals forces, H-bonding, and electrostatic interactions. The maximum adsorption capacity of BioNC for RhB adsorption was 1244.7 g L^{-1}. The RhB adsorption on BioNC followed the Langmuir isotherm and pseudo-second-order kinetics rate model. BioNC also showed excellent reusability following easy separation. The photo-degradation of RhB dye was also efficiently achieved using the CuS@corn starch/chitin hydrogel nanocomposite.[312] Under NIR irradiation, CuS promotes the formation of hydroxyl radicals from H_2O_2, which directly degrades the RhB dye. Another CuS-based 3D hydroxyethyl acrylate/N-methyl maleic acid hydrogel nanocomposite (P(HEA/NMMA)-CuS) also showed high photo-degradation efficiency for the antibiotic sulfamethoxazole under visible light.[313] Initially, the adsorption of sulfamethoxazole on the surface of P(HEA/NMMA)-CuS followed a Langmuir adsorption and pseudo-second-order kinetic model. The adsorbed sulfamethoxazole was photodegraded, following pseudo-first-order kinetics. The generation of active hydroxyl radicals was proven for the photo-degradation of sulfamethoxazole, and complete degradation was achieved by the formation of eight primary intermediates of sulfamethoxazole. Panchal et al.[298] prepared a sodium alginate/gelatin-based ZnS-hydrogel nanocomposite (SA-Gel-cl-PAAm/ZnS) for the removal of dyes via adsorption. SA-Gel-cl-PAAm/ZnS could efficiently remove 95.26% and 91.68% of the biebrich scarlet and CV dyes, respectively. The removal of biebrich scarlet followed the Langmuir isotherm and pseudo-first-order kinetics. In contrast, the removal of CV was followed by the Freundlich isotherm and pseudo-second-order kinetics. Desorption of dyes from the hydrogel nanocomposite was performed by treating the adsorbent in a 0.1 NaOH and 0.1 HCl solution, and it could be reused for several cycles.

The excellent regeneration ability of hydrogel nanocomposites enhances their potential for use as an environmentally friendly and efficient material for the removal of water pollutants from industrial wastewater. In summary, the most explored metal sulfide-based hydrogel nanocomposites for wastewater treatment involve MoS_2. However, there is a broad scope to examine the efficiency of several combinations of metal sulfides and hydrogels for wastewater treatment. Metal

sulfides are also known for their photocatalytic activity. Therefore, there is a need to study various metal sulfide and hydrogel nanocomposites for wastewater treatment as photocatalysts.

6.5. Graphene and Graphene Oxide-Based Hydrogel Nanocomposites

Graphene and its derivatives have been studied in various applications due to their outstanding characteristics.[314,315] However, graphene sheets are hydrophobic, and the strong π-π interactions between the graphene sheets lead to aggregation, which makes graphene sheets less ideal for direct application due to their poor stability. Therefore, much interest has been devoted to developing graphene-based nanocomposite materials for various applications.[316–319] Graphene-based nanocomposite materials can be easily synthesized and fabricated either by chemical functionalization or noncovalent modifications.[320,321] Constructing 3D graphene macroscopic structures, such as graphene-based hydrogels consisting of a porous structure embedded with graphene sheets, can partially overcome the intrinsic π-π interactions. 3D graphene-based hydrogels have great potential in various applications, including wastewater treatment, by enabling the diffusion of water pollutants into the 3D macroscopic structural network.[322–324] These nanocomposites exhibit enhanced adsorption efficiency due to increased surface area, improved mechanical strength and stability, thermal stability, high negative charge density, recyclability, and avoiding agglomeration of nanomaterials.[118] Owing to the high negative charge density and hydrophilic moieties in the GO skeleton, it is easy to disperse GO in polymer systems.

Graphene/alginate-based hydrogel nanocomposites have been actively used to remove various contaminants from wastewater.[325,327–331] Luo et al.[325] prepared a Y-immobilized-graphene oxide-alginate hydrogel nanocomposite (Y-GO-SA) for the simultaneous adsorption of heavy metal ion As(V) and antibiotic tetracycline (TC) from the wastewater. The co-adsorption of As(V) and TC was pH-dependent and showed the highest adsorption at pH 5 and 8, respectively. **Figure 23**A illustrates all the possible interactions for the adsorption of TC

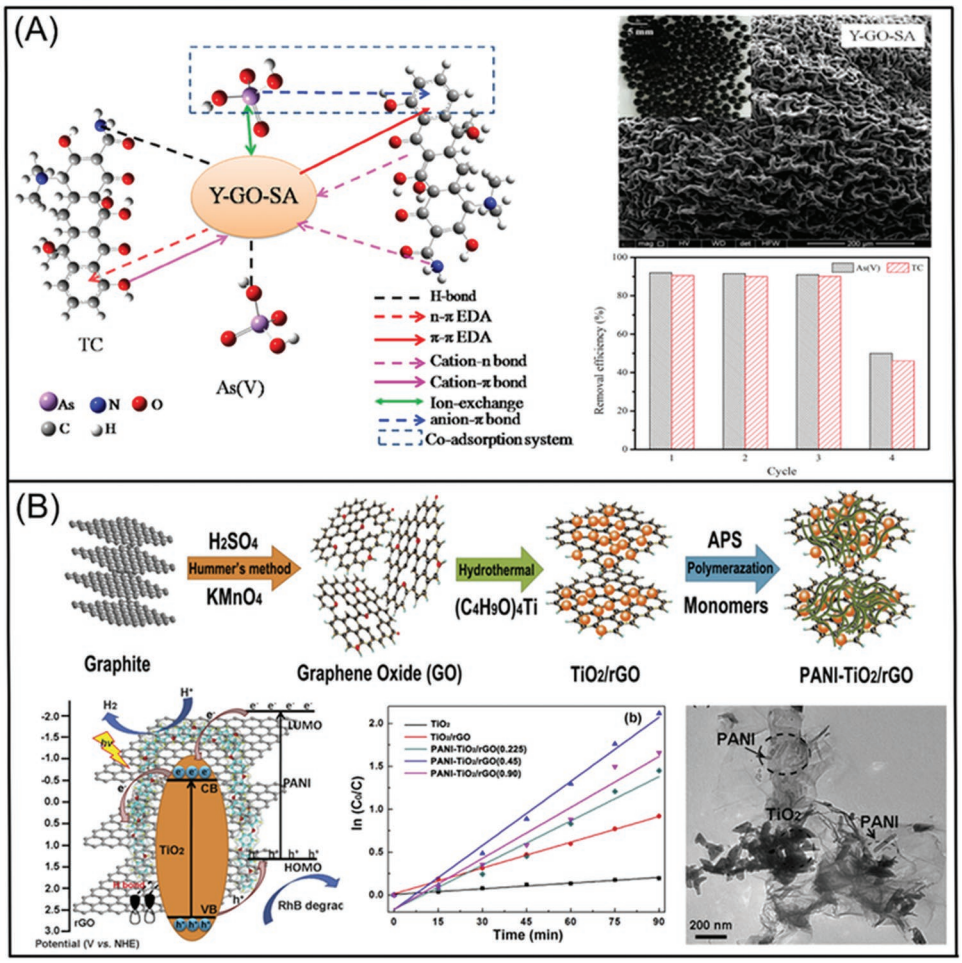

Figure 23. A) Schematic illustration of As(V) and TC co-adsorption mechanisms onto Y-GO-SA hydrogel nanocomposite; effect of pH on co-adsorption of TC and As(V) in binary system and recyclability of Y-GO-SA hydrogel nanocomposite for As(V) and TC removal for four cycles. Reproduced with permission.[325] Copyright 2020, Elsevier Science Ltd. B) The stepwise synthetic procedure, TEM image and photocatalytic efficiency of PANI-TiO_2/rGO hydrogel; photocatalytic mechanism of RhB in the presence of PANI-TiO_2/rGO hydrogel under visible light irradiation. Reproduced with permission.[326] Copyright 2020, Elsevier Science Ltd.

and As(V) on Y-GO-SA. The adsorption of TC was higher than that of As(V) on Y-GO-SA. This was ascribed to the presence of amino and hydroxyl groups on TC, which can easily form stable complexes with Y-GO-SA via multiple H-bonds, π-π electron-donor acceptor interaction between TC and GO, n-π electron donor-acceptor interaction between TC and SA.

Additionally, at pH 5, TC exists in a neutral or cationic form, which could bind to the adsorbed negatively charged As(V) through anion-π interactions through multilayer adsorption. As(V) adsorption was ascribed to H-bonding and ion exchange. Therefore, in the binary system, the adsorption of TC suppressed the adsorption of As(V) by occupying the active sites. In contrast, the adsorption of As(V) promoted the adsorption of TC via the formation of a sorbent-As-TC complex through anion-π interactions. The Y-GO-SA hydrogel also exhibits excellent reusability.

It has been noted that GO-based hydrogels are usually prepared via physical cross-linking approaches.[332] The absence of chemical cross-linkers also reduces the potential risk of toxicity. The primary interactions between the GO and polysaccharides in hydrogels are electrostatic forces. GO nanosheets and chitosan chains are cross-linked via electrostatic interactions between positively charged chitosan and negatively charged GO to form a chitosan/graphene oxide (GC) hydrogel network structure. A GC hydrogel column has been used to clean dye-contaminated wastewater, showing excellent adsorption potential toward cationic (MB and RhB) and anionic (MO and CR) dyes.[333] The hydrogel composite could easily be regenerated for successive adsorption cycles with retention of high adsorption efficiency.

A GO-impregnated chitosan-PVA hydrogel (GC-PVA) was prepared and evaluated for the adsorption of the CR dye under different experimental conditions from wastewater.[334] The adsorption of the CR dye was significantly improved after impregnating the chitosan-PVA hydrogel with GO. This might be due to the improved porosity and stability of the hydrogel nanocomposite following GO-impregnation.

Shen et al.[335] designed a highly porous and reactive hydrogel composed of live *Shewanella xiamenensis* BC01 bacteria encapsulated within an rGO network for the adsorption and biodegradation of the CR and MB dyes. Owing to synergetic effects, BC01-BCH showed exceptional decolorization performance and degraded the CR and MB dyes up to 99.8% and 97.3% in 55 h, respectively. Several graphene-based hydrogels have been studied as suitable adsorbents for the removal of water pollutants. **Table 4** summarizes the adsorption efficiency of different graphene-based hydrogel nanocomposites employed for the removal of several water pollutants.

In addition to adsorption, graphene-based hydrogel nanocomposites are also employed as efficient photocatalysts for the degradation of organic water pollutants. Ma et al.[326] prepared the PANI-TiO_2/rGO hydrogel nanocomposite via in situ polymerization of aniline on the surface of TiO_2/rGO. They observed excellent photocatalytic RhB degradation and H_2 evolution under visible light irradiation. A schematic presentation of the formation of PANI-TiO_2/rGO is presented in Figure 23B. PANI-TiO_2/rGO could effectively photodegrade 90.5% RhB within 90 min under visible light irradiation, which is significantly higher than pristine TiO_2 (24.7%). To achieve an effective photo-degradation, the loading of PANI was varied and optimized in the PANI-TiO_2/rGO hydrogel. As shown in Figure 23B, under light irradiation, TiO_2 and PANI generated e^- and h^+ charge carriers that were rapidly separated due to the rGO nanosheets, which restricted their recombination and promoted the photocatalytic reaction.

Similarly, Liang et al.[349] used the metal-free g-C_3N_4@PPy-rGO hydrogel as a photocatalyst to adsorb and photodegrade Cr(VI) and phenol from wastewater. The PPy and rGO in the hydrogel skeleton consist of a π-π conjugation system, which improves the separation of photo-generated charge carriers, alters the valence band edges of the g-C_3N_4, and enhances the photo-oxidation stability of the hydrogel nanocomposite material. Upon visible light exposure, g-C_3N_4 is excited and generates charge carriers, while rGO transfer the e^- to photo-reduce Cr(VI), and PPy transfer the holes to photo-oxidize the phenol. The synergic adsorption and photocatalysis degradation of water pollutants was achieved in situ, avoiding the complicated operation needed to recover and regenerate the catalyst following the reaction. The recyclability of g-C_3N_4@PPy-rGO hydrogel was maintained for ten consecutive cycles. **Table 5** summarizes the use of various graphene-based hydrogel nanocomposites for the photo-degradation of water pollutants. As evident from the ample number of examples, graphene-based hydrogel nanocomposites are one of the most widely explored classes of hydrogel nanocomposites as adsorbents as well as photocatalysts in water treatment applications. The ease of functionalization and excellent characteristics of graphene make it a popular choice for several applications. However, the photocatalytic applications of graphene-based hydrogel nanocomposites are scarce. In addition, there is a need to study various metallic/non-metallic/metal oxide NPs incorporated graphene-based hydrogel nanocomposites as photocatalysts for the treatment of wastewater.

6.6. CNTs and Other Carbonaceous Materials-Based Hydrogel Nanocomposites

Apart from graphene, other carbonaceous materials (e.g., CNTs, carbon spheres, carbon quantum dots, g-C_3N_4, and carbon nanofibers) have also been physically or chemically combined with hydrogel matrices and applied in various applications, including water treatment.[46,360]

Most recently, CNTs-based hydrogels have been utilized in wastewater treatment as adsorbents and photocatalysts.[361,362] Sun et al.[363] prepared an organic-inorganic hemicellulose-g-poly(methacrylic acid)/CNT composite hydrogel to adsorb the MB dye from the water. Various adsorption parameters, such as the effect of adsorbent amount, initial concentration of dye, contact time, and salt concentration, were also thoroughly investigated to optimize the adsorption conditions. 98% MB dye was successfully adsorbed from the contaminated water using 6 g L^{-1} hemicellulose-g-poly(methacrylic acid)/CNT hydrogel. FTIR was performed before and after adsorption to analyze the adsorption mechanism, and the results are shown in **Figure 24**A. The extra vibrational signatures that appear in the FTIR spectrum of the hydrogel following MB adsorption correspond to the functional groups of MB, confirming the

Table 4. Adsorption Capacity of various graphene-based hydrogels for water contaminants.

Graphene-based hydrogel	Water pollutant	Experimental conditions	Adsorption capacity [mg g^{-1}]	Ref.
3D graphene (3DG)	MB	T = RT t = 270 min	310	[336]
GO-loaded agarose hydrogel beads (GO-AgarBs)	RhB Orange G Aspirin	T = RT T = 5–12 h	321.7 132.1 196.4	[337]
Cellulose nanowhisker GO (GO/CNW) hydrogel	MB RhB	T = 298 K pH = 7 time = 20 & 40 min	122.5 62	[338]
β-cyclodextrin/chitosan functionalized GO (3D-GO/CS/β-CD)	MB	T = 298K time = 240 min pH = 12	1134	[339]
Prussian blue functionalized graphene (PB/rGOH)	Cs	T = 298 K time = 72 h	58.82	[340]
3D yttrium based-graphene oxide-sodium alginate (Y-GO-SA1.0)	F	T = 20 °C time = 48 h pH = 4	289	[331]
GO/Chitosan–PVA	CR	T = RT time = 150 min pH = 2	12.386	[334]
rGO–SA hydrogel microspheres	Phenol, Bisphenol A (BPA) tetracycline	T = 315.15 K time = 4 h pH = 6	26.12 17.31 14.12	[330]
GO/Chitosan	MB	T = 318 K time = 48 h pH = 7	275.5	[341]
Y-GO-SA	As (V) TC	T = RT time = 90 min pH = 5	274 478	[325]
Alginate/graphene double network (GAS) Alginate/graphene double network (GAD)	TC TC	T = 298K time = 20 h pH = 8	247 290	[329]
Lignosulfonate-modified graphene hydrogel (LGH)	Cr(VI)	T = 328K time = 18 h pH = 2	1743.9	[342]
Chitosan–polyethylenimine–GO (CS–PEI–GO)	Se	T = 298K time = 24 h pH = 3	1.62	[130]
GO-poly(2-hydroxyethyl methacrylate)	MB	T = 318.15K time = 45 min pH = 7	39.41	[343]
PVA/CMC-B@GO/Fe3O4/GQD	MB	T = 313K time = 4 h pH = 8	1000	[344]
Bacterial Cellulose/Polyvinyl Alcohol/Graphene Oxide/Attapulgite (BC/PVA/GO/APT)	Cu(II) Pb(II)	T = RT time = 360 min pH = 5 & 6	150.8 217.8	[345]
GO Reinforced Alginate/PVA Double Network Hydrogels	MB	T = 298 K time = 15 h pH = 6.5	480	[327]
3D RGO	Naproxen (NPX), Ibuprofen (IBP) Diclofenac (DFC)	T = RT time = 1 h pH = neutral	357 500 526	[346]
GO-starch nanocomposite (GO-HES)	MG	T = RT time = 30 h pH = 4.5	57.5	[347]
$CaCO_3$/PAN-PPy-modified GO/alginate	Cu(II)	T = 298 K time = 24 h pH = 5	291.2	[348]

Table 5. Photocatalytic degradation of various water pollutants using graphene-based hydrogels.

Graphene-based hydrogel	Water pollutant	Experimental Conditions	% Degradation	References
g-C_3N_4/GO/ polyacrylic acid (CGP)	MB RhB	Visible light Temp = RT time = 30 min	98 70.1	[350]
rGH-AgBr@rGO	BPA	Visible light time = 60 min	91.4	[351]
PANI-TiO_2/rGO	RhB	Visible light time = 90 min	90.5	[352]
Poly(vinyl alcohol)/poly(acrylic acid)/TiO_2/GO	Coomassie brilliant blue R-250 (CBB) MB	UV light pH = 10 time = 200 min	88 95	[353]
TiO_2/graphene	MB	UV light time = 30 min	100	[354]
P25–graphene	MB	UV light time = 60 min	96	[355]
N-doped graphene	Acridine orange (AO)	Visible light time = 5 h	70	[356]
ZnO/rGO–rGH hydrogel	Bisphonol A	UV lamp (250 W Hg) Temp = 25 ± 2 °C Time = 20 min	100	[357]
3D TiO_2-graphene hydrogel	Cr(VI)	UV lamp (250 W Hg) Temp = 25 ± 2 °C Time = 30 min	100	[358]
3D Ag_3PO_4-graphene hydrogel	Bisphenol A	Visible light (250 W metal halide) Temp = 25 ± 2 °C Time = 12 min	100	[359]
MoS_2–GO composite hydrogel	MB	Solar light Temp = RT Time = 60 min	99	[308]

adsorption of the MB dye on the hydrogel nanocomposite. Additionally, the pH of the solution was reduced from 5.3 to 3.35 after the adsorption of MB, suggesting that the adsorption took place via ion-exchange, as depicted in Figure 24A. The adsorption of MB followed the Freundlich isotherm and pseudo-second-order kinetics. In another study, CNTs were impregnated into chitosan hydrogel beads (CSBs), following four strategies: by dispersing CNTs in a) a chitosan solution (CSBN1), b) a sodium dodecyl sulfate (SDS) solution (CSBN2), c) a CS solution containing cetyltrimethylammonium bromide (CTAB) (CSBN3), and d) an SDS solution with CTAB and CS (CSBN4), and compared the adsorption of CR dye by each.[364] The Sips model was used to calculate the maximum adsorption capacity, and CSBN4 showed the largest (375.94 mg g^{-1}), while CSBN3 showed the lowest (121.07 mg g^{-1}) adsorption capacity for CR.

Baruah et al.[365] studied a carbon dots-chitosan hybrid hydrogel (CS-$NaSO_3$-CDs) for water remediation. The carbon dots in the hydrogel effectively improved the mechanical stability, water swelling characteristics, and adsorption of ions and water pollutants.[366] The CS-$NaSO_3$-CDs hydrogel nanocomposite film successfully adsorbs up to 94% Ca^{2+} and 70.8% Mg^{2+}, whereas the pristine CS-film could adsorb only 32.9% Ca^{2+}.[365] The adsorption of metal ions followed an ion-exchange mechanism for Na^+. **Table 6** lists notable carbon-based hydrogel nanocomposites as potential adsorbents for water pollutants.

Graphitic C_3N_4 (g-C_3N_4) is an attractive member of the carbonaceous materials family. It is frequently used as a metal-free photocatalyst due to its tunable electronic structure, excellent response to visible light, and chemical stability.[379,380] However, the low surface area, fast recombination of photo-induced electron-hole pairs, and difficulty in recycling limit the application of pristine g-C_3N_4. However, the construction of 3D structured g-C_3N_4 nanocomposites promotes charge separation, enhances the adsorption efficiency, and improves the surface area to expose more active sites.[381,382] Additionally, the separation of g-C_3N_4 hydrogel nanocomposites after the application is straightforward. Shafiee et al.[377] studied the adsorption-assisted photocatalytic potential of the g-C_3N_4/Co_3O_4/MWCNT nanocomposite stabilized in resorcinol formaldehyde hydrogel towards organic pollutant (RhB) degradation in water. They compared the surface area of all synthesized nanocomposites (hydrogel, g-C_3N_4 in hydrogel, Co_3O_4 in hydrogel, g-C_3N_4/Co_3O_4 in hydrogel, and g-C_3N_4/Co_3O_4/MWCNT in hydrogel). They found that g-C_3N_4/Co_3O_4/MWCNT in hydrogel exhibit the highest surface area. Figure 24B shows the removal efficiency of RhB under dark and light conditions, revealing that using all the prepared nanocomposites exhibit efficient catalytic efficiency toward the degradation of RhB. However, owing to its high active surface area, g-C_3N_4/Co_3O_4/MWCNT adsorb and degrade the most dye under dark and light conditions. Figure 24C shows the preparation of the PAAm/g-C_3N_4/PAA

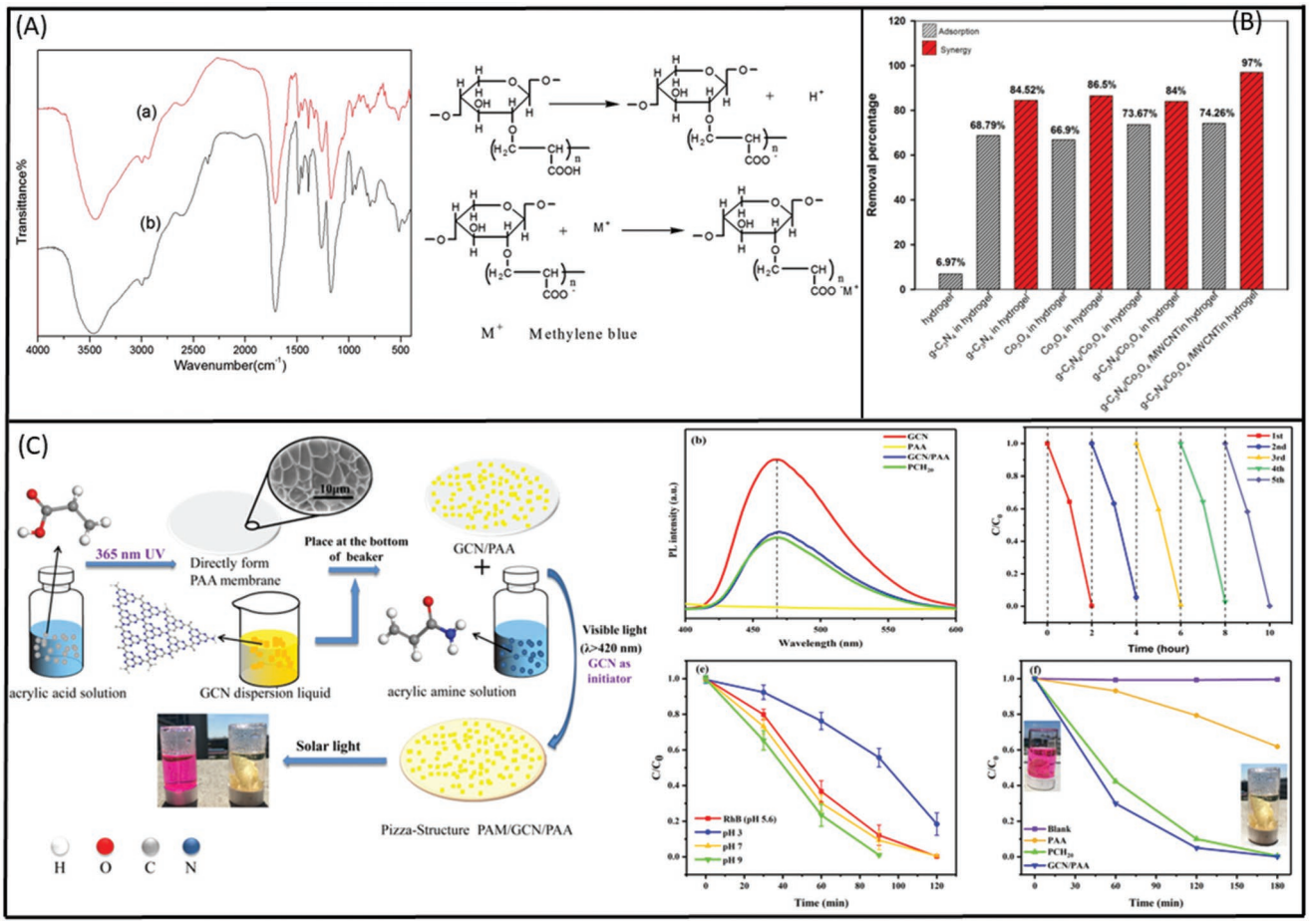

Figure 24. A) IR spectra of hydrogel nanocomposite (a) before and (b) after MB dye adsorption and most probable mechanism for MB adsorption on hemicellulose-g-poly(methacrylic acid)/CNT hydrogel nanocomposite. Reproduced with permission.[363] Copyright 2014, Wiley. B) Comparison of several hydrogel nanocomposites to remove RhB from wastewater. MWCNT/Co_3O_4/g-C_3N_4 shows the highest RhB removal percentage. Reproduced with permission.[377] Copyright 2019, Springer Nature. C) Schematic representation of the stepwise preparation of PCH20 and the RhB photo-degradation under solar light; PL spectra of all samples; effect of pH and photocatalytic performance of all samples on photodegradation of RhB; reusability characterization of PCH20 for five cycles. Reproduced with permission.[378] Copyright 2020, Elsevier Science Ltd.

hydrogel composite (PCH20) and its application in the photodegradation of RhB dye.[378] To prepare the PCH hydrogel, AA was polymerized under an inert atmosphere and UV irradiation, and g-C_3N_4 was added to the PAA film. The PAA/g-C_3N_4 composite was immersed in an AAm solution under visible light irradiation and nitrogen atmosphere to form PCH. The degradation of RhB was performed under solar light irradiation using PCH as a photocatalyst. The adsorption of RhB by PCH was ascribed to electrostatic interactions between carboxylate groups and RhB. Subsequently, g-C_3N_4 induced the photo-charge carriers to produce active species, which completely oxidized the RhB dye into CO_2 and H_2O (Figure 24C). The photodegradation is highly pH-dependent, as depicted in Figure 24C. Higher degradation was observed at pH > 5.6. As shown in Figure 24C, the photoluminescence spectra of all the synthesized materials suggest that introducing PAA into g-C_3N_4 or PAAm into PAA/g-C_3N_4, significantly increased the charge-carrier mobility and reduced the rate of charge-pair recombination. PCH was also found to be excellent recyclability for five cycles without compromising the photocatalytic activity.

In summary, it can be concluded that, in addition to graphene-based hydrogel nanocomposites, the study of carbon-based hydrogel nanocomposites in water treatment is sparse and need to be analyzed. CNT-based hydrogel nanocomposite is rarely investigated as a photocatalyst in water purification. Other carbon derivatives, such as quantum dots, carbon spheres, and carbon nanofibers, should also be incorporated into various hydrogels and investigated for water treatment.

6.7. Clay/LDHs-Based Hydrogel Nanocomposites

Clays are naturally occurring layered silicates of fine-sized particles with metal oxides and organic matter in trace amounts. Generally, natural clay consists of sheets of silicon and aluminum oxide in different ratios, for example, kaolinite (1:1), vermiculite and montmorillonite (2:1), and chlorite (2:2). The application of clay in water treatment is invaluable, because they are affordable, environmentally friendly, reliable, abundantly available, and exhibit good wettability. However, the poor

Table 6. Adsorption of water contaminants using various carbon-based hydrogels.

Carbon-based hydrogel	Water pollutant	Experimental conditions	Adsorption capacity [mg g^{-1}]	Ref.
Chitosan impregnated with CNT	CR	Temp 30 °C Time = 24 h pH 5	450.4	[367]
Carrageenan/MWCNT	CV	Temp 30 °C Time = 24 h pH 5	118	[368]
Tragacanth gum/carboxyl-functionalized CNT	MB	Temp 40 °C Time = 40 min pH 11	647	[369]
Chitosan/CNT	Phenol	Temp 30 °C Time = 120 min pH 6.5	404.2	[370]
Carbon dot cross-linked polyvinylpyrrolidone	MG CV Eosin Y	Temp RT Time = 12 h pH 8	20.16 23.11 30.45	[371]
CNT/GO/sodium alginate	CIP	Temp 25 °C Time = 60 h pH4-6	181	[372]
Chitosan/CNT	CR	Temp 30 °C Time = 24 h pH 5	423.34	[373]
Lignin/cellulose fibers/carbon dots	Cr(VI)	Temp RT Time = 200 min	599.9	[374]
Cellulose nanofibrils/ carbon dots	Fe(III) Ba(II) Pb(II) Cu(II)	Temp 25 °C Time = 100 min	769, 212, 2056 1246	[375]
CNT/Chitosan	CR	Temp 30 °C Time = 24 h pH 5	375.4	[364]
g-C_3N_4@SBC/CMC	MB	Temp 25 °C Time = 120 min pH 8	362.3	[376]

regeneration and low adsorption capacity demote the use of natural clays as adsorbents to clean the water. At the same time, the fabrication of clay into the polymer matrix as clay-based hydrogels is an advanced class of adsorbent materials, which can successfully remove contaminants from wastewater.[383] In clay-based hydrogels, the introduction of clay into the polymer matrix enhances the mechanical strength, water wettability, pH sensitivity, active surface area, easy regeneration, and reduces the cost. Moreover, the choice of clay and polymer matrix in hydrogel can be utilized to fabricate pollutant-specific adsorbents with high adsorption capacity.

The structure of clay generally exhibits negative charges. Therefore, clay-modified hydrogels have been used to remove cationic contaminants from wastewater.[384–386] Mahdavinia et al.[384] demonstrated the use of κ-carrageenan-g-poly(acrylamide)/sepiolite hydrogel nanocomposite for the removal of CR dye from wastewater. Nano sepiolite clay was used as filler in the hydrogel matrix without any chemical modification. The dye adsorption capacity of the hydrogel with sepiolite clay was higher than that of pristine hydrogel without clay. The same group also observed similar results upon using a sodium montmorillonite nanoclay embedded in a hydrogel for the removal of CV.[385,386] The inclusion of nanoclay enhances the negative charge density in a hydrogel and, thus, increases the adsorption capacity of cationic dyes. The adsorption of CV using sodium montmorillonite nanoclay-modified hydrogel followed the Freundlich isotherm and pseudo-second-order kinetics.[385] Recently, Qi et al.[387] employed a PDA/montmorillonite (MMT)-embedded pullulan hydrogel nanocomposite for the adsorption of CV dye. The hydrogel nanocomposite exhibited a high adsorption capacity (112.45 mg g^{-1}), following the Langmuir isotherm and pseudo-second-order kinetics. **Figure 25**A shows that PDA and MMT clay alone form a sludge in the water after the adsorption of CV dye and are hard to separate. However, co-doping PDA and MMT on the pullulan hydrogel improves the separation after the adsorption process and avoids secondary waste generation. The adsorption of CV on the hydrogel nanocomposite primarily involves electrostatic interactions between MMT and cationic CV dye and π-π interaction between the aromatic rings of the adsorbate and adsorbent (Figure 25A). The selectivity of the clay-based hydrogel towards cationic dyes was also investigated. As reported in Figure 25A,

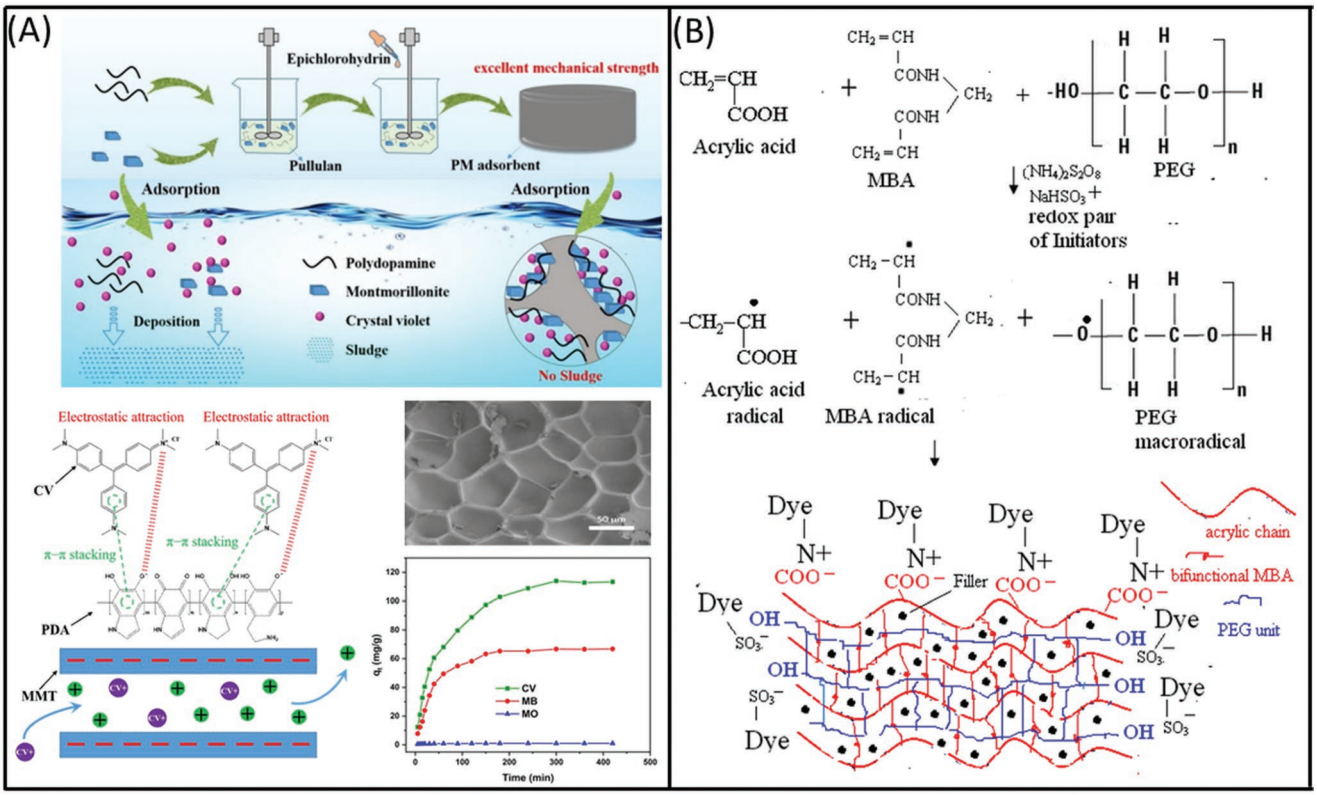

Figure 25. A) Synthesis and adsorption representation using PDA/MMT hydrogel; Adsorption mechanism of CV on PDA/MMT hydrogel and adsorption selectivity of PDA/MMT hydrogel. Reproduced with permission.[387] Copyright 2021, Elsevier Science Ltd. B) Representation of formation of the clay-based PEG/PAA hydrogel and its interaction with dyes. Reproduced with permission.[388] Copyright 2015, Elsevier Science Ltd.

the PDA/MMT-embedded pullulan hydrogel efficiently adsorb the cationic dyes (CV, MB) but failed to remove the anionic dye.

In addition to cationic pollutants, clay-based hydrogels have also been employed for the removal of anionic contaminants in wastewater. Ray et al.[388] synthesized a series of clay-based PEG/PAA hydrogels with different loadings of nano bentonite clay (0.5 wt.%, 1.0 wt.%, and 1.5 wt.%) as filler for the adsorption of CR and MV dye from wastewater. Figure 25B shows the synthesis of the PEG/PAA/nano bentonite clay-based hydrogel and its application in dye removal via adsorption. A crosslink co-polymerization was initiated in an aqueous PEG solution with AA using MBA as a crosslinker via free-radical polymerization. The concentration of PEG and MBA was varied to prepare a series of hydrogels. The best results were obtained for the hydrogel consisting of 6 wt.% PEG and 1 wt.% nano bentonite clay, showing adsorption capacities of 2227 and 1927 mg g^{-1} for CR and MV, respectively. A bentonite clay-incorporated cellulose-based hydrogel exhibited enhanced adsorption capacity toward anionic azo dyes.[389] The adsorption capacity reached 45.77 mg $g^{-1,}$ and the adsorption mechanism was governed by physisorption. **Table 7** summarizes the adsorption of various cationic pollutants using clay-based hydrogel nanocomposites.

LDHs, known as hydrotalcite, are synthetic clays with anionic layered exchange materials. They can be represented using the general formula $[M^{II}_{1-x}M^{III}_{x}(OH)_2]^{x+}(A^{n-})_{x/n}\ mH_2O$), where M^{II} and M^{III} are divalent and trivalent metallic cations, respectively, which are octahedrally coordinated to hydroxide anions.[402] A^{n-} are the replaceable interlayer anions in the LDH, which can be NO_3^-, Cl^-, or CO_3^{2-}, and water molecules are intercalated in the hydroxide layers of LDH. The value of x varies in the range of 0.2–0.33. LDH structures can easily be tuned during the synthesis for a targeted application. LDHs are a versatile class of 2D materials with distinct features, such as low cost, easily tunable structure, replaceable intercalated anions, high surface area, non-toxicity, and multiple chemical functionalities. These outstanding characteristics make LDHs popular in various applications, such as catalysis,[403] fuel cells,[404] adsorption,[402] super-capacitors,[405] CO_2 capture,[406] and drug delivery.[407] LDHs are also conducive to adsorbents for wastewater treatment due to their high surface area, tunable architecture, non-toxicity, low cost, and exchangeable anionic features.[408,409] Generally, in addition to adsorption via interactions with the functional groups on LDHs, contaminants intercalate into the layered structure of LDHs, which aids in the removal of water contaminants. However, LDHs exhibit low hydraulic conductivity, which makes them less suitable for water application.[410] Therefore, to avoid this issue, LDHs can be combined with other materials. LDHs-based hydrogels are also well-suited for water treatment applications.

Shan et al.[411] embedded different amounts of calcined LDH (CLDH, 0–10%, w/v) into alginate hydrogel beads to prepare hydrogel nanocomposite beads and investigated the suitability of the CLDH-alginate beads for the removal of PNP and p-aminophenol (PAP) from the water. **Figure 26**A

Table 7. Application of various clay-based hydrogel nanocomposites as adsorbents for organic/inorganic water pollutant removal.

Clay-based hydrogel	Water pollutant	Experimental conditions	Adsorption capacity [mg g^{-1}]	Ref.
Sodium alginate-g-poly(sodium acrylate-co-styrene)/ organo-illite/smectite	MB	Temp = 30, 40, and 50 °C Time: 180 min pH = 4	1843.46	[390]
Alginate–montmorillonite	Polychlorinated biphenyl (PCB)	Temp = 25 °C Time: 6 h	0.332	[391]
Poly (β-cyclodextrin-co-citric acid)/ bentonite	MB	Temp = 25 °C Time: 4.5 h pH = 6	806.45	[392]
Polyvinyl alcohol/carboxymethyl cellulose (CMC)/graphene oxide/ bentonite	MB	Temp = 30 °C Time: 240 min pH = 8	172.14	[393]
Montmorillonite supported-poly (acrylamide-co-acrylic acid)	MB	Temp = 30 °C Time: 20 min pH = 8	717.54	[394]
Chitosan–halloysite	MB MG	Temp = 30 °C Time: 120 min	270.27 303.03	[63]
Cellulose / Montmorillonite	MB	Temp = 30 °C Time: 40 h pH = 7	782.9	[395]
TiO_2 @ CMC- chitosan/montmorillonite	MB	Temp = 0, 30, and 60 °C Time: 120 min	283.9	[396]
CMC-cl-pAA/Fe_3O_4-C30B	MB	Temp = 25 and 45 °C Time: 85 min pH = 7	1081.60	[397]
PVA/ Chitosan/ Agar-agar @ Cloisite30B /Fe_3O_4	RhB MB	Temp = 298 K Time: 40 min pH = 7	780 800	[398]
Poly(N-isopropylacrylamide) (PNIPAm)/lithium magnesium silicate hydrate (LMSH)	Amaranth dye	Temp = 25 °C Time: 24 h pH = 2	1.33	[399]
Egg white/PVA/montmorillonite (EW/PVA/MMT)	MB	Temp = 37 °C Time: 720 min pH = 9	2.4	[400]
SAlg/dextrin-cl-PAA/bentonite	Paraquat	Temp = 25 °C Time: 260 min pH = 10	90.9	[401]

shows the removal of PNP and PAP using the various loadings of CLDH in CLDH-alginate beads. It is evident that the adsorption efficiency of alginate is significantly improved by the addition of CLDH, and CLDH-alginate beads could adsorb 98.23% PNP and 36.46% PAP from the wastewater, mainly via H-bonding and anionic exchange. To understand the complete mechanism of PNP and PAP adsorption, DFT theoretical calculations were also performed. Figure 26A shows that the theoretical binding distances for the oxygen atoms in PNP with hydrogen atoms of CLDH are closer than those of the nitrogen and oxygen atoms of PAP. Furthermore, the bond formation between PNP and CLDH is stable, which promotes the adsorption of PNP rather than PAP by the CLDH-alginate hydrogel beads.

A LDH/PAAm hydrogel nanocomposite was prepared via in situ free-radical polymerization using various Co/Al LDH loadings as crosslinkers (0.105%, 0.210%, 0.420%, 0.630%, 0.840%, 1.05%), AAm as monomer, and a $NaHSO_3$ and ammonium persulfate as redox initiator (Figure 26B).[412] The hydrogel formation was governed by the coordination and H-bonding interactions between the amide groups on AAm and hydroxyl groups on Co/Al LDH nanosheets. These LDH-based hydrogels showed a good affinity toward the adsorption of the anionic MO dye. Owing to the positive charge of Co/Al LDH, the adsorption of MO dye was initially fast, and the adsorption capacity of the hydrogel increased with increasing Co/Al LDH loading. The adsorption followed the Langmuir adsorption isotherm and pseudo-second-order kinetics. Moreover, the adsorption of the anionic MO dye was four times higher than that of the cationic MB dye using the Co/Al LDH/PAAm hydrogel (Figure 26B), suggesting that the positively charged Co/Al LDH in the hydrogel skeleton played a vital role in the adsorption of water contaminants.

An Agarose/LDH hydrogel nanocomposite exhibited high adsorption capacity of several anions (viz., SO_4^{2-}, I^-, and HPO_4^{2-}) at room temperature.[413] The adsorption of anions was governed by the ion-exchange mechanism with LDH in

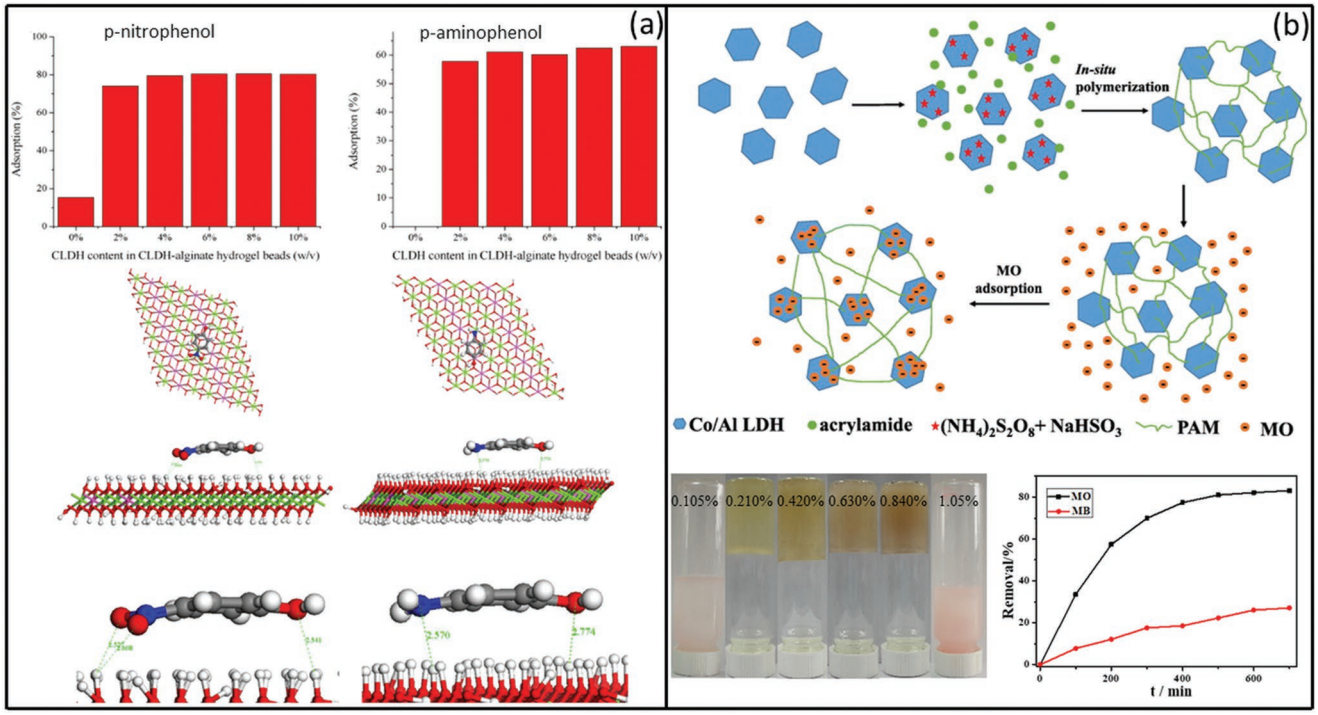

Figure 26. A) Effect of CLDH amount in CLDH-alginate hydrogel beads for PNP and PAP removal; Optimized geometrical structures of the PNP and PAP adsorption on CLDH. Reproduced with permission.[411] Copyright 2018, Elsevier Science. B) Schematic illustration of Co/Al-LDH/PAM NC hydrogel preparation through in situ polymerization and MO dye adsorption; the effect of Co/Al-LDH contents in Co/Al-LDH/PAM NC hydrogels for adsorption of MO and MB using Co/Al-LDH/PAM in the binary system. Reproduced with permission.[412] Copyright 2019, Elsevier Science Ltd.

the hydrogel nanocomposite. However, the hydrogel nanocomposite lacked selectivity. Recently, chloride-containing LDH-based superadsorbent was prepared by immersing PAA in an aqueous suspension of LDH particles.[414] Two types of LDHs were employed: chloride-containing LDH prepared by the co-precipitation method without further treatment (COP-LDH) and hydrothermally treated COP-LDH (HYD-LDH). Both LDH-based hydrogel nanocomposites were used for the adsorption of SO_4^{2-} anion from wastewater. During hydrogel formation, LDH particles were trapped between the macroscopic gaps within the polymer and improved the swelling properties of the hydrogel. Although the carboxylate group of the polymer had a negative effect on the adsorption of anions via electrostatic repulsion, the HYD-LDH-based hydrogel successfully adsorbs 86% of the SO_4^{2-} anion from water. Therefore, it can be concluded that clay/LDH-based hydrogel nanocomposites are highly efficient adsorptive materials and successfully adsorb both cationic and anionic contaminants. The low cost and abundant availability of clay/LDH make them desirable materials in water treatment applications. However, clay/LDH-based hydrogel nanocomposites have only been studied as adsorbent materials. Therefore, their potential as photocatalyst is yet to be explored.

6.8. MXene-Based Hydrogel Nanocomposites

Apart from the discussed materials, several other nanomaterials have been incorporated into hydrogels and used as adsorbents and photocatalysts to remove water contaminants. Still, they have not been explored much to the same extent. MXenes are a member of the 2D nanomaterial family and have been utilized in hydrogel matrix nanocomposites to enhance the water contaminant removal efficiency of hydrogels.[415–417] MXenes exhibit the general chemical formula, $M_{n+1}X_nT_x$, where M is an early transition metal (e.g., Mo, Nb, Ti, and V), X is carbon and/or nitrogen, T_x represents surface functional groups (e.g., −OH, −F, and −O), and n can be any number between 1 and 4.[418–420] The formulation of MXenes into a hydrogel matrix allows the preparation of MXene-based soft nanocomposites with tailorable properties. In addition, it enhances the stability of both nanocomposites, overcoming a common factor for their limited application.

Yang et al.[416] immobilized $Ti_3C_2T_x$ powder on SA to form SA-$Ti_3C_2T_x$ hydrogel beads and investigated its capability for the adsorption of MB dye from water solution. The effect of the mass ratio of $Ti_3C_2T_x$ and SA was also analyzed to optimize the adsorption of MB. As the MXene hydrogel content increased, the MB adsorption also increased. $Ti_3C_2T_x$/SA-30% showed the highest adsorption (98.04%) under the test conditions, while pristine SA could adsorb 45.51% MB. This MXene-based hydrogel could also be regenerated easily and used in successive cycles. The adsorption was observed to be well-fitted with pseudo-second-order kinetics and the Langmuir isotherm. The adsorption process was driven by both internal and external diffusion. Lu et al.[417] used the PAAm/MXene hydrogel nanocomposite for the removal of MB dye. The adsorption is mainly attributed to the electrostatic interaction between the cationic water pollutant and the negatively charged hydrogel

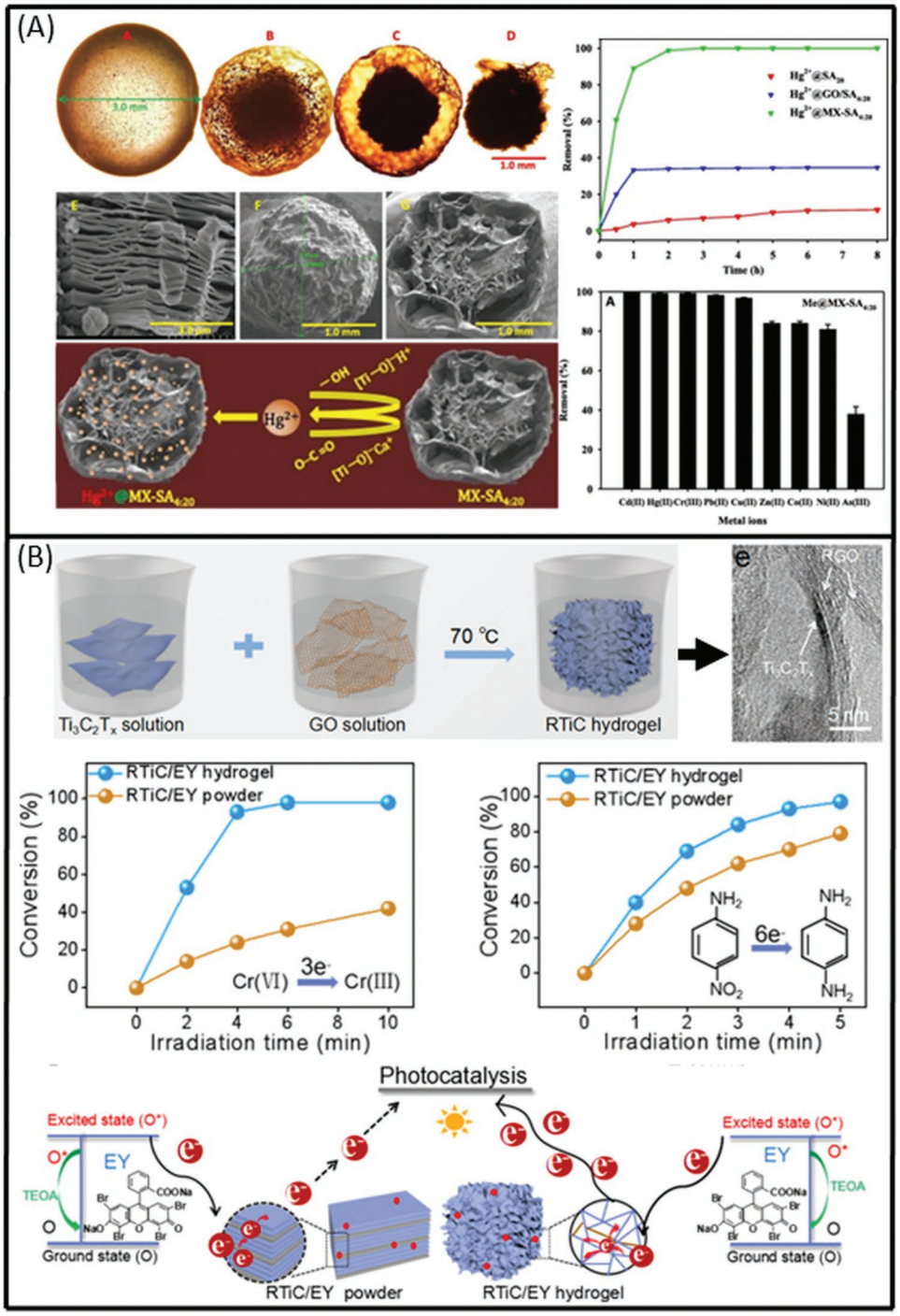

Figure 27. A) Optical microscopic images of $Ti_3C_2T_x$-SA4:20 (A) hydrogel (≈3 mm), (B) after vacuum freeze-drying (≈2 mm), (C) cross-sectional view, and (D) core of $Ti_3C_2T_x$-SA4:20 spheres; SEM images of $Ti_3C_2T_x$-SA before and after drying; Illustration of Hg^{2+} ions uptake onto $Ti_3C_2T_x$-SA4:20; Adsorption of Hg^{2+} using several hydrogel beads and adsorption of metal ions in the multi-component system using $Ti_3C_2T_x$-SA4:20. Reproduced with permission.[421] Copyright 2019, Elsevier Science Ltd. B) Fabrication process and HRTEM image of RTiC/EY hydrogel; Comparison of RTiC/EY powder and hydrogel for Cr(VI) and p-nitroaniline photocatalytic conversion; Mechanism of photocatalytic conversion of Cr(VI) and p-nitroaniline using RTiC/EY in the presence of visible light illumination. Reproduced with permission.[422] Copyright 2018, American Chemical Society.

nanocomposite, which promoted the multi-layer adsorption of MB dye in the pores of the hydrogel.

In another study, $Ti_3C_2T_x$-SA hydrogel spheres were prepared for the removal of mercury ions.[421] Optical images of $Ti_3C_2T_x$-SA hydrogel spheres revealed that the spheres are ≈3 mm in diameter in wet form and ≈2 mm in diameter in dry form (**Figure 27**A). In contrast, SEM images indicated a core-shell structure. $Ti_3C_2T_x$-SA absorbed Hg(II) with outstanding

adsorption capacity (932.84 mg g^{-1}), representing 100% removal efficiency. This adsorption efficiency of $Ti_3C_2T_x$-SA was substantially higher than that of pristine SA and GO/SA (Figure 27A). After Hg(II) adsorption, the hydrogel spheres were regenerated in an acidic medium and used for consecutive cycles. This hydrogel nanocomposite was also employed for the removal of several other toxic metals. It could remove Cr, Co, Ni, Cu, and Zn with 90% removal capacity and Pb, Hg, and Cd with 80% removal capacity (Figure 27A). The mechanism of toxic metal adsorption involves complex formation between [Ti—O]—H^+ and Hg^{2+}, electrostatic interactions, and ion exchange between Ca^{2+} and Hg^{2+}.

MXene-based hydrogels have also been explored for photocatalytic degradation. Chen et al.[422] developed an organic-free synthetic strategy to construct the $Ti_3C_2T_x$-based hydrogel (RTiC) based on a GO-assisted self-convergence process, as reported in Figure 27B. Furthermore, the $Ti_3C_2T_x$-based hydrogel was integrated with photosensitizer (Eosin Y) (RTiC/EY) and used to photodegrade Cr(VI) and p-nitroaniline in water. Under visible light illumination, the RTiC/EY hydrogel nanocomposite photocatalytically reduced Cr(VI) into Cr(III) with 99.3% efficiency in 10 min, whereas RTiC/EY powder could reduce only reduce 41.6%. Similarly, the RTiC/EY hydrogel nanocomposite catalyzed the photocatalytic hydrogenation of p-nitroaniline into p-phenylenediamine with 97% efficiency in 5 min. In comparison, the RTiC/EY powder could reduce only 79% under similar conditions (Figure 27B). Because structure dictates the characteristics and application of a material, the interconnected porous system of the RTiC/EY hydrogel plays a vital role in improving photocatalytic efficiency. The RTiC/EY hydrogel exhibits a high surface area (approximately twice that of the RTiC/EY powder), which improves the adsorption of the reactant and facilitates the interaction between the adsorbed reactant and photo-generated charge pairs for photocatalytic degradation. Despite several advantages, MXenes-based hydrogel nanocomposites are a sparsely explored class of hydrogel nanocomposites in wastewater treatment.

6.9. MOFs-Based Hydrogel Nanocomposites

MOFs are an emerging class of materials suitable for various applications, including wastewater treatment.[423] The outstanding characteristics of MOFs, such as high surface area, tunable porosity, various functional groups, and ease of modification without altering the framework topology, make them popular candidates as an adsorbent and catalyst in water purification. However, MOFs have several challenges to their practical applications, such as high rigidity, brittleness, and less-than-satisfactory processability.[424] Therefore, designing stable and flexible MOF-based nanocomposites represents a significant step toward improving the practical performance of MOFs. Hydrogels based on MOFs have traditionally been considered one of the most effective methods to enhance the stability and utility of MOFs. Although MOF-based hydrogels have been explored for wastewater treatment, it is still a relatively unexplored material class for environmental remediation.

The 3D network of a hydrogel promotes the dispersion of the crystalline MOF material, which enhances the potential of nanocomposite in water purification. Controlling the diffusion kinetics and sustaining the hierarchical porosities of MOFs in hydrogel nanocomposites is one of the significant challenges for the practical handling of the material. Entrapping the MOFs in the hydrogel is one solution to address this limitation. Polymers have also been widely used to grow and disperse MOFs due to their adjustable functionalities. Recently, a MOF-based hydrogel was prepared in situ by using a zinc hydroxide PAAm composite as the precursor gel.[425] The prepared ZIF-8-PAAm MOF-hydrogel nanocomposite could efficiently remove humic acid from contaminated water, exhibiting a maximum adsorption capacity of 111.5 mg g^{-1}. The nanocomposite exhibited the high porosity of ZIF-8 and swelling characteristics of the hydrogel.

Zhu et al.[426] reported a straightforward in situ growth method to prepare a MOF-alginate nanocomposite, which was used to remove RhB dye via adsorption from contaminated water efficiently. Shi et al.[36] reported a one-step synthesis method to prepare alginate-based Co-MOF hydrogel nanocomposite to adsorb TC from wastewater. The one-step synthesis strategy involved the concurrent gelation of the hydrogel matrix and the formation of the MOF via the simultaneous chelation of CO^{2+} with alginate and 2-methylimidazole (ligand). The MOF-based hydrogel showed excellent adsorption characteristics towards TC (adsorption capacity of 364.89 mg g^{-1}) and favorable reusability. Electrostatic interactions were the driving force between the negatively charged adsorbate and positively charged adsorbent.

3D printing technology is a fascinating approach to creating innumerable high-resolution structures from digital models.[427] This technique has been widely used to tailor the shapes of composite materials for various applications, including biomedicine and catalysts.[428,429] It is also a promising strategy to assemble MOFs into hydrogels. Zhan et al.[430] 3D printed MOF-based hydrogel for water remediation. **Figure 28** shows the preparation technique of 3D printed MOF-based hydrogel and its application in wastewater purification. To prepare the hydrogel, the synthesized MOF (Cu-BTC) was mixed with the polymer solution (SA and gelatin) and used as ink in the 3D printing. Three different shapes (i.e., square, hexagonal, and circle) of the hydrogel material were printed and crosslinked with $CaCl_2$, which further enhanced the mechanical stability (Figure 28A). The hydrogel nanocomposite was used to adsorb five organic dyes (i.e., MB, RhB, MG, MV, and auramine O). Upon introducing the 3D printed MOF-based hydrogel nanocomposite to the dye-contaminated water, it rapidly absorbed the water and dye and swelled to a large extent (Figure 28B). The adsorption of cationic dyes in the hydrogel was mainly governed by electrostatic forces and van der Waals attraction. The swelled 3D printed hydrogel could be easily regenerated in HCl and reused several times. Among the five dyes investigated, the 3D printed MOF-based hydrogel showed excellent potential for the adsorption of MB and MV dyes.

Another 3D printed MOF-based hydrogel was prepared using HKUST-1 and SA-based hydrogel and used for the removal of the dyes MB and Rhodamine 6G (R6G).[152] The printed MOF-based hydrogel exhibits high mechanical strength and could be stretched up to 453% of its original length and could adsorb 96.3% and 33.3% of the MB and R6G dyes, respectively. One of the major advantages of 3D printed hydrogels

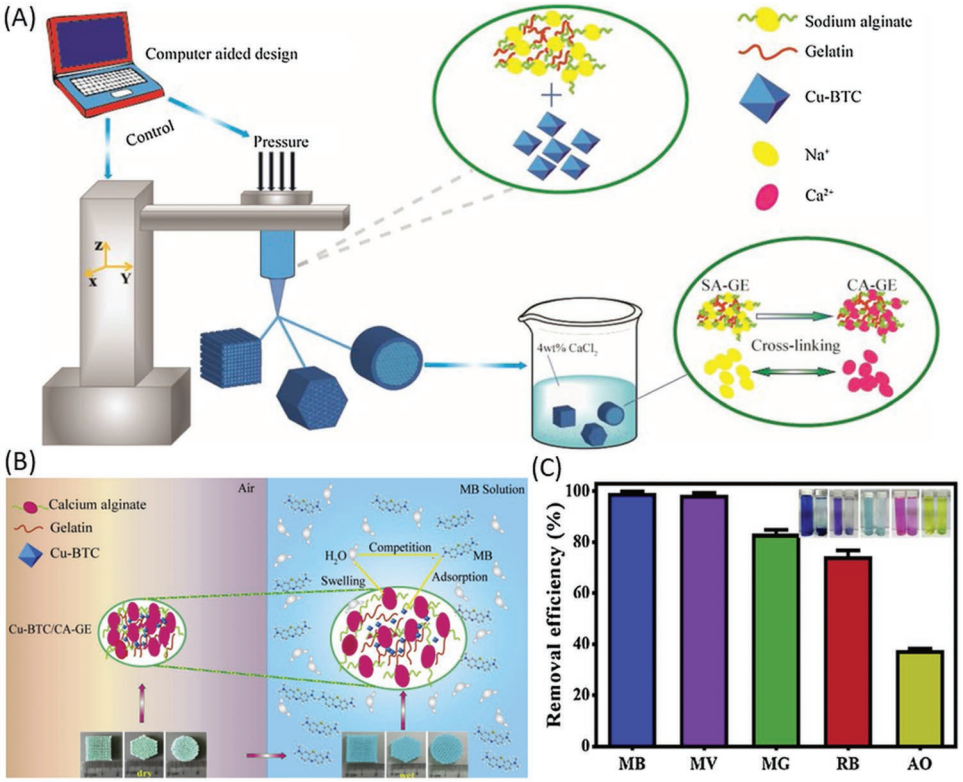

Figure 28. A) Schematic illustration of the preparation of 3D printed MOF-based hydrogel, B) swelling behavior and adsorption of MB dye using 3D printed MOF-based hydrogels, and C) The removal efficiency of hydrogel towards various dyes in the aqueous medium. Reproduced with permission.[430] Copyright 2020, Elsevier Science Ltd.

is the ability to generate a diverse range of shapes with low waste. Graphene-based MOF hydrogels have also been explored to remove water contaminants. One-step synthesis of a highly porous MOF@rGO hydrogel composite was reported for the removal of organic pollutants from wastewater via adsorption and photo-degradation.[431] MOF NPs are decorated on the rGO walls by metal-oxygen covalent bonding and robust electrostatic interactions. The prepared hydrogel nanocomposite could adsorb oil, heavy metal ions, and organic dye from the wastewater and degrades the MB dye under UV irradiation. Analogous MOF-based hydrogels are promising materials for environmental remediation with a wide range of options in shapes, functional groups, high mechanical strength, and excellent regeneration ability. Therefore, there is a need to explore MOF-based hydrogel nanocomposites in water treatment and investigate the effect of their shapes and functional groups on their efficiency as adsorbents and photocatalysts.

7. Conclusion and Future Directions

Hydrogels and their nanocomposites in wastewater purification/treatment are proven to effectively remove a broad class of water pollutants through adsorption and photocatalysis. Many hydrogel properties, such as high-water retention, fast swelling kinetics, fast diffusion process, large surface area, high porosity, ease of modification, permeability, hydrophilicity, and insolubility in water, are conducive to their application in water purification applications. Furthermore, incorporating nanomaterials into hydrogels enhances their overall performance towards eliminating pollutants and improves recyclability and reusability, which improves their applicability in industrial applications. This review encompassed fundamental aspects of hydrogels, gelation chemistry, and the preparation of hydrogel nanocomposite, and discussed the improvement of properties upon the incorporation of nanostructured materials into hydrogels. Additionally, an overview of the most important literature in water treatment using hydrogel nanocomposite as adsorbents and photocatalysts is provided and critically assessed. Various aspects are discussed, such as the recovery and reusability of the hydrogel and adsorption/photocatalytic mechanisms. Among different hydrogel nanocomposites, carbonaceous (e.g., graphene, GO, and CNTs) hydrogels are the most explored adsorbents for effective water treatment due to their large surface area, high porosity, unique surface properties, high chemical stability, easy modification, simple regeneration, and reusability. Magnetic hydrogel nanocomposites are also popular due to their straightforward recovery. At the same time, naturally occurring polysaccharides, such as cellulose (including HEC, MC, and nanocellulose), gums (viz. GG, Gg, and GK), chitin, chitosan, and alginate, were commonly employed to fabricate hydrogel nanocomposites due to high adsorption performance, fast kinetics, and reusability. For photocatalysis, semiconductor metal oxides (viz. TiO_2), g-C_3N_4, CuS, CdS, and graphene-based hydrogel nanocomposites are mainly implemented for photocatalytic degradation of organic

Figure 29. Challenges and opportunities of hydrogel nanocomposites as emerging materials for water treatment applications.

and inorganic contaminants in water treatment due to high surface area, high ionic conduction, and high photogenerated charge carriers. Based on the studied literature, the following reaction scopes and directions are recommended to address current limitations in hydrogel nanocomposite-based wastewater treatment technologies to achieve their full potential and utilization in large-scale water treatment (**Figure 29**).

Despite being well-studied materials, the interactions between hydrogel and H_2O, solvent molecules, or nanomaterials are not entirely understood on a fundamental level. There is a need to fully elucidate the factors that control these interactions by tailoring the constituents of hydrogels. Advanced characterization techniques/tools should be implemented to investigate the polymer-matter interactions and hydrogel-interface interactions with solvents, light/phonon, and electric charge carriers. Additionally, advanced characterization would be helpful in predicting a more precise adsorption/photocatalysis mechanism on hydrogels. Furthermore, the properties prediction using computational modeling based on different polymer backbone interactions with water/solvents is relatively under-explored, possibly owing to the formidable complexity of modeling large molecules such as a polymer.

The cost of hydrogel nanocomposites is a serious challenge that impedes the commercialization of these potent materials for water treatment. Affordable large-scale production of hydrogel materials would reduce the overall cost of the process. Furthermore, 3D printing of hydrogels has emerged as a promising method for developing custom-optimized, bio-based, reusable, and scalable water purification objects (filters, meshes, and membranes). 3D or 4D printing of hydrogel materials provide various surface functionalities with different topographies and morphological shapes that will further enhance performance and ensure their applicability on a large scale. However, very few studies have been conducted on 3D-printed hydrogels for water purification. Thus, more dedicated research is needed to develop intelligent water technologies at an affordable cost. Additionally, the advanced technology integration in the production process would make it a continuous process, reducing costs.

Most of the investigations for water treatment using hydrogel nanocomposites involve lab-based synthetic polluted water consisting of a single pollutant, rather than industrial wastewater with multiple contaminants, such as salts, inorganic ions, and surfactants, besides the primary pollutant. The lab approach may not be able to develop effective adsorbents/photocatalysts to resolve the pollutant problem of real industrial wastewater. Therefore, pilot-scale remediation studies are required to treat mimic industrial water with multiple pollutant systems to validate the knowledge gained for the industrial scale.

Adsorption has been recognized as an effective method for water treatment, but it results in secondary environmental waste. Most of the reported studies investigate the removal of pollutants with little effort dedicated to separating, regenerating, and valorizing the spent adsorbents. Adding magnetic materials to hydrogels is advantageous for saving energy, time, and cost to separate the material after adsorption/photocatalysis. The efficient regeneration/recovery of spent adsorbents depends on the selection of regeneration methods, stability of sorbent materials, type of eluents, and recycling times while ensuring the stability and reusability of the materials. To reduce the environmental footprint, the best way to valorize the secondary waste is to apply it directly/indirectly in sensors, energy, and photocatalysis/catalysis applications and as feed additives, soil conditioners, bioactive, and antibacterial compounds.[432] Moreover, a circular approach could also be used by combining two or three different applications to reduce secondary waste to a minimum.[33] However, smart strategies are still needed to solve the issue of secondary waste in adsorption processes. On the other hand, effective photocatalysis does not produce secondary environmental waste as it completely degrades the pollutant into water and carbon dioxide.

Many hydrogel nanocomposites do not demonstrate high adsorption capacity after regeneration. The pre-treatment, chemical, and physical modifications (with polymers or inorganic materials) of a hydrogel can improve the overall adsorption/photocatalysis performance, regeneration, and recyclability. Pre- and post-treatment of hydrogel materials could introduce additional functions that would synergistically enhance the functionalities for water purification and allow them to be explored in various emerging applications.

Hydrogel nanocomposites with high thermal/mechanical stability and increased swelling capacity are required for wastewater treatment at the high-temperature conditions of the industrial waste stream—repeated swelling-deswelling results in a decrease in mechanical strength and, consequently, loss of performance. Chemical cross-linking enhances mechanical stability and performance. Moreover, it is further necessary to explore new ways to improve the mechanical resilience of

composites with, for example, improvement in self-healing capability after a swelling. The problems associated with pH sensitivity, chemical/thermal stability, and swelling ratio still need to be addressed for the full-scale implementation of hydrogel nanocomposites.

Moreover, it is challenging to transfer results from laboratory batch studies to industrial water treatment plants due to up-scaling constraints. This can be solved by integrating data science/machine learning into water treatment technology. Furthermore, the performance of an adsorbent/photocatalyst is greatly affected by the complexity of water elements in real wastewater. Applying advanced machine learning models to batch-study performance data and characteristics of materials could quickly predict the practicability of a material based on the kind of targeted water-effluent system. Thus, technology integration offers a rapid and higher water technology transfer success rate for real-world applications. Furthermore, the economic feasibility of a process is equally vital for large-scale operations.

The utilization of nanomaterials for environmental applications has been an ongoing concern and the subject of debate over environmental safety and potential risks. It has been noted that the incorporation of nanomaterials into nanocomposites could reduce their toxicity.[433] Herein, developing hydrogel nanocomposites with biocompatible polymers and nanomaterials via transforming the nanomaterials suspension/powder to 3D interconnected macroscopic polymers could prevent the leakage of nanomaterials, promoting water protection and sustainability. Furthermore, hydrogel nanocomposites have been proven as valuable materials for water purification, but more research should be conducted on their toxicity to elucidate the potential risks and toxicological effects on human health and the environment.

Despite recent progress, photocatalysis based on hydrogel nanocomposites is still in the budding phase of development. Many hurdles remain to enhance photocatalytic performance and stability to fulfill the requirement of pilot-scale/industrial operations. Besides having high surface area, exposed active sites, and high adsorption capacity, the efficiency of hydrogel nanocomposite-based photocatalysts is not highly satisfactory, possibly due to the high recombination of photo-generated charge carriers and several thermodynamic constraints. Most reported studies focused on casual co-mixing of semiconductor photocatalysts and gel networks, which restricts the ample exposure of photo-catalytically active sites. Hydrogel dryness is a serious problem, resulting in complicated operation, difficult separation, and secondary waste due to catalyst leakage. Therefore, innovative strategies are needed to improve the photocatalytic performance of 3D hydrogel nanocomposites for effective water treatment. To solve the drawbacks of existing hydrogel-based photocatalysts, pre-treatment, such as interfacial modification of polymer monomers and photocatalytic materials and modulation of the gel matrix, would be beneficial for obtaining effective performance and recyclability of photocatalytic hydrogels.

Furthermore, the photoelectric synergy may enhance photocatalytic efficiency as the electric field would boost the charge separation and migration in an interconnected 3D network and resolve the problem of thermodynamic constraints. Moreover, combined integrated hydrogel technologies may be developed using the concept of adsorption synergized photocatalysis to overcome issues of water treatment and CO_2 capture and conversion. Hydrogel materials can also be implemented in seawater desalination, atmospheric moisture harvesting, anti-biofouling/microbial treatment, and solar water evaporation to resolve the scarcity of clean water.

Overall, this review encourages more scientific interest in the tailorable synthesis of hydrogel and hydrogel nanocomposites for applications in water and wastewater treatment using adsorption and photocatalysis. It would also inspire researchers to apply hydrogel nanocomposites in energy applications (e.g., batteries, supercapacitors, and electro-/photo-catalyst for energy production), wearable electronics, and biomedical applications due to their versatile properties and flexibility.

Acknowledgements

N.K. and R.G. contributed equally to this work. The authors acknowledge the funding support from the Department of Science and Innovation (C6ACH77), the Council for Scientific and Industrial Research (C6ACH20), and the University of Johannesburg (086310), for their financial support.

Conflict of Interest

The authors declare no conflict of interest.

Keywords

3D printed hydrogels, biopolymer-based materials, hydrogels, nanomaterials, surface chemistry, water

Received: June 20, 2022
Revised: September 19, 2022
Published online: November 30, 2022

[1] T. Oki, S. Kanae, *Science* **2006**, *313*, 1068.
[2] M. M. Mekonnen, A. Y. Hoekstra, *Sci. Adv.* **2016**, *2*, e1500323.
[3] S. S. Ray, R. Gusain, N. Kumar, *Carbon nanomaterial-based adsorbents for water purification: Fundamentals and applications*, Elsevier, Amsterdam **2020**.
[4] I. V. Kirstein, A. Gomiero, J. Vollertsen, *Curr. Opin. Toxicol.* **2021**, *28*, 70.
[5] R. Bain, R. Johnston, T. Slaymaker, *npj Clean Water* **2020**, *3*, 37.
[6] S. Bolisetty, M. Peydayesh, R. Mezzenga, *Chem. Soc. Rev.* **2019**, *48*, 463.
[7] V. K. Gupta, I. Ali, T. A. Saleh, A. Nayak, S. Agarwal, *RSC Adv.* **2012**, *2*, 6380.
[8] N. Yanar, P. Kallem, M. Son, H. Park, S. Kang, H. Choi, *J. Ind. Eng. Chem.* **2020**, *91*, 1.
[9] B. P. Chaplin, *Acc. Chem. Res.* **2019**, *52*, 596.
[10] S. K. Loeb, P. J. J. Alvarez, J. A. Brame, E. L. Cates, W. Choi, J. Crittenden, D. D. Dionysiou, Q. Li, G. Li-Puma, X. Quan, D. L. Sedlak, T. David Waite, P. Westerhoff, J.-H. Kim, *Environ. Sci. Technol.* **2019**, *53*, 2937.
[11] S. S. Ray, A. O. C. Iroegbu, *ACS Omega* **2021**, *6*, 4511.
[12] J. R. Werber, C. O. Osuji, M. Elimelech, *Nat. Rev. Mater.* **2016**, *1*, 16018.

[13] R. Zhang, Y. Liu, M. He, Y. Su, X. Zhao, M. Elimelech, Z. Jiang, *Chem. Soc. Rev.* **2016**, *45*, 5888.
[14] B. Wang, W. Liang, Z. Guo, W. Liu, *Chem. Soc. Rev.* **2015**, *44*, 336.
[15] A. Mudhoo, D. Mohan, C. U. Pittman, G. Sharma, M. Sillanpää, *J. Environ. Chem. Eng.* **2021**, *9*, 105380.
[16] D. Zhu, Q. Zhou, *Environ. Nanotechnol., Monit. Manage.* **2019**, *12*, 100255.
[17] M. Ateia, D. E. Helbling, W. R. Dichtel, *ACS Mater. Lett.* **2020**, *2*, 1532.
[18] M. Mahinroosta, Z. Jomeh Farsangi, A. Allahverdi, Z. Shakoori, *Mater. Today Chem.* **2018**, *8*, 42.
[19] I. Gibas, H. Janik, *Chem. Chem. Technol.* **2010**, *4*, 297.
[20] K. Sharma, B. Kaith, V. Kumar, S. Kalia, V. Kumar, H. Swart, *Geoderma* **2014**, *232*, 45.
[21] M. C. Catoira, L. Fusaro, D. Di Francesco, M. Ramella, F. Boccafoschi, *J. Mater. Sci.: Mater. Med.* **2019**, *30*, 115.
[22] B. Maji, S. Maiti, *Carbohydr. Polym.* **2021**, *251*, 117095.
[23] L. Weerasundara, B. Gabriele, A. Figoli, Y.-S. Ok, J. Bundschuh, *Crit. Rev. Environ. Sci. Technol.* **2021**, *51*, 1970.
[24] V. Sinha, S. Chakma, *J. Environ. Chem. Eng.* **2019**, *7*, 103295.
[25] P. Mohammadzadeh Pakdel, S. J. Peighambardoust, *J. Environ. Manage.* **2018**, *217*, 123.
[26] P. Mohammadzadeh Pakdel, S. J. Peighambardoust, *Carbohydr. Polym.* **2018**, *201*, 264.
[27] W. Cui, J. Ji, Y.-F. Cai, H. Li, R. Ran, *J. Mater. Chem. A* **2015**, *3*, 17445.
[28] A. K. Gaharwar, N. A. Peppas, A. Khademhosseini, *Biotechnol. Bioeng.* **2014**, *111*, 441.
[29] Z. Wu, P. Zhang, H. Zhang, X. Li, Y. He, P. Qin, C. Yang, *J. Hazard. Mater.* **2022**, *421*, 126754.
[30] K. Yu, D. Wang, Q. Wang, *Polymers* **2018**, *10*, 880.
[31] G. Sharma, B. Thakur, M. Naushad, A. Kumar, F. J. Stadler, S. M. Alfadul, G. T. Mola, *Environ. Chem. Lett.* **2018**, *16*, 113.
[32] H. Mittal, A. Al Alili, P. P. Morajkar, S. M. Alhassan, *Int. J. Biol. Macromol.* **2021**, *167*, 1248.
[33] N. Kumar, H. Mittal, S. M. Alhassan, S. S. Ray, *ACS Sustainable Chem. Eng.* **2018**, *6*, 17011.
[34] N. Kumar, H. Mittal, V. Parashar, S. S. Ray, J. C. Ngila, *RSC Adv.* **2016**, *6*, 21929.
[35] X. Zhang, I. Elsayed, C. Navarathna, G. T. Schueneman, E. I. B. Hassan, *ACS Appl. Mater. Interfaces* **2019**, *11*, 46714.
[36] Y. Zhuang, Y. Kong, X. Wang, B. Shi, *New J. Chem.* **2019**, *43*, 7202.
[37] C. Duan, C. Liu, X. Meng, K. Gao, W. Lu, Y. Zhang, L. Dai, W. Zhao, C. Xiong, W. Wang, Y. Liu, Y. Ni, *Carbohydr. Polym.* **2020**, *230*, 115642.
[38] X. Wang, X. Wang, J. Yin, N. Li, Z. Zhang, Y. Xu, L. Zhang, Z. Qin, T. Jiao, *Composites, Part B* **2022**, *241*, 110052.
[39] J. Ma, M. Zhang, M. Ji, L. Zhang, Z. Qin, Y. Zhang, L. Gao, T. Jiao, *Int. J. Biol. Macromol.* **2021**, *193*, 2221.
[40] A. Katzenberg, A. Raman, N. L. Schnabel, A. L. Quispe, A. I. Silverman, M. A. Modestino, *React. Chem. Eng.* **2020**, *5*, 377.
[41] W. Lei, N. Suzuki, C. Terashima, A. Fujishima, *Front. Energy* **2021**, *15*, 577.
[42] W. Jiang, Y. Zhu, G. Zhu, Z. Zhang, X. Chen, W. Yao, *J. Mater. Chem. A* **2017**, *5*, 5661.
[43] E. M. Ahmed, *J. Adv. Res.* **2015**, 6, 105.
[44] S. Nangia, S. Warkar, D. Katyal, *J. Macromol. Sci., Part A* **2018**, *55*, 747.
[45] K. Yang, Q. Han, B. Chen, Y. Zheng, K. Zhang, Q. Li, J. Wang, *Int. J. Nanomed.* **2018**, *13*, 2217.
[46] J. Anjali, V. K. Jose, J.-M. Lee, *J. Mater. Chem. A* **2019**, *7*, 15491.
[47] A. G. Pereira, F. H. Rodrigues, A. T. Paulino, A. F. Martins, A. R. Fajardo, *J. Cleaner Prod.* **2021**, *284*, 124703.
[48] L. Weerasundara, B. Gabriele, A. Figoli, Y.-S. Ok, J. Bundschuh, *Crit. Rev. Environ. Sci. Technol.* **2021**, *51*, 1970.
[49] M. Khan, I. M. Lo, *Water Res.* **2016**, *106*, 259.
[50] Y. Zhang, Q. Cheng, C. Wang, H. Li, X. Han, Z. Fan, G. Su, D. Pan, Z. Li, *Chemosphere* **2021**, *279*, 130927.
[51] S. Perumal, R. Atchudan, T. N. J. I. Edison, R. S. Babu, P. Karpagavinayagam, C. Vedhi, *Metals* **2021**, *11*, 864.
[52] K. Zhang, X. Luo, L. Yang, Z. Chang, S. Luo, *ACS ES&T Water* **2021**, *1*, 1098.
[53] F. N. Muya, C. E. Sunday, P. Baker, E. Iwuoha, *Water Sci. Technol.* **2015**, *73*, 983.
[54] V. Van Tran, D. Park, Y.-C. Lee, *Environ. Sci. Pollut. Res.* **2018**, *25*, 24569.
[55] F. Ganji, F. S. Vasheghani, F. E. Vasheghani, *Iran. Polym. J.* **2010**, *19*, 375.
[56] Y. S. Zhang, A. Khademhosseini, *Science* **2017**, *356*, eaaf3627.
[57] Y. Sekine, T. Ikeda-Fukazawa, *J. Chem. Phys.* **2009**, *130*, 034501.
[58] Y. Du, E. Lo, S. Ali, A. Khademhosseini, *Proc. Natl. Acad. Sci. USA* **2008**, *105*, 9522.
[59] K. Haraguchi, *Colloid Polym. Sci.* **2011**, *289*, 455.
[60] A. Sydney Gladman, E. A. Matsumoto, R. G. Nuzzo, L. Mahadevan, J. A. Lewis, *Nat. Mater.* **2016**, *15*, 413.
[61] S. V. Murphy, A. Atala, *Nat. Biotechnol.* **2014**, *32*, 773.
[62] G. Nie, Y. Zang, W. Yue, M. Wang, A. Baride, A. Sigdel, S. Janaswamy, *Carbohydr. Polym. Technol. Appl.* **2021**, *2*, 100074.
[63] Q. Peng, M. Liu, J. Zheng, C. Zhou, *Microporous Mesoporous Mater.* **2015**, *201*, 190.
[64] X. Wang, S. Jing, Z. Hou, Y. Liu, X. Qiu, Y. Liu, Y. Tan, *J. Mater. Sci.* **2018**, *53*, 15009.
[65] N. M. Oliveira, Y. S. Zhang, J. Ju, A.-Z. Chen, Y. Chen, S. R. Sonkusale, M. R. Dokmeci, R. L. Reis, J. F. Mano, A. Khademhosseini, *Chem. Mater.* **2016**, *28*, 3641.
[66] B. E. Kelly, I. Bhattacharya, H. Heidari, M. Shusteff, C. M. Spadaccini, H. K. Taylor, *Science* **2019**, *363*, 1075.
[67] G. A. Appuhamillage, D. R. Berry, C. E. Benjamin, M. A. Luzuriaga, J. C. Reagan, J. J. Gassensmith, R. A. Smaldone, *Polym. Int.* **2019**, *68*, 964.
[68] F. Ullah, M. B. H. Othman, F. Javed, Z. Ahmad, H. M. Akil, *Mater. Sci. Eng., C* **2015**, *57*, 414.
[69] E. C. Muniz, G. Geuskens, *J. Mater. Sci.: Mater. Med.* **2001**, *12*, 879.
[70] K. Y. Lee, D. J. Mooney, *Chem. Rev.* **2001**, *101*, 1869.
[71] Z. Fang, A. Zhang, P. Wu, G. Yu, *ACS Mater. Lett.* **2019**, *1*, 158.
[72] D. K. Nandakumar, S. K. Ravi, Y. Zhang, N. Guo, C. Zhang, S. C. Tan, *Energy Environ. Sci.* **2018**, *11*, 2179.
[73] Y. Zhao, B. Liu, L. Pan, G. Yu, *Energy Environ. Sci.* **2013**, *6*, 2856.
[74] F. Zhao, Y. Shi, L. Pan, G. Yu, *Acc. Chem. Res.* **2017**, *50*, 1734.
[75] T. Nezakati, A. Seifalian, A. Tan, A. M. Seifalian, *Chem. Rev.* **2018**, *118*, 6766.
[76] K. Varaprasad, G. M. Raghavendra, T. Jayaramudu, M. M. Yallapu, R. Sadiku, *Mater. Sci. Eng., C* **2017**, *79*, 958.
[77] S. Sugihara, S. Kanaoka, S. Aoshima, *Macromolecules* **2004**, *37*, 1711.
[78] H. Fan, J. Wang, Z. Tao, J. Huang, P. Rao, T. Kurokawa, J. P. Gong, *Nat. Commun.* **2019**, *10*, 5127.
[79] X. Zhou, Y. Guo, F. Zhao, G. Yu, *Acc. Chem. Res.* **2019**, *52*, 3244.
[80] J.-Y. Sun, X. Zhao, W. R. K. Illeperuma, O. Chaudhuri, K. H. Oh, D. J. Mooney, J. J. Vlassak, Z. Suo, *Nature* **2012**, *489*, 133.
[81] Z. Wei, J. H. Yang, J. Zhou, F. Xu, M. Zrínyi, P. H. Dussault, Y. Osada, Y. M. Chen, *Chem. Soc. Rev.* **2014**, *43*, 8114.
[82] Y. Liu, Y.-H. Hsu, A. P.-H. Huang, S.-h. Hsu, *ACS Appl. Mater. Interfaces* **2020**, *12*, 40108.
[83] M. Hua, S. Wu, Y. Ma, Y. Zhao, Z. Chen, I. Frenkel, J. Strzalka, H. Zhou, X. Zhu, X. He, *Nature* **2021**, *590*, 594.
[84] Z. He, C. Wu, M. Hua, S. Wu, D. Wu, X. Zhu, J. Wang, X. He, *Matter* **2020**, *2*, 723.
[85] Y. Yang, H. Zhao, Z. Yin, J. Zhao, X. Yin, N. Li, D. Yin, Y. Li, B. Lei, Y. Du, W. Que, *Mater. Horiz.* **2018**, *5*, 1143.

[86] T. Zhao, G. Wang, D. Hao, L. Chen, K. Liu, M. Liu, *Adv. Funct. Mater.* **2018**, *28*, 1800793.
[87] H. Guo, T. Nakajima, D. Hourdet, A. Marcellan, C. Creton, W. Hong, T. Kurokawa, J. P. Gong, *Adv. Mater.* **2019**, *31*, 1900702.
[88] S. Hong, Y. Shi, R. Li, C. Zhang, Y. Jin, P. Wang, *ACS Appl. Mater. Interfaces* **2018**, *10*, 28517.
[89] A. Uliniuc, M. Popa, T. Hamaide, M. Dobromir, *Cellul. Chem. Technol.* **2012**, *46*, 1.
[90] M. Kumari, G. S. Chauhan, *J. Appl. Polym. Sci.* **2011**, *119*, 363.
[91] V. K. Thakur, M. K. Thakur, *Int. J. Biol. Macromol.* **2015**, *72*, 834.
[92] N. Bhattarai, J. Gunn, M. Zhang, *Adv. Drug Delivery Rev.* **2010**, *62*, 83.
[93] J. L. Ifkovits, J. A. Burdick, *Tissue Eng.* **2007**, *13*, 2369.
[94] N. Ranganathan, R. Joseph Bensingh, M. Abdul Kader, S. K. Nayak, in *Cellulose-Based Superabsorbent Hydrogels*, (Ed: M. I. H. Mondal), Springer International Publishing, Cham **2018**.
[95] Y. Chen, D. Ding, Z. Mao, Y. He, Y. Hu, W. Wu, X. Jiang, *Biomacromolecules* **2008**, *9*, 2609.
[96] T. Ogata, K. Nagayoshi, T. Nagasako, S. Kurihara, T. Nonaka, *React. Funct. Polym.* **2006**, *66*, 625.
[97] R. Sato, R. Noma, H. Tokuyama, *Eur. Polym. J.* **2015**, *66*, 91.
[98] K. T. Nguyen, J. L. West, *Biomaterials* **2002**, *23*, 4307.
[99] R. Reeves, A. Ribeiro, L. Lombardo, R. Boyer, J. B. Leach, *Polymers* **2010**, *2*, 252.
[100] T. Qunyi, Z. Ganwei, *Carbohydr. Polym.* **2005**, *62*, 74.
[101] H. Mittal, V. Kumar, S. M. Alhassan, S. S. Ray, *Int. J. Biol. Macromol.* **2018**, *114*, 283.
[102] H. Mittal, S. S. Ray, M. Okamoto, *Macromol. Mater. Eng.* **2016**, *301*, 496.
[103] E. Karadağ, D. Saraydın, O. Güven, *Macromol. Mater. Eng.* **2001**, *286*, 34.
[104] S. G. Abd Alla, M. Sen, A. W. M. El-Naggar, *Carbohydr. Polym.* **2012**, *89*, 478.
[105] K. Saini, *PharmaTutor* **2017**, *5*, 27.
[106] H. M. Said, S. G. Abd Alla, A. W. M. El-Naggar, *React. Funct. Polym.* **2004**, *61*, 397.
[107] A. Panda, S. B. Manohar, S. Sabharwal, Y. K. Bhardwaj, A. B. Majali, *Radiat. Phys. Chem.* **2000**, *58*, 101.
[108] W. E. Hennink, C. F. van Nostrum, *Adv. Drug Delivery Rev.* **2002**, *54*, 13.
[109] J. K. Stille, *Macromolecules* **1981**, *14*, 870.
[110] M. S. Rehmann, K. M. Skeens, P. M. Kharkar, E. M. Ford, E. Maverakis, K. H. Lee, A. M. Kloxin, *Biomacromolecules* **2017**, *18*, 3131.
[111] H. Shih, C.-C. Lin, *Biomacromolecules* **2012**, *13*, 2003.
[112] A. Rajbhandary, B. L. Nilsson, in *Gels Handbook: Fundamentals, Properties and Applications*, Vol. *1*, World Scientific Publishing Co Pte Ltd, Singapore **2016**, pp. 219–250.
[113] A. S. Hoffman, *Adv. Drug Delivery Rev.* **2012**, *64*, 18.
[114] M. F. Akhtar, M. Hanif, N. M. Ranjha, *Saudi Pharm. J.* **2016**, *24*, 554.
[115] J. M. Rosiak, F. Yoshii, *Nucl. Instrum. Methods Phys. Res., Sect. B* **1999**, *151*, 56.
[116] R. Gusain, N. Kumar, S. S. Ray, *Coord. Chem. Rev.* **2020**, *405*, 213111.
[117] S. Merino, C. Martín, K. Kostarelos, M. Prato, E. Vázquez, *ACS Nano* **2015**, *9*, 4686.
[118] Y. Zhuang, F. Yu, H. Chen, J. Zheng, J. Ma, J. Chen, *J. Mater. Chem. A* **2016**, *4*, 10885.
[119] T. Khampieng, S. Wongkittithavorn, S. Chaiarwut, P. Ekabutr, P. Pavasant, P. Supaphol, *J. Drug Delivery Sci. Technol.* **2018**, *44*, 91.
[120] Y. Chen, P. Pötschke, J. Pionteck, B. Voit, H. Qi, *ACS Omega* **2019**, *4*, 5117.
[121] S. Sershen, S. Westcott, N. Halas, J. West, *Appl. Phys. Lett.* **2002**, *80*, 4609.
[122] V. Pardo-Yissar, R. Gabai, A. N. Shipway, T. Bourenko, I. Willner, *Adv. Mater.* **2001**, *13*, 1320.
[123] C. Wang, N. T. Flynn, R. Langer, *Adv. Mater.* **2004**, *16*, 1074.
[124] G. Marcelo, M. López-González, F. Mendicuti, M. P. Tarazona, M. Valiente, *Macromolecules* **2014**, *47*, 6028.
[125] A. Skardal, J. Zhang, L. McCoard, S. Oottamasathien, G. D. Prestwich, *Adv. Mater.* **2010**, *22*, 4736.
[126] B. Xu, Y. Liu, J. Yuan, P. Wang, Q. Wang, *Polymers* **2018**, *10*, 1362.
[127] H. Wu, G. Yu, L. Pan, N. Liu, M. T. McDowell, Z. Bao, Y. Cui, *Nat. Commun.* **2013**, *4*, 1943.
[128] C. C. Piras, P. Slavik, D. K. Smith, *Angew. Chem., Int. Ed.* **2020**, *59*, 853.
[129] M. T. Taghizadeh, V. Siyahi, H. Ashassi-Sorkhabi, G. Zarrini, *Int. J. Biol. Macromol.* **2020**, *147*, 1018.
[130] P. C. Bandara, J. V. D. Perez, E. T. Nadres, R. G. Nannapaneni, K. J. Krakowiak, D. F. Rodrigues, *ACS Appl. Polym. Mater.* **2019**, *1*, 2668.
[131] G.-B. Fu, R. Xie, J.-W. Qin, X.-B. Deng, X.-J. Ju, W. Wang, Z. Liu, L.-Y. Chu, *Ind. Eng. Chem. Res.* **2021**, *60*, 8762.
[132] D. A. Patiño-Ruiz, G. De Ávila, C. Alarcón-Suesca, Á. D. González-Delgado, A. Herrera, *ACS Omega* **2020**, *5*, 26463.
[133] A. Khalil, N. Ali, A. M. Asiri, T. Kamal, S. B. Khan, J. Ali, *Cellulose* **2021**, *28*, 11299.
[134] I. Lee, C. W. Park, S. S. Yoon, H.-M. Yang, *Chemosphere* **2019**, *224*, 776.
[135] K. Mikula, D. Skrzypczak, B. Ligas, A. Witek-Krowiak, *SN Appl. Sci.* **2019**, *1*, 643.
[136] T. Nonaka, A. Yasunaga, T. Ogata, S. Kurihara, *J. Appl. Polym. Sci.* **2006**, *99*, 449.
[137] I. Gholamali, M. Yadollahi, *Int. J. Biol. Macromol.* **2020**, *160*, 724.
[138] M. A. Mudassir, S. Z. Hussain, S. Kousar, H. Zhang, T. M. Ansari, I. Hussain, *ACS Appl. Mater. Interfaces* **2021**, *13*, 27400.
[139] Q. Cao, J. Barrio, M. Antonietti, B. Kumru, M. Shalom, B. V. K. J. Schmidt, *ACS Appl. Polym. Mater.* **2020**, *2*, 3346.
[140] A. C. Yu, H. Chen, D. Chan, G. Agmon, L. M. Stapleton, A. M. Sevit, M. W. Tibbitt, J. D. Acosta, T. Zhang, P. W. Franzia, R. Langer, E. A. Appel, *Proc. Natl. Acad. Sci. USA* **2016**, *113*, 14255.
[141] Y. Yang, W. Pu, X. Xu, B. Wei, C. D. Wood, *Chem. Commun.* **2019**, *55*, 2849.
[142] A. Teleki, F. L. Haufe, A. M. Hirt, S. E. Pratsinis, G. A. Sotiriou, *RSC Adv.* **2016**, *6*, 21503.
[143] R. E. M. Lutton, E. Larrañeta, M.-C. Kearney, P. Boyd, A. D. Woolfson, R. F. Donnelly, *Int. J. Pharm.* **2015**, *494*, 417.
[144] L. A. J. Rutgeerts, A. H. Soultan, R. Subramani, B. Toprakhisar, H. Ramon, M. C. Paderes, W. M. De Borggraeve, J. Patterson, *Chem. Commun.* **2019**, *55*, 7323.
[145] S. Mallakpour, E. Azadi, C. M. Hussain, *Adv. Colloid Interface Sci.* **2021**, *293*, 102436.
[146] H. Yang, H. Yuan, Q. Hu, W. Liu, D. Zhang, *Appl. Surf. Sci.* **2020**, *504*, 144445.
[147] M. A. Skylar-Scott, J. Mueller, C. W. Visser, J. A. Lewis, *Nature* **2019**, *575*, 330.
[148] J. Yuan, C. Yi, H. Jiang, F. Liu, G. J. Cheng, *ACS Appl. Polym. Mater.* **2021**, *3*, 699.
[149] N. Fijoł, A. Aguilar-Sánchez, A. P. Mathew, *Chem. Eng. J.* **2022**, *430*, 132964.
[150] N. Fijoł, H. N. Abdelhamid, B. Pillai, S. A. Hall, N. Thomas, A. P. Mathew, *RSC Adv.* **2021**, *11*, 32408.
[151] Y. Song, B. Wang, P. Altemose, C. Kowall, L. Li, *Ind. Eng. Chem. Res.* **2020**, *59*, 21058.
[152] W. Liu, O. Erol, D. H. Gracias, *ACS Appl. Mater. Interfaces* **2020**, *12*, 33267.
[153] H. Baniasadi, R. Ajdary, J. Trifol, O. J. Rojas, J. Seppälä, *Carbohydr. Polym.* **2021**, *266*, 118114.
[154] M. Shahbazi, H. Jäger, S. J. Ahmadi, M. Lacroix, *Carbohydr. Polym.* **2020**, *240*, 116211.
[155] M. Hamidi, A. Azadi, P. Rafiei, *Adv. Drug Delivery Rev.* **2008**, *60*, 1638.

[156] J. Kollár, M. Mrlík, D. Moravčíková, Z. Kroneková, T. Liptaj, I. Lacík, J. Mosnáček, *Macromolecules* **2016**, *49*, 4047.
[157] L. Tan, B. Tan, *Chem. Soc. Rev.* **2017**, *46*, 3322.
[158] Y. Huang, M. Zeng, J. Ren, J. Wang, L. Fan, Q. Xu, *Colloids Surf. A* **2012**, *401*, 97.
[159] A. Rashidzadeh, A. Olad, D. Salari, A. Reyhanitabar, *J. Polym. Res.* **2014**, *21*, 344.
[160] J. P. Baker, L. H. Hong, H. W. Blanch, J. M. Prausnitz, *Macromolecules* **1994**, *27*, 1446.
[161] J. P. Baker, H. W. Blanch, J. M. Prausnitz, *Polymer* **1995**, *36*, 1061.
[162] A. E. English, S. Mafé, J. A. Manzanares, X. Yu, A. Y. Grosberg, T. Tanaka, *J. Chem. Phys.* **1996**, *104*, 8713.
[163] H. Salimi-Kenari, F. Mollaie, E. Dashtimoghadam, M. Imani, B. Nyström, *Carbohydr. Polym.* **2018**, *181*, 141.
[164] H. Yu, D. W. Grainger, *J. Appl. Polym. Sci.* **1993**, *49*, 1553.
[165] Y. Guo, J. Bae, Z. Fang, P. Li, F. Zhao, G. Yu, *Chem. Rev.* **2020**, *120*, 7642.
[166] K.-i. Hoshino, T. Nakajima, T. Matsuda, T. Sakai, J. P. Gong, *Soft Matter* **2018**, *14*, 9693.
[167] M. Guvendiren, S. Yang, J. A. Burdick, *Adv. Funct. Mater.* **2009**, *19*, 3038.
[168] J. Fu, *J. Polym. Sci., Part B: Polym. Phys.* **2018**, *56*, 1336.
[169] J. Fan, Z. Shi, M. Lian, H. Li, J. Yin, *J. Mater. Chem. A* **2013**, *1*, 7433.
[170] I. Tokarev, S. Minko, *Soft Matter* **2009**, *5*, 511.
[171] S. Chatterjee, P. C.-l. Hui, *Polymers* **2021**, *13*, 2086.
[172] T. Jiang, X. Zhao, X. Yin, R. Yang, G. Tan, *Appl. Energy* **2021**, *287*, 116573.
[173] T. Garg, S. Singh, A. K. Goyal, *Crit Rev Ther Drug Carrier Syst* **2013**, 30.
[174] G. Cirillo, T. Spataro, M. Curcio, U. G. Spizzirri, F. P. Nicoletta, N. Picci, F. Iemma, *Mater. Sci. Eng., C* **2015**, *48*, 499.
[175] H. Yim, M. Kent, S. Mendez, S. Balamurugan, S. Balamurugan, G. Lopez, S. Satija, *Macromolecules* **2004**, *37*, 1994.
[176] A. Saad, R. Mills, H. Wan, M. A. Mottaleb, L. Ormsbee, D. Bhattacharyya, *J. Membr. Sci.* **2020**, *599*, 117821.
[177] Q. Shi, H. Liu, D. Tang, Y. Li, X. Li, F. Xu, *NPG Asia Mater.* **2019**, *11*, 64.
[178] S. Jana, J. Ray, B. Mondal, S. Pradhan, T. Tripathy, *Colloids Surf. A* **2018**, *553*, 472.
[179] B. H. Kim, F. Liu, Y. Yu, H. Jang, Z. Xie, K. Li, J. Lee, J. Y. Jeong, A. Ryu, Y. Lee, *Adv. Funct. Mater.* **2018**, *28*, 1803149.
[180] R. Demir-Cakan, M. R. Palacin, L. Croguennec, *J. Mater. Chem. A* **2019**, *7*, 20519.
[181] H. Zhang, W. Niu, S. Zhang, *Chem. Eng. J.* **2020**, *387*, 124105.
[182] B. Yang, W. Yuan, *ACS Appl. Mater. Interfaces* **2019**, *11*, 16765.
[183] Q. Guan, G. Lin, Y. Gong, J. Wang, W. Tan, D. Bao, Y. Liu, Z. You, X. Sun, Z. Wen, *J. Mater. Chem. A* **2019**, *7*, 13948.
[184] Z. Lei, P. Wu, *Nat. Commun.* **2019**, *10*, 3429.
[185] S. Xia, S. Song, G. Gao, *Chem. Eng. J.* **2018**, *354*, 817.
[186] C. K. Chiang, C. R. Fincher, Y. W. Park, A. J. Heeger, H. Shirakawa, E. J. Louis, S. C. Gau, A. G. MacDiarmid, *Phys. Rev. Lett.* **1977**, *39*, 1098.
[187] Y. Wang, Y. Ding, X. Guo, G. Yu, *Nano Res.* **2019**, *12*, 1978.
[188] R. Prabhakar, D. Kumar, *Polym.-Plast. Technol. Eng.* **2016**, *55*, 46.
[189] M. Wang, Y. Chen, R. Khan, H. Liu, C. Chen, T. Chen, R. Zhang, H. Li, *Colloids Surf. A* **2019**, *567*, 139.
[190] X. Jing, H.-Y. Mi, X.-F. Peng, L.-S. Turng, *Carbon* **2018**, *136*, 63.
[191] P. He, J. Wu, X. Pan, L. Chen, K. Liu, H. Gao, H. Wu, S. Cao, L. Huang, Y. Ni, *J. Mater. Chem. A* **2020**, *8*, 3109.
[192] W. W. Focke, G. E. Wnek, Y. Wei, *J. Phys. Chem.* **1987**, *91*, 5813.
[193] J. Stejskal, O. E. Bogomolova, N. V. Blinova, M. Trchová, I. Šeděnková, J. Prokeš, I. Sapurina, *Polym. Int.* **2009**, *58*, 872.
[194] D. Zhou, L. Zhang, S. Guo, *Water Res.* **2005**, *39*, 3755.
[195] H. Mittal, A. Al Alili, P. P. Morajkar, S. M. Alhassan, *Colloids Surf. A* **2021**, *630*, 127533.
[196] H. Mittal, A. Al Alili, P. P. Morajkar, S. M. Alhassan, *J. Mol. Liq.* **2021**, *323*, 115034.
[197] Z. Mohammadi, S. Shangbin, C. Berkland, J.-t. Liang, *Chem. Eng. J.* **2017**, *307*, 496.
[198] M. Akter, M. Bhattacharjee, A. K. Dhar, F. B. A. Rahman, S. Haque, T. U. Rashid, S. M. F. Kabir, *Gels* **2021**, *7*, 30.
[199] X. Yang, D. Wang, *ACS Appl. Energy Mater.* **2018**, *1*, 6657.
[200] R. Gusain, N. Kumar, S. S. Ray, in *Photocatalysts in Advanced Oxidation Processes for Wastewater Treatment*, John Wiley & Sons, USA **2020**.
[201] A. L. Linsebigler, G. Lu, J. T. Yates, *Chem. Rev.* **1995**, *95*, 735.
[202] N. Kumar, S. Kumar, R. Gusain, N. Manyala, S. Eslava, S. S. Ray, *ACS Appl. Energy Mater.* **2020**, *3*, 9897.
[203] A. L. Luna, S. Papadopoulos, T. Kyburz, E. Tervoort, L. Novotny, M. Niederberger, *J. Mater. Chem. A* **2021**, *9*, 22380.
[204] E. Caló, V. V. Khutoryanskiy, *Eur. Polym. J.* **2015**, *65*, 252.
[205] H. M. Shewan, J. R. Stokes, *J. Food Eng.* **2013**, *119*, 781.
[206] M. R. Guilherme, F. A. Aouada, A. R. Fajardo, A. F. Martins, A. T. Paulino, M. F. Davi, A. F. Rubira, E. C. Muniz, *Eur. Polym. J.* **2015**, *72*, 365.
[207] F. N. Muya, C. E. Sunday, P. Baker, E. Iwuoha, *Water Sci. Technol.* **2016**, *73*, 983.
[208] M. Khan, I. M. C. Lo, *Water Res.* **2016**, *106*, 259.
[209] K. Varaprasad, Y. M. Mohan, S. Ravindra, N. N. Reddy, K. Vimala, K. Monika, B. Sreedhar, K. M. Raju, *J. Appl. Polym. Sci.* **2010**, *115*, 1199.
[210] V. R. Babu, C. Kim, S. Kim, C. Ahn, Y.-I. Lee, *Carbohydr. Polym.* **2010**, *81*, 196.
[211] B. Plackal Adimuriyil George, N. Kumar, H. Abrahamse, S. S. Ray, *Sci. Rep.* **2018**, *8*, 14368.
[212] G. Babaladimath, V. Badalamoole, *Polym. Bull.* **2019**, *76*, 4215.
[213] J. Singh, A. Dhaliwal, *J. Polym. Environ.* **2021**, *29*, 71.
[214] B. K. Bhangi, S. K. Ray, *Int. J. Biol. Macromol.* **2020**, *144*, 801.
[215] L. Tang, F. Tang, M. Li, L. Li, *Colloids Surf. A* **2018**, *553*, 618.
[216] C. Gao, Q. An, Z. Xiao, S. Zhai, B. Zhai, Z. Shi, *Carbohydr. Polym.* **2018**, *181*, 744.
[217] T.-D. Nguyen, C.-H. Dang, D.-T. Mai, *Carbohydr. Polym.* **2018**, *197*, 29.
[218] B. Wang, M. Ran, G. Fang, T. Wu, Q. Tian, L. Zheng, L. Romero-Zerón, Y. Ni, *Cellulose* **2020**, *27*, 6995.
[219] M. S. Chavali, M. P. Nikolova, *SN Appl. Sci.* **2019**, *1*, 607.
[220] R. Gusain, K. Gupta, P. Joshi, O. P. Khatri, *Adv. Colloid Interface Sci.* **2019**, *272*, 102009.
[221] K. Gupta, P. Joshi, R. Gusain, O. P. Khatri, *Coord. Chem. Rev.* **2021**, *445*, 214100.
[222] S. H. S. Chan, T. Yeong Wu, J. C. Juan, C. Y. Teh, *J. Chem. Technol. Biotechnol.* **2011**, *86*, 1130.
[223] M. S. Sri Abirami Saraswathi, A. Nagendran, D. Rana, *J. Mater. Chem. A* **2019**, *7*, 8723.
[224] S. Ghosh, A. Das, *Toxicol. Environ. Chem.* **2015**, *97*, 491.
[225] R. Daghrir, P. Drogui, D. Robert, *Ind. Eng. Chem. Res.* **2013**, *52*, 3581.
[226] K. S. Varma, R. J. Tayade, K. J. Shah, P. A. Joshi, A. D. Shukla, V. G. Gandhi, *Water-Energy Nexus* **2020**, *3*, 46.
[227] L. M. Anaya-Esparza, J. M. Ruvalcaba-Gómez, C. I. Maytorena-Verdugo, N. González-Silva, R. Romero-Toledo, S. Aguilera-Aguirre, A. Pérez-Larios, E. Montalvo-González, *Materials* **2020**, *13*, 811.
[228] N. Neghi, M. Kumar, D. Burkhalov, *Chem. Eng. J.* **2019**, *359*, 963.
[229] P. Lei, F. Wang, X. Gao, Y. Ding, S. Zhang, J. Zhao, S. Liu, M. Yang, *J. Hazard. Mater.* **2012**, *227*, 185.
[230] U. M. Garusinghe, V. S. Raghuwanshi, W. Batchelor, G. Garnier, *Sci. Rep.* **2018**, *8*, 2306.
[231] F. Magalhães, F. C. C. Moura, R. M. Lago, *Desalination* **2011**, *276*, 266.
[232] L. Liu, M. Yue, J. Lu, J. Hu, Y. Liang, W. Cui, *Appl. Surf. Sci.* **2018**, *456*, 645.

[233] W. Cui, J. He, H. Wang, J. Hu, L. Liu, Y. Liang, *Appl. Catal., B* **2018**, *232*, 232.
[234] M. Thomas, G. A. Naikoo, M. U. D. Sheikh, M. Bano, F. Khan, *J. Photochem. Photobiol., A* **2016**, *327*, 33.
[235] S. Thakur, S. Pandey, O. A. Arotiba, *Carbohydr. Polym.* **2016**, *153*, 34.
[236] Z. Wu, X. Chen, B. Yuan, M.-L. Fu, *Chemosphere* **2020**, *239*, 124745.
[237] T. Tamer, W. Abou-Taleb, G. Roston, M. Mohyeldin, A. Omer, R. Khalifa, A. Hafez, *Environ. Nanotechnol., Monit. Manage.* **2018**, *10*, 112.
[238] H. Mittal, A. Maity, S. S. Ray, *Chem. Eng. J.* **2015**, *279*, 166.
[239] H. Mittal, S. S. Ray, *Int. J. Biol. Macromol.* **2016**, *88*, 66.
[240] S. Çınar, Ü. H. Kaynar, T. Aydemir, S. C. Kaynar, M. Ayvacıklı, *Int. J. Biol. Macromol.* **2017**, *96*, 459.
[241] H. Mittal, P. P. Morajkar, A. Al Alili, S. M. Alhassan, *J. Polym. Environ.* **2020**, *28*, 1637.
[242] T. Zeng, Y. Yu, Z. Li, J. Zuo, Z. Kuai, Y. Jin, Y. Wang, A. Wu, C. Peng, *Mater. Chem. Phys.* **2019**, *231*, 105.
[243] X. Jiao, Y. Gutha, W. Zhang, *Colloids Surf., B* **2017**, *149*, 184.
[244] S. A. Bhat, F. Zafar, A. U. Mirza, A. H. Mondal, A. Kareem, Q. M. R. Haq, N. Nishat, *Arabian J. Chem.* **2020**, *13*, 5724.
[245] N. Singh, S. Kumari, N. Goyal, S. Khan, *Environ. Nanotechnol., Monit. Manage.* **2021**, *15*, 100444.
[246] S. Vahidhabanu, D. Karuppasamy, A. I. Adeogun, B. R. Babu, *RSC Adv.* **2017**, *7*, 5669.
[247] E. Makhado, S. Pandey, K. D. Modibane, M. Kang, M. J. Hato, *Int. J. Biol. Macromol.* **2020**, *162*, 60.
[248] S. Thakur, B. Sharma, A. Thakur, V. K. Gupta, W. F. Alsanie, C. Makatsoris, V. K. Thakur, *Bioresour. Technol.* **2022**, *348*, 126708.
[249] B. R. Motshabi, K. E. Ramohlola, K. D. Modibane, D. Kumar, M. J. Hato, E. Makhado, *Mater. Lett.* **2022**, *315*, 131924.
[250] S. K. Samanta, B. Mandal, T. Tripathy, *J. Appl. Polym. Sci.* **2022**, *139*, e52465.
[251] A. Dhanya, K. Aparna, *Procedia Technol.* **2016**, *24*, 611.
[252] J. Zhou, B. Hao, L. Wang, J. Ma, W. Cheng, *Sep. Purif. Technol.* **2017**, *176*, 193.
[253] L. Bergamonti, C. Bergonzi, C. Graiff, P. P. Lottici, R. Bettini, L. Elviri, *Water Res.* **2019**, *163*, 114841.
[254] R. Su, S. Ge, H. Li, Y. Su, Q. Li, W. Zhou, B. Gao, Q. Yue, *Sci. Total Environ.* **2019**, *693*, 133657.
[255] D. Arikal, A. Kallingal, *Environ. Technol.* **2021**, *42*, 2278.
[256] H. Yang, K. Zhang, R. Shi, A. Tang, *J. Am. Ceram. Soc.* **2007**, *90*, 1370.
[257] S. Iqbal, M. Javed, M. A. Qamar, A. Bahadur, M. Fayyaz, A. Akbar, H. O. Alsaab, N. S. Awwad, H. A. Ibrahium, *ChemistrySelect* **2022**, *7*, 202103694.
[258] D. Mehta, S. Mazumdar, S. Singh, *J. Water Process Eng.* **2015**, *7*, 244.
[259] S. Saber-Samandari, S. Saber-Samandari, H. Joneidi-Yekta, M. Mohseni, *Chem. Eng. J.* **2017**, *308*, 1133.
[260] G. Sharma, A. Kumar, C. Chauhan, A. Okram, S. Sharma, D. Pathania, S. Kalia, *Sustainable Chem. Pharm.* **2017**, *6*, 96.
[261] J. Wang, X. Li, Q. Cheng, F. Lv, C. Chang, L. Zhang, *Carbohydr. Polym.* **2020**, *229*, 115470.
[262] X.-F. Sun, B. Liu, Z. Jing, H. Wang, *Carbohydr. Polym.* **2015**, *118*, 16.
[263] C. Shen, Y. Shen, Y. Wen, H. Wang, W. Liu, *Water Res.* **2011**, *45*, 5200.
[264] T. Lü, R. Ma, K. Ke, D. Zhang, D. Qi, H. Zhao, *Chem. Eng. J.* **2021**, *408*, 127327.
[265] G. R. Mahdavinia, A. Massoudi, A. Baghban, E. Shokri, *J. Environ. Chem. Eng.* **2014**, *2*, 1578.
[266] M. El-Arnaoutya, M. Eid, O. Sallam, A. Mostafa, *Arab J. Nucl. Sci. Appl.* **2015**, *48*, 10.
[267] C. Dong, J. Lu, B. Qiu, B. Shen, M. Xing, J. Zhang, *Appl. Catal., B* **2018**, *222*, 146.
[268] H. Wang, C. Wang, X. Cui, L. Qin, R. Ding, L. Wang, Z. Liu, Z. Zheng, B. Lv, *Appl. Catal., B* **2018**, *221*, 169.
[269] I. S. Pinto, P. H. Pacheco, J. V. Coelho, E. Lorençon, J. D. Ardisson, J. D. Fabris, P. P. de Souza, K. W. Krambrock, L. C. Oliveira, M. C. Pereira, *Appl. Catal., B* **2012**, *119*, 175.
[270] C. Duan, C. Liu, X. Meng, K. Gao, W. Lu, Y. Zhang, L. Dai, W. Zhao, C. Xiong, W. Wang, *Carbohydr. Polym.* **2020**, *230*, 115642.
[271] G. Sharma, A. Kumar, S. Sharma, H. Ala'a, M. Naushad, A. A. Ghfar, T. Ahamad, F. J. Stadler, *Sep. Purif. Technol.* **2019**, *211*, 895.
[272] O. Ghazy, M. G. Hamed, M. Breky, E. H. Borai, *Colloids Surf. A* **2021**, *621*, 126613.
[273] M. Khan, I. M. C. Lo, *J. Hazard. Mater.* **2017**, *322*, 195.
[274] D. P. Facchi, A. L. Cazetta, E. A. Canesin, V. C. Almeida, E. G. Bonafé, M. J. Kipper, A. F. Martins, *Chem. Eng. J.* **2018**, *337*, 595.
[275] C. Zhang, Y. Dai, Y. Wu, G. Lu, Z. Cao, J. Cheng, K. Wang, H. Yang, Y. Xia, X. Wen, W. Ma, C. Liu, Z. Wang, *Carbohydr. Polym.* **2020**, *234*, 115882.
[276] Y. Meng, C. Li, X. Liu, J. Lu, Y. Cheng, L.-P. Xiao, H. Wang, *Sci. Total Environ.* **2019**, *685*, 847.
[277] G. R. Mahdavinia, S. Mousanezhad, H. Hosseinzadeh, F. Darvishi, M. Sabzi, *Carbohydr. Polym.* **2016**, *147*, 379.
[278] F. Halouane, Y. Oz, D. Meziane, A. Barras, J. Juraszek, S. K. Singh, S. Kurungot, P. K. Shaw, R. Sanyal, R. Boukherroub, A. Sanyal, S. Szunerits, *J. Colloid Interface Sci.* **2017**, *507*, 360.
[279] S. Mola ali abasiyan, G. R. Mahdavinia, *Environ. Sci. Pollut. Res.* **2018**, *25*, 14977.
[280] Y. Zhu, J. Hu, J. Wang, *Prog. Nucl. Energy* **2014**, *71*, 172.
[281] S. Dong, Y. Wang, *Water Res.* **2016**, *88*, 852.
[282] Z. Sekhavat Pour, M. Ghaemy, *RSC Adv.* **2015**, *5*, 64106.
[283] A. Pourjavadi, M. Nazari, S. H. Hosseini, *RSC Adv.* **2015**, *5*, 32263.
[284] M. Mirabedini, M. Kassaee, S. Poorsadeghi, *Arabian J. Sci. Eng.* **2017**, *42*, 115.
[285] H. Mittal, N. Ballav, S. B. Mishra, *J. Ind. Eng. Chem.* **2014**, *20*, 2184.
[286] S. C. N. Tang, P. Wang, K. Yin, I. M. C. Lo, *Environ. Eng. Sci.* **2010**, *27*, 947.
[287] H. Rezazadeh, P. N. Moghadam, S. Ehsanimehr, A. R. Fareghi, *J. Elastomers Plast.* **2020**, *52*, 70.
[288] A. Sayed, G. A. Mahmoud, H. Said, A. A. Diab, *Mater. Chem. Phys.* **2022**, *280*, 125731.
[289] S. Karimi, H. Namazi, *Int. J. Biol. Macromol.* **2022**, *205*, 128.
[290] T. Wan, J. Wang, S. He, T. Wang, Y. Zheng, F. Xie, Q. Tang, *Polym. Bull.* **2022**, https://doi.org/10.1007/s00289-022-04220-3.
[291] F. Hassanzadeh-Afruzi, A. Maleki, E. N. Zare, *Int. J. Biol. Macromol.* **2022**, *203*, 445.
[292] B. Jia, D. Liu, C. Niu, Q. Yu, J. Ren, Q. Liu, H. Wang, *RSC Adv.* **2022**, *12*, 4417.
[293] H. E. Ali, S. M. Nasef, Y. H. Gad, *Carbohydr. Polym.* **2022**, *283*, 119149.
[294] N. Singh, S. Yadav, S. K. Mehta, A. Dan, *J. Macromol. Sci., Part A* **2022**, *59*, 271.
[295] P. Chen, X. Liu, R. Jin, W. Nie, Y. Zhou, *Carbohydr. Polym.* **2017**, *167*, 36.
[296] Y. Yue, S. Shen, W. Cheng, G. Han, Q. Wu, J. Jiang, *Colloids Surf. A* **2021**, 128035.
[297] L. Chen, C. He, J. Yin, S. Chen, W. Zhao, C. Zhao, *Environ. Technol.* **2022**, *43*, 355.
[298] Priya, A. K. Sharma, B. S. Kaith, V. Tanwar, J. K. Bhatia, N. Sharma, S. Bajaj, S. Panchal, *Int. J. Biol. Macromol.* **2019**, *129*, 214.
[299] Y. Liu, H. Chen, Q. Mo, X. Yang, J. Wang, X. Lin, D. Shang, Y. Li, Y. Zhang, *J. Hazard. Mater.* **2021**, *416*, 126262.
[300] Y. Liu, Y. Huang, C. Zhang, W. Li, C. Chen, Z. Zhang, H. Chen, J. Wang, Y. Li, Y. Zhang, *Environ. Pollut.* **2020**, *264*, 114739.

[301] R. Gusain, N. Kumar, E. Fosso-Kankeu, S. S. Ray, *ACS Omega* **2019**, *4*, 13922.
[302] A. T. Massey, R. Gusain, S. Kumari, O. P. Khatri, *Ind. Eng. Chem. Res.* **2016**, *55*, 7124.
[303] R. Gusain, N. Kumar, F. Opoku, P. P. Govender, S. S. Ray, *ACS Appl. Nano Mater.* **2021**, *4*, 4721.
[304] N. Kumar, E. Fosso-Kankeu, S. S. Ray, *ACS Appl. Mater. Interfaces* **2019**, *11*, 19141.
[305] G. Wei, J. Wei, J. Zhou, Y. Chen, D. Wu, Q. Wang, *Chem. Eng. J.* **2020**, *382*, 123018.
[306] N. Karaca, N. Ocal, N. Arsu, S. Jockusch, *J. Photochem. Photobiol., A* **2016**, *331*, 22.
[307] M. Dargahi, H. Ghasemzadeh, A. Torkaman, *Polym. Bull.* **2019**, *76*, 5039.
[308] Y. Ding, Y. Zhou, W. Nie, P. Chen, *Appl. Surf. Sci.* **2015**, *357*, 1606.
[309] N. Meng, J. Cheng, Y. Zhou, W. Nie, P. Chen, *Appl. Surf. Sci.* **2017**, *396*, 310.
[310] H. Hosseinzadeh, N. Bahador, *J. Mol. Liq.* **2017**, *240*, 630.
[311] A. K. Sharma, B. S. Kaith, S. Panchal, J. K. Bhatia, S. Bajaj, V. Tanwar, N. Sharma, *J. Environ. Manage.* **2019**, *231*, 380.
[312] Y. Xiong, B. Luo, G. Chen, J. Cai, Q. Jiang, B. Gu, X. Wang, *Polymers* **2019**, *11*, 1393.
[313] J. Yang, Z. Li, H. Zhu, *Appl. Catal., B* **2017**, *217*, 603.
[314] Y. Zhu, S. Murali, W. Cai, X. Li, J. W. Suk, J. R. Potts, R. S. Ruoff, *Adv. Mater.* **2010**, *22*, 3906.
[315] N. Kumar, R. Salehiyan, V. Chauke, O. Joseph Botlhoko, K. Setshedi, M. Scriba, M. Masukume, S. S. Ray, *FlatChem* **2021**, *27*, 100224.
[316] V. B. Mohan, K.-t. Lau, D. Hui, D. Bhattacharyya, *Composites, Part B* **2018**, *142*, 200.
[317] A. T. Lawal, *Biosens. Bioelectron.* **2019**, *141*, 111384.
[318] M. I. Fadlalla, P. S. Kumar, V. Selvam, S. G. Babu, *J. Mater. Sci.* **2020**, *55*, 7156.
[319] T. Jiao, H. Zhao, J. Zhou, Q. Zhang, X. Luo, J. Hu, Q. Peng, X. Yan, *ACS Sustainable Chem. Eng.* **2015**, *3*, 3130.
[320] H. B. Kulkarni, P. Tambe, G. M. Joshi, *Compos. Interfaces* **2018**, *25*, 381.
[321] X. Ji, L. Cui, Y. Xu, J. Liu, *Compos. Sci. Technol.* **2015**, *106*, 25.
[322] H. Lu, S. Zhang, L. Guo, W. Li, *RSC Adv.* **2017**, *7*, 51008.
[323] B. Y. Z. Hiew, L. Y. Lee, X. J. Lee, S. Thangalazhy-Gopakumar, S. Gan, S. S. Lim, G.-T. Pan, T. C.-K. Yang, W. S. Chiu, P. S. Khiew, *Process Saf. Environ. Prot.* **2018**, *116*, 262.
[324] H. Zhao, T. Jiao, L. Zhang, J. Zhou, Q. Zhang, Q. Peng, X. Yan, *Sci. China Mater.* **2015**, *58*, 811.
[325] J. He, F. Ni, A. Cui, X. Chen, S. Deng, F. Shen, C. Huang, G. Yang, C. Song, J. Zhang, *Sci. Total Environ.* **2020**, *701*, 134363.
[326] J. Ma, J. Dai, Y. Duan, J. Zhang, L. Qiang, J. Xue, *Renewable Energy* **2020**, *156*, 1008.
[327] C. Liu, H. Liu, T. Xiong, A. Xu, B. Pan, K. Tang, *Polymers* **2018**, *10*, 835.
[328] Y. Kong, Y. Zhuang, B. Shi, *J. Hazard. Mater.* **2020**, *382*, 121060.
[329] Y. Zhuang, F. Yu, J. Ma, J. Chen, *J. Colloid Interface Sci.* **2017**, *507*, 250.
[330] J. Feng, H. Ding, G. Yang, R. Wang, S. Li, J. Liao, Z. Li, D. Chen, *J. Colloid Interface Sci.* **2017**, *508*, 387.
[331] J. He, A. Cui, F. Ni, S. Deng, F. Shen, G. Yang, *J. Colloid Interface Sci.* **2018**, *531*, 37.
[332] C. Liu, H. Liu, K. Tang, K. Zhang, Z. Zou, X. Gao, *J. Polym. Environ.* **2020**, *28*, 984.
[333] T. S. Vo, T. T. B. C. Vo, J. W. Suk, K. Kim, *Nano Convergence* **2020**, *7*, 4.
[334] L. Das, P. Das, A. Bhowal, C. Bhattachariee, *Environ. Technol. Innovation* **2020**, *18*, 100664.
[335] L. Shen, Z. Jin, W. Xu, X. Jiang, Y.-x. Shen, Y. Wang, Y. Lu, *Ind. Eng. Chem. Res.* **2019**, *58*, 7817.
[336] M. Kheirabadi, M. Samadi, E. Asadian, Y. Zhou, C. Dong, J. Zhang, A. Z. Moshfegh, *J. Colloid Interface Sci.* **2019**, *537*, 66.
[337] C. Cheng, Y. Cai, G. Guan, L. Yeo, D. Wang, *Angew. Chem., Int. Ed.* **2018**, *57*, 11177.
[338] K. Soleimani, A. D. Tehrani, M. Adeli, *Ecotoxicol. Environ. Saf.* **2018**, *147*, 34.
[339] Y. Liu, S. Huang, X. Zhao, Y. Zhang, *Colloids Surf. A* **2018**, *539*, 1.
[340] Z. Wang, Q. Tu, S. Zheng, J. J. Urban, S. Li, B. Mi, *Nano Lett.* **2017**, *17*, 7289.
[341] Q. Zhang, F. Zhang, X. Xu, C. Zhou, D. Lin, *ACS Nano* **2018**, *12*, 1096.
[342] Y. Sun, X. Liu, X. Lv, T. Wang, B. Xue, *J. Cleaner Prod.* **2021**, *295*, 126406.
[343] D. Kharismadewi, Y. Haldorai, V. H. Nguyen, D. Tuma, J.-J. Shim, *Compos. Interfaces* **2016**, *23*, 719.
[344] N. Sarkar, G. Sahoo, S. K. Swain, *J. Mol. Liq.* **2020**, *302*, 112591.
[345] S. Song, Z. Liu, J. Zhang, C. Jiao, L. Ding, S. Yang, *Materials* **2020**, *13*, 3703.
[346] N. Umbreen, S. Sohni, I. Ahmad, N. U. Khattak, K. Gul, *J. Colloid Interface Sci.* **2018**, *527*, 356.
[347] A. Onder, M. R. Kıvanç, S. Durmuş, P. Ilgin, H. Ozay, O. Ozay, *J. Polym. Environ.* **2022**, *30*, 2928.
[348] W. Zhang, J. Ou, M. Tang, Q. He, A. Long, S. Luo, S. Sun, J. Wan, Y. Gao, L. Zhou, B. Wang, H. Wang, *Chem. Eng. J.* **2022**, *431*, 133375.
[349] Y. Liang, X. Wang, W. An, Y. Li, J. Hu, W. Cui, *Appl. Surf. Sci.* **2019**, *466*, 666.
[350] K. T. T. Myint, Y. Liu, H. Niu, J. Chen, Z. Jiao, *Catal. Surv. Asia* **2021**, *25*, 159.
[351] F. Chen, W. An, L. Liu, Y. Liang, W. Cui, *Appl. Catal., B* **2017**, *217*, 65.
[352] C. Manjunath, K. Ramesh, G. Manavendra, *Renew. Energy* **2019**, *133*, 2016.
[353] Y.-E. Moon, G. Jung, J. Yun, H.-I. Kim, *Mater. Sci. Eng., B* **2013**, *178*, 1097.
[354] Z. Zhang, F. Xiao, Y. Guo, S. Wang, Y. Liu, *ACS Appl. Mater. Interfaces* **2013**, *5*, 2227.
[355] C. Hou, Q. Zhang, Y. Li, H. Wang, *J. Hazard. Mater.* **2012**, *205*, 229.
[356] Y. Jiang, S. Chowdhury, R. Balasubramanian, *Chem. Eng. J.* **2017**, *327*, 751.
[357] C. Liu, M. Yue, L. Liu, Y. Rui, W. Cui, *RSC Adv.* **2018**, *8*, 22402.
[358] Y. Li, W. Cui, L. Liu, R. Zong, W. Yao, Y. Liang, Y. Zhu, *Appl. Catal., B* **2016**, *199*, 412.
[359] C. Mu, Y. Zhang, W. Cui, Y. Liang, Y. Zhu, *Appl. Catal., B* **2017**, *212*, 41.
[360] S. Roy, A. Baral, A. Banerjee, *Chemistry* **2013**, *19*, 14950.
[361] F. Mashkoor, A. Nasar, *Environ. Chem. Lett.* **2020**, *18*, 605.
[362] M. A. M. Ali, A. M. Alsabagh, M. W. Sabaa, R. A. El-Salamony, R. R. Mohamed, R. E. Morsi, *Iran. Polym. J.* **2020**, *29*, 455.
[363] X.-F. Sun, Q. Ye, Z. Jing, Y. Li, *Polym. Compos.* **2014**, *35*, 45.
[364] S. Chatterjee, T. Chatterjee, S.-R. Lim, S. H. Woo, *Bioresour. Technol.* **2011**, *102*, 4402.
[365] U. Baruah, A. Konwar, D. Chowdhury, *Nanoscale* **2016**, *8*, 8542.
[366] S. Singh, R. Jelinek, *ACS Appl. Polym. Mater.* **2020**, *2*, 2810.
[367] S. Chatterjee, M. W. Lee, S. H. Woo, *Bioresour. Technol.* **2010**, *101*, 1800.
[368] H. Hosseinzadeh, *Pol. J. Chem. Technol.* **2015**, *17*, 70.
[369] S. Mallakpour, F. Tabesh, *Int. J. Biol. Macromol.* **2021**, *166*, 722.
[370] D. C. Alves, J. O. Goncalves, B. B. Coseglio, T. A. Burgo, G. L. Dotto, L. A. Pinto, T. R. Cadaval Jr., *J. Environ. Chem. Eng.* **2019**, *7*, 103460.
[371] S. Nayak, S. R. Prasad, D. Mandal, P. Das, *J. Hazard. Mater.* **2020**, *392*, 122287.
[372] J. Ma, Z. Jiang, J. Cao, F. Yu, *Chemosphere* **2020**, *242*, 125188.
[373] S. Chatterjee, M. W. Lee, S. H. Woo, *Carbon* **2009**, *47*, 2933.
[374] H. Yuan, J. Peng, T. Ren, Q. Luo, Y. Luo, N. Zhang, Y. Huang, X. Guo, Y. Wu, *Sci. Total Environ.* **2021**, *760*, 143395.
[375] X. Guo, D. Xu, H. Yuan, Q. Luo, S. Tang, L. Liu, Y. Wu, *J. Mater. Chem. A* **2019**, *7*, 27081.
[376] Z. Chen, Y. Pan, P. Cai, *Int. J. Biol. Macromol.* **2022**, *205*, 37.

[377] M. R. M. Shafiee, J. Parhizkar, S. Radfar, *J. Mater. Sci.: Mater. Electron.* **2019**, *30*, 12475.
[378] K. T. Myint, G. G. Jia, H. J. Niu, J. Chen, Z. Jiao, *Sci. Total Environ.* **2020**, *705*, 135821.
[379] J. Wen, J. Xie, X. Chen, X. Li, *Appl. Surf. Sci.* **2017**, *391*, 72.
[380] S. Asadzadeh-Khaneghah, A. Habibi-Yangjeh, *J. Cleaner Prod.* **2020**, *276*, 124319.
[381] C. Hu, Y. R. Lin, H. C. Yang, *ChemSusChem* **2019**, *12*, 1794.
[382] G. Sharma, A. Kumar, M. Naushad, P. Dhiman, B. Thakur, A. García-Peñas, F. J. Stadler, *Materials* **2022**, *15*, 2549.
[383] S. A. Khan, T. A. Khan, *J. Environ. Chem. Eng.* **2021**, *9*, 105575.
[384] G. R. Mahdavinia, A. Asgari, *Polym. Bull.* **2013**, *70*, 2451.
[385] G. R. Mahdavinia, B. Massoumi, K. Jalili, G. Kiani, *J. Polym. Res.* **2012**, *19*, 9947.
[386] H. Hosseinzadeh, S. Zoroufi, G. R. Mahdavinia, *Polym. Bull.* **2015**, *72*, 1339.
[387] X. Qi, Q. Zeng, X. Tong, T. Su, L. Xie, K. Yuan, J. Xu, J. Shen, *J. Hazard. Mater.* **2021**, *402*, 123359.
[388] R. Bhattacharyya, S. K. Ray, *Chem. Eng. J.* **2015**, *260*, 269.
[389] S. P. Santoso, A. Kurniawan, F. E. Soetaredjo, K.-C. Cheng, J. N. Putro, S. Ismadji, Y.-H. Ju, *Cellulose* **2019**, *26*, 3339.
[390] Y. Wang, W. Wang, A. Wang, *Chem. Eng. J.* **2013**, *228*, 132.
[391] S. Barreca, S. Orecchio, A. Pace, *Appl. Clay Sci.* **2014**, *99*, 220.
[392] A. Heydari, H. Sheibani, *RSC Adv.* **2015**, *5*, 82438.
[393] H. Dai, Y. Huang, H. Huang, *Carbohydr. Polym.* **2018**, *185*, 1.
[394] W. Wang, J. Wang, Y. Zhao, H. Bai, M. Huang, T. Zhang, S. Song, *Environ. Pollut.* **2020**, *257*, 113574.
[395] N. Peng, D. Hu, J. Zeng, Y. Li, L. Liang, C. Chang, *ACS Sustainable Chem. Eng.* **2016**, *4*, 7217.
[396] W. Wang, J. Ni, L. Chen, Z. Ai, Y. Zhao, S. Song, *Int. J. Biol. Macromol.* **2020**, *165*, 1.
[397] N. Malatji, E. Makhado, K. E. Ramohlola, K. D. Modibane, T. C. Maponya, G. R. Monama, M. J. Hato, *Environ. Sci. Pollut. Res.* **2020**, *27*, 44089.
[398] N. Sarkar, G. Sahoo, R. Das, S. K. Swain, *ACS Appl. Nano Mater.* **2018**, *1*, 1188.
[399] H. Bai, Q. Zhang, T. He, G. Zheng, G. Zhang, L. Zheng, S. Ma, *Appl. Clay Sci.* **2016**, *124*, 157.
[400] H. Khadivi, M. Sirousazar, V. Abbasi-Chianeh, E. Jalilnejad, *J. Polym. Environ.* **2022**, *30*, 3186.
[401] S. Thakur, A. Verma, P. Raizada, O. Gunduz, D. Janas, W. F. Alsanie, F. Scarpa, V. K. Thakur, *Chemosphere* **2022**, *291*, 133002.
[402] M. Daud, A. Hai, F. Banat, M. B. Wazir, M. Habib, G. Bharath, M. A. Al-Harthi, *J. Mol. Liq.* **2019**, *288*, 110989.
[403] T. Li, H. N. Miras, Y.-F. Song, *Catalysts* **2017**, *7*, 260.
[404] K. Charradi, Z. Ahmed, P. Aranda, R. Chtourou, *Appl. Clay Sci.* **2019**, *174*, 77.
[405] A.-L. Yan, X.-C. Wang, J.-P. Cheng, *Nanomaterials* **2018**, *8*, 747.
[406] Z.-z. Yang, J.-j. Wei, G.-m. Zeng, H.-q. Zhang, X.-f. Tan, C. Ma, X.-c. Li, Z.-h. Li, C. Zhang, *Coord. Chem. Rev.* **2019**, *386*, 154.
[407] V. A. Shirin, R. Sankar, A. P. Johnson, H. Gangadharappa, K. Pramod, *J. Controlled Release* **2022**, *343*, 724.
[408] M. Zubair, M. Daud, G. McKay, F. Shehzad, M. A. Al-Harthi, *Appl. Clay Sci.* **2017**, *143*, 279.
[409] N. Kumar, L. Reddy, V. Parashar, J. C. Ngila, *J. Environ. Chem. Eng.* **2017**, *5*, 1718.
[410] J.-H. Kim, J.-K. Kang, S.-C. Lee, S.-B. Kim, *Appl. Clay Sci.* **2019**, *170*, 1.
[411] R. Shan, Y. He, T. Zi, G. Wang, X. Liu, Z. Han, T. Zhang, Y. Zhu, *Water, Air, Soil Pollut.* **2018**, *229*, 329.
[412] X.-J. Yang, P. Zhang, P. Li, Z. Li, W. Xia, H. Zhang, Z. Di, M. Wang, H. Zhang, Q. J. Niu, *J. Mol. Liq.* **2019**, *280*, 128.
[413] T. Hibino, *Appl. Clay Sci.* **2014**, *87*, 150.
[414] T. Hibino, *Appl. Clay Sci.* **2021**, *211*, 106188.
[415] W. Hu, L. Xie, H. Zeng, *J. Colloid Interface Sci.* **2020**, *568*, 36.
[416] Z.-H. Zhang, J.-Y. Xu, X.-L. Yang, *Mater. Chem. Phys.* **2021**, *260*, 124123.
[417] F. Chen, R. Wang, H. Chen, H. Lu, *Polym.-Plast. Technol. Mater.* **2021**, *60*, 1568.
[418] M. M. Tunesi, R. A. Soomro, X. Han, Q. Zhu, Y. Wei, B. Xu, *Nano Convergence* **2021**, *8*, 5.
[419] Y.-Z. Zhang, J. K. El-Demellawi, Q. Jiang, G. Ge, H. Liang, K. Lee, X. Dong, H. N. Alshareef, *Chem. Soc. Rev.* **2020**, *49*, 7229.
[420] O. Folorunso, N. Kumar, Y. Hamam, R. Sadiku, S. S. Ray, *FlatChem* **2021**, *29*, 100281.
[421] A. Shahzad, M. Nawaz, M. Moztahida, J. Jang, K. Tahir, J. Kim, Y. Lim, V. S. Vassiliadis, S. H. Woo, D. S. Lee, *Chem. Eng. J.* **2019**, *368*, 400.
[422] Y. Chen, X. Xie, X. Xin, Z.-R. Tang, Y.-J. Xu, *ACS Nano* **2019**, *13*, 295.
[423] B.-M. Jun, Y. A. J. Al-Hamadani, A. Son, C. M. Park, M. Jang, A. Jang, N. C. Kim, Y. Yoon, *Sep. Purif. Technol.* **2020**, *247*, 116947.
[424] Y. Chen, S. Li, X. Pei, J. Zhou, X. Feng, S. Zhang, Y. Cheng, H. Li, R. Han, B. Wang, *Angew. Chem., Int. Ed.* **2016**, *55*, 3419.
[425] O. Maan, P. Song, N. Chen, Q. Lu, *Adv. Mater. Interfaces* **2019**, *6*, 1801895.
[426] H. Zhu, Q. Zhang, S. Zhu, *ACS Appl. Mater. Interfaces* **2016**, *8*, 17395.
[427] X. Zhou, C.-j. Liu, *Adv. Funct. Mater.* **2017**, *27*, 1701134.
[428] Y. S. Zhang, K. Yue, J. Aleman, K. Mollazadeh-Moghaddam, S. M. Bakht, J. Yang, W. Jia, V. Dell'Erba, P. Assawes, S. R. Shin, M. R. Dokmeci, R. Oklu, A. Khademhosseini, *Ann. Biomed. Eng.* **2017**, *45*, 148.
[429] A. Davó-Quiñonero, D. Sorolla-Rosario, E. Bailón-García, D. Lozano-Castelló, A. Bueno-López, *J. Hazard. Mater.* **2019**, *368*, 638.
[430] R. Pei, L. Fan, F. Zhao, J. Xiao, Y. Yang, A. Lai, S.-F. Zhou, G. Zhan, *J. Hazard. Mater.* **2020**, *384*, 121418.
[431] J. Mao, M. Ge, J. Huang, Y. Lai, C. Lin, K. Zhang, K. Meng, Y. Tang, *J. Mater. Chem. A* **2017**, *5*, 11873.
[432] D. Harikishore Kumar Reddy, K. Vijayaraghavan, J. A. Kim, Y.-S. Yun, *Adv. Colloid Interface Sci.* **2017**, *242*, 35.
[433] I. E. Mejías Carpio, C. M. Santos, X. Wei, D. F. Rodrigues, *Nanoscale* **2012**, *4*, 4746.

Neeraj Kumar is currently a senior researcher at Council for Scientific and Industrial Research (CSIR), Pretoria, South Africa. He obtained his Ph.D. degree in chemistry from the University of Johannesburg in 2017. His research interests focus on controllable synthesis and processing of 2D nanomaterials, especially graphene, MXenes, and metal chalcogenides and their organic/inorganic nanocomposites for environmental and energy applications, including water treatment, photo-catalysis, photoelectro-catalysis, CO_2 capture and conversion, and energy storage.

Rashi Gusain is a research associate at the University of Johannesburg and a visiting researcher at CSIR-Pretoria, South Africa. She received her Ph.D. degree in chemical science from CSIR-Indian Institute of Petroleum, India in 2016. Her expertise is in organic and inorganic synthesis, ionic liquids, nanomaterials, tribology, photo-catalysis, and water purification. Her current research interest is the development of inorganic nanomaterials for photo-degradation of organic water contaminants and CO_2 capture and conversion.

Sadanand Pandey is currently a research professor in the Department of Chemistry, at Yeungnam University, South Korea. He was a Kothari fellow at the world's prestigious Indian Institute of Science (2011–2013) and an NRF scientist at the University of Johannesburg, South Africa (2014–2018). Research interests include the synthesis and processing of bio-based organic-inorganic Nanocomposites for energy storage, water purification, and biomedical fields.

Suprakas Sinha Ray is a chief researcher in polymer nanocomposites at the Council for Scientific and Industrial Research (CSIR), Pretoria, South Africa. He was awarded a Ph.D. in physical chemistry by the University of Calcutta in 2001 and is director of the Department of Science and Technology (DST)-CSIR, Nanotechnology Innovation Centre, and manager of the Centre for Nanostructures and Advanced Materials. He is also affiliated with the University of Johannesburg as a distinguished visiting professor of applied chemistry. Prof. Ray's current research focus is on polymer-based advanced nanostructured materials and their applications.